University of Alberta

DNA Separation in Nanoporous Microfluidic Devices

by

Neda Nazemifard

A thesis submitted to the Faculty of Graduate Studies and Research
in partial fulfillment of the requirements for the degree of

Doctor of Philosophy

Mechanical Engineering

Spring 2011
Edmonton, Alberta

To my parents and my husband

ABSTRACT

This dissertation investigates the size based separation of DNA molecules in nanoparticle arrays under asymmetric pulsed electrophoresis. Crystalline arrays of nanoparticles within microfluidic channels are fabricated using colloidal self-assembly, yielding structures with pore sizes ranging from a few nanometers to a few hundred nanometers. Angular separation of DNA molecules is achieved in these matrices using asymmetric pulsed field electrophoresis. The DNA migration mechanism in highly confined pores and the impact of pulse frequency and field magnitudes on DNA separation are studied. It is observed that in confinements smaller than the persistence length of DNA, the DNA molecule is fully stretched and can be treated as a persistent chain due to its bending elasticity. The frequency response of DNA separation is also investigated, showing four distinct regions in frequency response curve; a low frequency rise, a plateau, a subsequent decline, and a second plateau at higher frequencies. It is shown that this frequency response is governed by the relation between the pulse time, relaxation time, and the reorientation time of DNA. Real-time videos of single DNA migrating under high frequency pulsed electric field show the DNA no longer follows the ratchet mechanism seen at lower frequencies, but reptates along the average direction of the two electric fields. A freely-jointed-chain model of DNA is developed to calculate the frequency response of a chain under a pulsed external force. The model exhibits a similar variation of angular separation with frequency.

Finally, the role of order within a separation matrix on DNA separation efficiency is studied systematically. Colloidal arrays with two different sized nanoparticles mixed in various proportions are prepared, yielding structures with different degrees of disorder. Radial distribution functions and orientational order parameters are calculated to characterize the scale of disorder. The DNA separation resolution is quantified for each structure, showing a strong dependence on order within the structure. Ordered structures give better separation resolution than highly disordered structures. However, the variation of separation performance with order is not monotonic, showing a small, but statistically significant improvement in structures with short range order compared to those with long range order.

Acknowledgment

It has been an unforgettable experience and I like to thank a number of people for making the last four years of my life such an amazing time.

I had the chance to work with one of the brightest scientists I ever met as my supervisor, Dr. Jed Harrison. His sharp understanding of the physical problems, his insightful guidance, and his keen sense of humour came to my rescue, whenever I knocked on his door for help. But, maybe the most important thing I take from working with Jed is how he integrates his meticulous scientific integrity and professional attitude with his zest for excellence in all aspects of his research. I truly feel blessed to have the chance to be his student.

I have also been lucky to work with two exceptional professors from the beginning of my graduate study, Drs. Subir Bhattacharjee and Jacob Masliyah. I am thankful to Subir for patiently teaching me the invaluable skill of scientific communication. I am thankful to him for his trust, encouragement, and uncountable words of advice. He taught me, by his own example that the key to a successful future in science is passion and a never-ending thirst for learning.

I am short of words to express my gratitude to my supervisor and mentor, Dr. Jacob Masliyah. His vision, his devotion to his students, and his extraordinary understanding of scientific concepts have been a great source of inspiration and comfort throughout my graduate study. Through his mentorship, I learned to never lose track of the bigger picture in the horizon and to never forget the people around me and their impact on my work.

I thank Dr. David Nobes for being in my supervisory committee and for his help with fluorescence microscopy. I like to thank the members of my examining committee: Dr. Charles Lucy and Dr. Michael Lipsett for reviewing my thesis. I like to specially thank Dr. Michael Lipsett for his insightful comments during my candidacy exam, which helped me to develop a more profound understanding of the multiphysics nature of this research. I would like to specially thank Dr. Gary Slater for accepting to come to Edmonton as the external examiner in my defence.

I would like to acknowledge the financial support provided by NSERC Graham Bell Graduate Student Scholarship (CGSD) and Alberta Ingenuity Scholarship in Nanotechnology, which supported me throughout my PhD.

I am also thankful to my friends and lab mates for their support, friendship, and help. I thank Jeff, Tania, Shahnawaz, James, Yujuan, Wenmin, Ledi, and Abebaw. I would like to specially thank my friend, Shahnawaz, for teaching me the alphabets of doing experiments and for all our brainstorming discussions. I also like to thank Dr. Abebaw Jemere for his help and friendship.

No words can fully express my gratitude to my parents and my brother for their love and sacrifice. They have supported me in any and every possible way throughout my education. Without their constant encouragement, I could have never enjoyed my years of being a student, as much as I did. A special thank goes to my purring, fluffy friend, Khepel, for never leaving my side while I was writing this thesis. Finally, I would like to sincerely thank my husband, Farshid, for his understanding and support, and for being with me through ups and downs. I feel lucky to have such a caring companion to spend the rest of my life with.

Table of Contents

List of Tables

List of Figures

List of Symbols

a_p	particle radius (m)
b	Kuhn length (m)
d	diameter of the smaller particle in a binary packed structure (m)
d_p	pore size (m)
d_{ch}	channel size (m)
D	diameter of the larger particle in a binary packed structure (m)
D_{dif}	diffusion coefficient (m^2s^{-1})
e	elementary charge of an electron (4.355×10^{-19} C)
E_1, E_2	applied electric fields (Vm^{-1})
f	frequency (Hz)
f^*	scaled frequency
g(r)	radial distribution function
k_b	Boltzmann constant (1.381×10^{-23} JK^{-1})
L	DNA apparent length (m)
$L_{contour}$	DNA contour length (m)
M	DNA molecular weight (Da)
n_∞	bulk number concentration of the ions in an electrolyte (m^{-3})
N	number of Kuhn segments

N_p	number of particles in an electron micrograph of a packed structure
p	persistence length of DNA (m)
q_k	electric charge associated with a Kuhn segment (C)
q_{total}	total electric charge of DNA (C)
Q	total electric charge of a particle (C)
r	radial distance from the centre of a particle (m)
R_g	gyration radius of a polymer (m)
R_N	end to end distance of an ideal polymer chain (m)
Rs	separation resolution
Rs_{bed}	separation resolution arising solely from the separation bed
Rs*	scaled separation resolution
t_{or}	reorientation time of DNA (s)
t_p	time taking DNA molecule to move one column in nanoparticle array (s)
T	absolute temperature (K)
T_p	pulse time (s)
U	electrophoretic velocity (ms^{-1})
w	width of a DNA molecule (m)
w_b	band width (m)
z	valence of ions

Greek symbols

α	angle between the two applied electric fields (º)
β	angle between a line connecting two particles in a packed bed and the horizontal direction (º)
ε	scaled electric force applied on a DNA
ε_0	vacuum permittivity (8.854×10^{-12}, Fm^{-1})
ε_r	relative permittivity of an electrolyte
η	buffer viscosity ($kgm^{-1}s^{-1}$)
θ	deflection angle of DNA streams (º)
θ_{max}	maximum deflection angle of DNA streams
κ^{-1}	Debye length (m)
λ	Odijk segment (m)
μ_1, μ_2	DNA electrophoretic mobilities in the direction of E_1 and E_2 ($m^2V^{-1}s^{-1}$)
μ_0	DNA mobility in a free solution ($m^2V^{-1}s^{-1}$)
ξ	friction coefficient of a bead in the Rouse bead-spring model (kgs^{-1})
ξ_k	friction coefficient associated with a Kuhn segment (kgs^{-1})
ξ_{total}	total friction coefficient of DNA molecule (kgs^{-1})
ς	zeta potential of a particle (V)
σ^2_{bed}	variance of the fluorescence intensity profile associated with the separation bed (m^2)

σ^2_{inj}	variance of the fluorescence intensity profile associated with the injection channel (m^2)
σ^2_{total}	variance of the fluorescence intensity profile at the separation chamber (m^2)
τ_0	Kuhn segment relaxation time (s)
τ_p	relaxation time of the p-th mode (s)
τ_r	longest relaxation time of a DNA molecule
χ_{700}	volume fraction of 700 nm particles in a bidisperse suspension of 320 and 700 nm particles
ψ	orientational order parameter

Abbreviations

APFE	asymmetric pulsed field electrophoresis
bp	base pair
BRF	biased reptation with fluctuation
BRM	biased reptation model
CSA	colloidal self assembly
CV	coefficient of variation
DNA	Deoxyribonucleic acid
GE	gel electrophoresis
HGP	Human Genome Project
PCR	polymerase chain reaction
PD	peak distance

PDMS	Polydimethylsiloxane
PFGE	pulsed field gel electrophoresis
TBE	tris borate Ethylenediaminetetraacetic acid
TIRF	total internal reflection fluorescence microscopy

CHAPTER 1
INTRODUCTION

1.1 Introduction

With the completion of the Human Genome Project[1] (HGP) in 2003, scientists now possess a library of information that has a potential to revolutionize human health, medicine, and environment. Separation of DNA by size is at the core of DNA analysis, which was the underlying technology utilized in conducting and completing the HGP.[2-4] The same underlying technology also took part in the recent breakthrough in synthetic biology, the creation of a bacterium with an artificial genome in 2010, by two biologists, Craig Venter and Hamilton Smith.[5] DNA separation technology is used in many life-sciences applications, including forensic, environmental, pharmaceutical, and medical researches.[6-10] With a number of disease-related genes already being identified, DNA analysis can further facilitate understanding the relation between genes and disease, which may ultimately result in the development of new treatments for complex diseases such as cancer.[11-15] The continuous and steady growth of these genetically related technologies, however, rely heavily on improved techniques for DNA separation, which needs to be high in speed, high in throughput, and low in cost without compromising the separation resolution.[16-19]

Due to the negative electric charge of DNA molecules in aqueous solutions, electrophoresis has been the preferred method of size separation for these molecules.[8, 20] DNA molecules in free solutions under an electrophoretic force adopt a "free-draining-coil" conformation, meaning that both the electric force and the hydrodynamic friction force vary in a similar fashion with the molecular size, resulting in a migration rate that is molecular size-independent.[21-25] By conducting electrophoresis in a sieving matrix, a size-dependent mobility is induced through interactions of the molecule with the porous structure.[8, 26-28] Agarose and polyacrylamide hyrogels are the two widely used separation matrices, which, combined with the electrophoresis technique, form the basis of conventional Gel Electrophoresis (GE) for size separation of DNA.[29-31] Gel electrophoresis can successfully resolve DNA molecules up to 10 kbp.[30-33] In 1984, Schwartz and Cantor[34] developed a variation on the standard GE protocol, by introducing a pulsed electric field instead of a constant electric field. The method became known as Pulsed Field Gel Electrophoresis (PFGE). Using PFGE, DNA molecules up to 50 Mbp can be separated.[35]

In practice, both GE and PFGE are conducted in either slab-gel or capillary configurations. However, there are some drawbacks associated with each configuration. In slab-gel configuration, a new gel should be cast prior to each separation run, a large amount of DNA sample is required, and due to the large scale of the device, the separation is conducted using low electric fields to suppress problems associated with Joule heating, resulting in long separation times of a few days.[36, 37] Capillary electrophoresis is performed in thin capillaries

of 50-100 μm, so higher electric fields can be applied, since the generated heat is easily dissipated due to the small scale of the device. However, due to the one-dimensional geometry of capillaries, for separation of large DNA molecules, only field inversion electrophoresis can be applied, where the two pulsed electric fields are applied in opposite directions, resulting in significant reduction in migration rate of DNA molecules despite the high values of the applied electric fields.[38, 39]

With advances in micro and nanofabrication techniques during the last decade, the application of micro and nanofluidic devices for separation and analysis of DNA molecules has been proposed, investigated, and devised in a variety of designs and materials.[40-45] Microfluidic systems have common characteristics which make them an excellent candidate to replace the conventional methods of DNA size separation.[46-48]

1.2 Objectives and Scope

The design and fabrication of fast, affordable, high throughput devices for high resolution separation of DNA molecules which can be integrated in lab-on-a-chip systems is still an ongoing challenge. This research is centred around the challenges involved in electrophoretic DNA separation methods in microfluidic devices. A microfluidic device for size separation of DNA has been developed in our group, based on the colloidal self assembly (CSA) approach.[49, 50] In this device, a self assembled nanoparticle array serves as a separation matrix for pulsed field DNA electrophoresis. The promising preliminary results proved the

feasibility of using nanoparticle array as a sieving matrix for DNA separation, but the full potential of the self assembly approach for DNA separation and the separation mechanism of DNA in our device is still unknown. The first objective of this thesis is to investigate the scope and limitations of the self assembly approach in the range of confinement sizes it can provide, and their structural robustness at high electric fields. The simplicity inherent in CSA provides a unique opportunity to fabricate ordered structures where the size of confinement can easily be altered from hundreds of nanometres to just a few nanometres. Taking advantage of this possibility, the effects of confinement size on DNA separation performance under strong asymmetric pulsed fields were investigated.

The second objective of this thesis is to investigate the role of separation matrix architecture on DNA separation performance. Most separation matrices used for DNA separation are either highly disordered such as gels or highly ordered, such as microfabricated arrays. Using the self assembly approach, we fashioned highly ordered and highly disordered structures as well as structures in between, systematically tuning the order. So, in addition to confinement size, the role of confinement geometry or architecture on separation performance is also investigated.

Asymmetric pulsed field electrophoresis is the latest subcategory of the more general, well-studied pulsed field electrophoresis technique. Although the overall separation mechanism for pulsed field electrophoresis is known, the separation mechanism specific to the asymmetric pulsed field electrophoresis within a nanoparticle array structure has not been fully investigated. Our

fractionation device serves as a reliable tool to study the DNA migration mechanism under asymmetric pulsed electric fields. The third objective of this thesis is to investigate the migration mechanism of DNA molecules in order to explain the somewhat complicated separation behaviour of DNA under asymmetric pulsed electric fields and the effects of different experimental parameters on the separation performance. A combination of the self assembly approach and high resolution real-time videomicroscopy of single DNA molecules was used to observe the DNA dynamics. The relation between basic polymer properties such as persistence length or characteristic relaxation time of DNA and the separation behaviour within an ordered, nanoporous array across a large range of frequencies was established. An attempt was also made to relate DNA separation behaviour observed in asymmetric pulsed field electrophoresis to the existing knowledge in the literature for pulsed field gel electrophoresis.

The specific objectives of this thesis can be summarized as:

- To study elements of the separation mechanism of DNA molecules under asymmetric pulsed field electrophoresis in nanoparticle arrays.
- To identify the key parameters governing the separation performance of DNA molecules in asymmetric pulsed electric field method.
- To explore and visualize DNA migration in nanoscale confinements under strong pulsed electric fields.
- To investigate the role of the separation matrix architecture on DNA separation performance in nanoporous materials.

1.3 Background Review

An alternative to the conventional, macro scale DNA separation techniques is application of microfluidic systems for DNA separation. Micro and nanofluidic technologies have common characteristics, making them a potential replacement for the conventional methods of DNA fractionation. Due to the high surface to volume ratio in microfluidic systems, the heat transfer is much faster in these systems compared to the macro scale devices. For DNA separation, better heat transfer means application of much higher electric fields is possible, which directly results in significantly faster separation processes.[51-53] In contrast to a slab-gel apparatus that requires millilitre sample volumes, microfluidic systems require only a few nanolitre sample volumes.[54]

Microfluidic systems are potentially portable and can be deployed in field locations for use in a variety of forensic, diagnostic, and biosensing applications. Attempts have been made to miniaturize other DNA analysis elements such as DNA purification, polymerase chain reaction (PCR) amplification, and detection, so along with a DNA separation unit, they can form self-contained DNA analysis system. These lab-on-a-chip concepts provide field equipment that does not rely on pre-existing laboratory infrastructures.[18, 45, 55-60] Hopwood et al.[61] devised a multistep microfluidic device for an on-site forensic investigation, which allows DNA purification, amplification by PCR, and collection of the amplified product for delivery to an integral capillary electrophoresis chip to produce a DNA profile compatible with the data format of DNA databases. Mathies's group[43, 56, 62]

developed a high-performance genetic analysis unit that combines high-throughput microfluidic emulsion generator with PCR. In another study, Quake's group[18, 63] reported the use of single-molecule methods to sequence an individual human genome, which enabled analysis of human genomic information without the need for cloning, amplification or ligation. Their device is intended to facilitate application of genome sequencing to personal genomics.

Since their early days, micro and nanofluidic system opened new opportunities in developing new materials and unique mechanisms for DNA separation that could not be realized in conventional methods. Austin's group[52, 64] designed a "DNA prism", where an array of micron-scale posts served as a separation matrix for continuous-flow separation of DNA under asymmetric pulsed electric fields. The DNA prism sorts DNA molecules in different directions according to their molecular sizes, much as a prism deflects light of different wavelengths at different angles. Another separation mechanism called "entropic trapping" was realized by Craighead's group.[65-67] They invented a nanofluidic device, consisting of many narrow constrictions and wider regions that cause size-dependent trapping (entropic trapping) of DNA. This process creates electrophoretic mobility differences, thus enabling efficient separation without the use of a gel or pulsed electric fields. Viovy's group[53, 68] designed a microfluidic DNA separation device, where the separation matrix is made with columns of paramagnetic micron-size particles assembled upon applying a magnetic field. Baba's group[69, 70] established a nanofabrication technique for constructing nanopillars in a quartz microchip. The size of pillars and the spacing

between pillars are designed as a DNA sieving matrix for optimal separation of large DNA fragments. DNA molecules were successfully separated within 10 s under a direct current electric field.

In addition to microfabricated matrices for DNA separation, colloidal self assembled structures were also employed within microfluidic devices for DNA separation. Compared to nanofabricated structures, self assembled structures are easier to fabricate and lower in cost. The migration and conformations of DNA molecules in self assembled silica particle arrays were studied by the Wirth's group.[71] Their results suggested self assembling inorganic materials can serve as possible alternatives to gels for higher speed electrophoresis. The self assembled array in their device was fabricated using conventional vertical deposition procedures. A new colloidal self assembly technique highly compatible with the microfluidic approach was developed by the Harrison group[49, 50] to form crack-free, macro scale, self assembled arrays within microfluidic devices. They designed a microfluidic DNA separation device, which used the self assembled nanoparticle array as a sieving matrix for separation of DNA molecules under pulsed electric fields.

Not only does the micro and nanofluidic approach provide an opportunity to examine different separation matrices for DNA fractionation, it also provides a platform to discover innovative separation methods, which do not rely on separation media. A matrix-free method of DNA separation proposed and developed by Slater et al.[21, 72] Their method was based on labelling DNA with a large, uncharged molecule to overcome the DNA free-draining property. The

resulting methodology is called end-labelled free-solution electrophoresis. In another attempt, similar to early works of Fung and Yeung[73] in using capillaries for DNA separation, Wang et al.[74] reported using a narrow microchannel to hydrodynamically separate a wide range of DNA fragments in a single run and in a few minutes without the need for gels or wall coatings. Pel et al.[75] demonstrated a unique parameter for DNA separation in a microfluidic device that results from the nonlinear response of DNA to superposition of synchronous, time-varying electrophoretic fields. In another study, using nanofabrication techniques, Salieb-Beugelaar et al.[76, 77] investigated the transport behavior of lambda-DNA (48 kbp) in fused silica nanoslits upon application of electric fields of different strengths. Their preliminary experiments show that the migration rate of DNA in nanoslits is size-dependent, suggesting that high field electrophoresis in nanoslits can be used for DNA separation.

The ability of nanofluidic systems to approach molecular size scales enables scientists to target single DNA molecules. Numerous DNA molecular properties such as conformational, dynamic, and entropic properties have been directly probed in micro and nanofluidic devices. Austin's group[78-82] demonstrated a new method to fabricate single fluidic-channels with a width of a few nanometres to measure DNA extensions and relaxation times in nanochannels. Their observations showed that below a critical width, there is a crossover in the polymer physics due to the confinement effects. Using nanofabrication techniques, Doyle's group[83-85] experimentally investigated the influence of slit-like confinement on the coil-stretch transition of single DNA

molecules and relaxation times of DNA in nanoscale confinement. Cheng et al.[74, 86] reported on the creation of micro-curvilinear flow through a microfluidic device to observe real-time dynamics of DNA under mechanical stimulation, including stretching and bending. They found that the flexible DNA molecules exhibited multimodal responses related to both the elongation and bending dynamics dictated by their locations within the curvilinear flow.

Despite all the above advances in developing microfluidic based separation devices for DNA, the design and fabrication of microfluidic devices for DNA size separation still pose a variety of challenges, such as the need to achieve high-resolution separations over distances of a few centimetres or less, the complicated nanofabrication techniques that usually require sophisticated facilities and time-consuming, expensive fabrication procedures.[17, 42, 76, 87] These challenges suggest that further investigation and research is needed to transform the concept of a commercial, affordable, hand-held DNA analysis system into reality.

1.4 Organization of the Thesis

In this chapter, a general overview of DNA size separation has been presented. The overall objectives and scope of this study have also been laid out. In Chapter 2, we discuss the principles of electrophoretic methods of DNA size separation. Different migration mechanisms of DNA in separation media under electrophoretic force are discussed. A brief description of polymer physics in free

solutions as well as nanoscale confinements is also presented, to facilitate our discussions in the following chapters.

In Chapter 3, the effect of the void size that confines DNA, which will be referred to as the confinement, on DNA separation is studied. Ordered nanoparticle arrays with confinements as small as a few nanometres (~ 15 nm) are fabricated using the colloidal self assembly approach. The mechanism of DNA transport in ordered, highly confined pores was studied under asymmetric pulsed electric field. DNA separation was conducted in ordered arrays with different pore sizes. A simple geometric model is developed to explain the separation of DNA molecules and its variation with experimental parameters such as electric field strength, pulse frequency, pore size, and DNA size. The model shows a poor agreement with experimental results in larger confinements. It is only in the smallest confinement of 15 nm that a quantitative fit of the geometric model with the experimental result is observed. Existing theories of DNA migration mechanism and DNA stretching in nanoscale confinement are employed to explain the agreement between the model and the experiment in nanoscale confinement.

In Chapter 4, we study the frequency behaviour of DNA separation under asymmetric pulsed electric fields. Four distinct regimes are observed in the separation-frequency curve. High quality real-time movies of DNA migration were acquired using Total Internal Fluorescence Microscopy (TIRF). These movies were employed to understand the migration mechanism of DNA in each frequency regime. The effect of DNA reorientation and relaxation times on

separation behaviour was also studied. A numerical analysis of DNA based on a freely-jointed-chain model was also developed, to help understand the frequency behaviour of DNA chain under asymmetric pulsed fields.

In Chapter 5, we investigate the role of order in a separation matrix on DNA separation performance. Using the colloidal self assembly approach, monodisperse suspensions of nanoparticles were used to fabricate highly ordered structures. Bidisperse suspensions, on the other hand, provide disordered structures, where the degree of disorder can be systematically changed by varying the volume fractions of the two particles in suspension. Different analytical parameters were calculated to characterize each structure. A DNA separation experiment was conducted in each structure and the separation band distance, band width, and separation resolution were measured and calculated. The results show that DNA separation is significantly affected by the degree of disorder in the separation matrix. A non-monotonic behaviour of DNA separation with the degree of order is observed.

Finally, in Chapter 6, a summary of the key observations in this study is provided and some directions for future research in this field are suggested.

1.5 REFERENCES

1. Gibbs, R.A., J.W. Belmont, P. Hardenbol, T.D. Willis, F.L. Yu, H.M. Yang, L.Y. Ch'ang, W. Huang, B. Liu, Y. Shen, et al., *The international hapmap project.* **Nature**, *2003*. 426: p. 789-796.
2. Baba, Y., *Analysis of disease-causing genes and DNA-based drugs by capillary electrophoresis - towards DNA diagnosis and gene therapy for human diseases.* **Journal of Chromatography B**, *1996*. 687: p. 271-302.
3. Kan, C.W., C.P. Fredlake, E.A.S. Doherty, and A.E. Barron, *DNA sequencing and genotyping in miniaturized electrophoresis systems.* **Electrophoresis**, *2004*. 25: p. 3564-3588.
4. Ugaz, V.M., R.D. Elms, R.C. Lo, F.A. Shaikh, and M.A. Burns, *Microfabricated electrophoresis systems for DNA sequencing and genotyping applications: Current technology and future directions.* **Philosophical Transactions of the Royal Society a-Mathematical Physical and Engineering Sciences**, *2004*. 362: p. 1105-1129.
5. Gibson, D.G., J.I. Glass, C. Lartigue, V.N. Noskov, R.Y. Chuang, M.A. Algire, G.A. Benders, M.G. Montague, L. Ma, M.M. Moodie, et al., *Creation of a bacterial cell controlled by a chemically synthesized genome.* **Science**, *2010*. 329: p. 52-56.
6. Ferreira, G.N.M., G.A. Monteiro, D.M.F. Prazeres, and J.M.S. Cabral, *Downstream processing of plasmid DNA for gene therapy and DNA vaccine applications.* **Trends in Biotechnology**, *2000*. 18: p. 380-388.

7. Issaq, H.J., *A decade of capillary electrophoresis.* **Electrophoresis**, *2000*. 21: p. 1921-1939.

8. Viovy, J.L., *Electrophoresis of DNA and other polyelectrolytes: Physical mechanisms.* **Reviews of Modern Physics**, *2000*. 72: p. 813-872.

9. Ryu, D.D.Y. and D.H. Nam, *Recent progress in biomolecular engineering.* **Biotechnology Progress**, *2000*. 16: p. 2-16.

10. Jansen, R.C. and J.P. Nap, *Genetical genomics: The added value from segregation.* **Trends in Genetics**, *2001*. 17: p. 388-391.

11. Sharon, D., R. Chen, and M. Snyder, *Systems biology approaches to disease marker discovery.* **Disease Markers**, *2010*. 28: p. 209-224.

12. Moreno, C., J. Lazar, H.J. Jacob, and A.E. Kwitek, *Comparative genomics for detecting human disease genes*, in *Genetic dissection of complex traits, 2nd edition*. *2008*. p. 655-697.

13. Michlmayr, A. and R. Oehler, *'omics': State of the art in vitro techniques employed in surgical research.* **European Surgery-Acta Chirurgica Austriaca**, *2010*. 42: p. 127-133.

14. van't Veer, L.J., H.Y. Dai, M.J. van de Vijver, Y.D.D. He, A.A.M. Hart, M. Mao, H.L. Peterse, K. van der Kooy, M.J. Marton, A.T. Witteveen, et al., *Gene expression profiling predicts clinical outcome of breast cancer.* **Nature**, *2002*. 415: p. 530-536.

15. Hedenfalk, I., D. Duggan, Y.D. Chen, M. Radmacher, M. Bittner, R. Simon, P. Meltzer, B. Gusterson, M. Esteller, O.P. Kallioniemi, et al.,

Gene-expression profiles in hereditary breast cancer. **New England Journal of Medicine**, *2001*. 344: p. 539-548.

16. Wang, D.J. and S. Bodovitz, *Single cell analysis: The new frontier in 'omics'.* **Trends in Biotechnology**, *2010*. 28: p. 281-290.
17. van den Berg, A., H.G. Craighead, and P.D. Yang, *From microfluidic applications to nanofluidic phenomena.* **Chemical Society Reviews**, *2010*. 39: p. 899-900.
18. Lee, C.C., T.M. Snyder, and S.R. Quake, *A microfluidic oligonucleotide synthesizer.* **Nucleic Acids Research**, *2010*. 38: p. 2514-2521.
19. Wan, F., J. Zhang, and B. Chu, *Advances in electrophoretic techniques for DNA sequencing and oligonucleotide analysis*, in *Advances in chromatography, vol 47*. *2009*. p. 59-125.
20. Landers, J.P., R.P. Oda, T.C. Spelsberg, J.A. Nolan, and K.J. Ulfelder, *Capillary electrophoresis - a powerful microanalytical technique for biologically-active molecules.* **Biotechniques**, *1993*. 14: p. 98-111.
21. Heller, C., G.W. Slater, P. Mayer, N. Dovichi, D. Pinto, J.L. Viovy, and G. Drouin, *Free-solution electrophoresis of DNA.* **Journal of Chromatography A**, *1998*. 806: p. 113-121.
22. Slater, G.W. and S.Y. Wu, *Reptation, entropic trapping, percolation, and rouse dynamics of polymers in random-environments.* **Physical Review Letters**, *1995*. 75: p. 164-167.

23. Shafer, R.H., N. Laiken, and B.H. Zimm, *Radial migration of DNA-molecules in cylindrical flow .1. Theory of free-draining model.* **Biophysical Chemistry**, *1974*. 2: p. 180-184.

24. Rasmusson, M. and B. Akerman, *Dynamic mobility of DNA.* **Langmuir**, *1998*. 14: p. 3512-3516.

25. Stellwagen, N.C., C. Gelfi, and P.G. Righetti, *The free solution mobility of DNA.* **Biopolymers**, *1997*. 42: p. 687-703.

26. Noolandi, J., J. Rousseau, G.W. Slater, C. Turmel, and M. Lalande, *Self-trapping and anomalous dispersion of DNA in electrophoresis.* **Physical Review Letters**, *1987*. 58: p. 2428-2431.

27. Slater, G.W. and J. Noolandi, *The biased reptation model of DNA gel-electrophoresis - mobility vs molecular-size and gel concentration.* **Biopolymers**, *1989*. 28: p. 1781-1791.

28. Zimm, B.H., *Lakes-straits model of field-inversion gel-electrophoresis of DNA.* **Journal of Chemical Physics**, *1991*. 94: p. 2187-2206.

29. Southern, E.M., *Detection of specific sequences among DNA fragments separated by gel-electrophoresis.* **Journal of Molecular Biology**, *1975*. 98: p. 503-517.

30. Panyim, S. and R. Chalkley, *High resolution acrylamide gel electrophoresis of histones.* **Archives of Biochemistry and Biophysics**, *1969*. 130: p. 337-346.

31. Loening, U.E., *Fractionation of high-molecular-weight ribonucleic acid by polyacrylamide-gel electrophoresis.* **Biochemical Journal**, *1967*. 102: p. 251-257.

32. Laurell, C.B., *Quantitative estimation of proteins by electrophoresis in agarose gel containing antibodies.* **Analytical Biochemistry**, *1966*. 15: p. 45-52.

33. Peacock, A.C. and C.W. Dingman, *Resolution of multiple ribonucleic acid species by polyacrylamide gel electrophoresis.* **Biochemistry**, *1967*. 6: p. 1818-1827.

34. Schwartz, D.C. and C.R. Cantor, *Separation of yeast chromosome-sized dnas by pulsed field gradient gel-electrophoresis.* **Cell**, *1984*. 37: p. 67-75.

35. Bustamante, C., S. Gurrieri, and S.B. Smith, *Towards a molecular description of pulsed-field gel-electrophoresis.* **Trends in Biotechnology**, *1993*. 11: p. 23-30.

36. Burns, M.A., B.N. Johnson, S.N. Brahmasandra, K. Handique, J.R. Webster, M. Krishnan, T.S. Sammarco, P.M. Man, D. Jones, D. Heldsinger, et al., *An integrated nanoliter DNA analysis device.* **Science**, *1998*. 282: p. 484-487.

37. Verpoorte, E., *Microfluidic chips for clinical and forensic analysis.* **Electrophoresis**, *2002*. 23: p. 677-712.

38. Dolnik, V., S.R. Liu, and S. Jovanovich, *Capillary electrophoresis on microchip.* **Electrophoresis**, *2000*. 21: p. 41-54.

39. Woolley, A.T., D. Hadley, P. Landre, A.J. deMello, R.A. Mathies, and M.A. Northrup, *Functional integration of pcr amplification and capillary electrophoresis in a microfabricated DNA analysis device.* **Analytical Chemistry**, *1996*. 68: p. 4081-4086.

40. Sanders, G.H.W. and A. Manz, *Chip-based microsystems for genomic and proteomic analysis.* **Trac-Trends in Analytical Chemistry**, *2000*. 19: p. 364-378.

41. Albargheuthi, M.N. and A.E. Barron, *Polymeric matrices for DNA sequencing by capillary electrophoresis.* **Electrophoresis**, *2000*. 21: p. 4096-4111.

42. Arora, A., G. Simone, G.B. Salieb-Beugelaar, J.T. Kim, and A. Manz, *Latest developments in micro total analysis systems.* **Analytical Chemistry**, *2010*. 82: p. 4830-4847.

43. Blazej, R.G., P. Kumaresan, and R.A. Mathies, *Microfabricated bioprocessor for integrated nanoliter-scale sanger DNA sequencing.* **Proceedings of the National Academy of Sciences of the United States of America**, *2006*. 103: p. 7240-7245.

44. Braiman, A., F. Rudakov, and T. Thundat, *Highly selective separation of DNA fragments using optically directed transport.* **Applied Physics Letters**, *2010*. p.96-99.

45. Chin, C.D., V. Linder, and S.K. Sia, *Lab-on-a-chip devices for global health: Past studies and future opportunities.* **Lab on a Chip**, *2007*. 7: p. 41-57.

46. Harrison, D.J., K. Fluri, K. Seiler, Z.H. Fan, C.S. Effenhauser, and A. Manz, *Micromachining a miniaturized capillary electrophoresis-based chemical-analysis system on a chip.* **Science**, *1993*. 261: p. 895-897.

47. Harrison, D.J., A. Manz, Z.H. Fan, H. Ludi, and H.M. Widmer, *Capillary electrophoresis and sample injection systems integrated on a planar glass chip.* **Analytical Chemistry**, *1992*. 64: p. 1926-1932.

48. Kulrattanarak, T., R.G.M. van der Sman, C. Schroen, and R.M. Boom, *Classification and evaluation of microfluidic devices for continuous suspension fractionation.* **Advances in Colloid and Interface Science**, *2008*. 142: p. 53-66.

49. Zeng, Y., M. He, and D.J. Harrison, *Microfluidic self-patterning of large-scale crystalline nanoarrays for high-throughput continuous DNA fractionation.* **Angewandte Chemie-International Edition**, *2008*. 47: p. 6388-6391.

50. Zeng, Y. and D.J. Harrison, *Self-assembled colloidal arrays as three-dimensional nanofluidic sieves for separation of biomolecules on microchips.* **Analytical Chemistry**, *2007*. 79: p. 2289-2295.

51. Chou, H.P., C. Spence, A. Scherer, and S. Quake, *A microfabricated device for sizing and sorting DNA molecules.* **Proceedings of the National Academy of Sciences of the United States of America**, *1999*. 96: p. 11-13.

52. Duke, T.A.J., R.H. Austin, E.C. Cox, and S.S. Chan, *Pulsed-field electrophoresis in microlithographic arrays.* **Electrophoresis**, *1996*. 17: p. 1075-1079.

53. Doyle, P.S., J. Bibette, A. Bancaud, and J.L. Viovy, *Self-assembled magnetic matrices for DNA separation chips.* **Science**, *2002*. 295: p. 2237-2237.

54. Margulies, M., M. Egholm, W.E. Altman, S. Attiya, J.S. Bader, L.A. Bemben, J. Berka, M.S. Braverman, Y.J. Chen, Z.T. Chen, et al., *Genome sequencing in microfabricated high-density picolitre reactors.* **Nature**, *2005*. 437: p. 376-380.

55. Waggoner, P.S. and H.G. Craighead, *Micro- and nanomechanical sensors for environmental, chemical, and biological detection.* **Lab on a Chip**, *2007*. 7: p. 1238-1255.

56. Zeng, Y., R. Novak, J. Shuga, M.T. Smith, and R.A. Mathies, *High-performance single cell genetic analysis using microfluidic emulsion generator arrays.* **Analytical Chemistry**, *2010*. 82: p. 3183-3190.

57. Persson, F. and J.O. Tegenfeldt, *DNA in nanochannels-directly visualizing genomic information.* **Chemical Society Reviews**, *2010*. 39: p. 985-999.

58. Levy, S.L. and H.G. Craighead, *DNA manipulation, sorting, and mapping in nanofluidic systems.* **Chemical Society Reviews**, *2010*. 39: p. 1133-1152.

59. Le Gac, S. and A. van den Berg, *Single cells as experimentation units in lab-on-a-chip devices.* **Trends in Biotechnology**, *2010*. 28: p. 55-62.

60. Gupta, K., D.H. Kim, D. Ellison, C. Smith, A. Kundu, J. Tuan, K.Y. Suh, and A. Levchenko, *Lab-on-a-chip devices as an emerging platform for stem cell biology.* **Lab on a Chip**, *2010*. 10: p. 2019-2031.

61. Hopwood, A.J., C. Hurth, J.N. Yang, Z. Cai, N. Moran, J.G. Lee-Edghill, A. Nordquist, R. Lenigk, M.D. Estes, J.P. Haley, et al., *Integrated microfluidic system for rapid forensic DNA analysis: Sample collection to DNA profile.* **Analytical Chemistry**, *2010*. 82: p. 6991-6999.

62. Liu, P. and R.A. Mathies, *Integrated microfluidic systems for high-performance genetic analysis.* **Trends in Biotechnology**, *2009*. 27: p. 572-581.

63. Pushkarev, D., N.F. Neff, and S.R. Quake, *Single-molecule sequencing of an individual human genome.* **Nature Biotechnology**, *2009*. 27: p. 847-U101.

64. Huang, L.R., J.O. Tegenfeldt, J.J. Kraeft, J.C. Sturm, R.H. Austin, and E.C. Cox, *A DNA prism for high-speed continuous fractionation of large DNA molecules.* **Nature Biotechnology**, *2002*. 20: p. 1048-1051.

65. Levy, S.L., J.T. Mannion, J. Cheng, C.H. Reccius, and H.G. Craighead, *Entropic unfolding of DNA molecules in nanofluidic channels.* **Nano Letters**, *2008*. 8: p. 3839-3844.

66. Han, J.Y. and H.G. Craighead, *Characterization and optimization of an entropic trap for DNA separation.* **Analytical Chemistry**, *2002*. 74: p. 394-401.

67. Han, J. and H.G. Craighead, *Separation of long DNA molecules in a microfabricated entropic trap array.* **Science**, *2000*. 288: p. 1026-1029.

68. Minc, N., C. Futterer, K. Dorfman, A. Bancaud, C. Gosse, C. Goubault, and J.L. Viovy, *Quantitative microfluidic separation of DNA in self-assembled magnetic matrixes.* **Analytical Chemistry**, *2004*. 76: p. 3770-3776.

69. Tabuchi, M., M. Ueda, N. Kaji, Y. Yamasaki, Y. Nagasaki, K. Yoshikawa, K. Kataoka, and Y. Baba, *Nanospheres for DNA separation chips.* **Nature Biotechnology**, *2004*. 22: p. 337-340.

70. Kaji, N., Y. Tezuka, Y. Takamura, M. Ueda, T. Nishimoto, H. Nakanishi, Y. Horiike, and Y. Baba, *Separation of long DNA molecules by quartz nanopillar chips under a direct current electric field.* **Analytical Chemistry**, *2004*. 76: p. 15-22.

71. Zhang, H. and M.J. Wirth, *Electromigration of single molecules of DNA in a crystalline array of 300-nm silica colloids.* **Analytical Chemistry**, *2005*. 77: p. 1237-1242.

72. Meagher, R.J., J.I. Won, L.C. McCormick, S. Nedelcu, M.M. Bertrand, J.L. Bertram, G. Drouin, A.E. Barron, and G.W. Slater, *End-labeled free-solution electrophoresis of DNA.* **Electrophoresis**, *2005*. 26: p. 331-350.

73. Fung, E.N. and E.S. Yeung, *High-speed DNA-sequencing by using mixed poly(ethylene oxide) solutions in uncoated capillary columns.* **Analytical Chemistry**, *1995*. 67: p. 1913-1919.

74. Wang, X.Y., V. Veerappan, C. Cheng, X. Jiang, R.D. Allen, P.K. Dasgupta, and S.R. Liu, *Free solution hydrodynamic separation of DNA fragments from 75 to 106 000 base pairs in a single run.* **Journal of the American Chemical Society**, *2010*. 132: p. 40-45.

75. Pel, J., D. Broemeling, L. Mai, H.L. Poon, G. Tropini, R.L. Warren, R.A. Holt, and A. Marziali, *Nonlinear electrophoretic response yields a unique parameter for separation of biomolecules.* **Proceedings of the National Academy of Sciences of the United States of America**, *2009*. 106: p. 14796-14801.

76. Salieb-Beugelaar, G.B., K.D. Dorfman, A. van den Berg, and J.C.T. Eijkel, *Electrophoretic separation of DNA in gels and nanostructures.* **Lab on a Chip**, *2009*. 9: p. 2508-2523.

77. Salieb-Beugelaar, G.B., J. Teapal, J. van Nieuwkasteele, D. Wijnperle, J.O. Tegenfeldt, F. Lisdat, A. van den Berg, and J.C.T. Eijkel, *Field-dependent DNA mobility in 20 nm high nanoslits.* **Nano Letters**, *2008*. 8: p. 1785-1790.

78. Liang, X.G., K.J. Morton, R.H. Austin, and S.Y. Chou, *Single sub-20 nm wide, centimeter-long nanofluidic channel fabricated by novel nanoimprint mold fabrication and direct imprinting.* **Nano Letters**, *2007*. 7: p. 3774-3780.

79. Reisner, W., K.J. Morton, R. Riehn, Y.M. Wang, Z.N. Yu, M. Rosen, J.C. Sturm, S.Y. Chou, E. Frey, and R.H. Austin, *Statics and dynamics of*

single DNA molecules confined in nanochannels. **Physical Review Letters**, *2005*. 94.

80. Tegenfeldt, J.O., C. Prinz, H. Cao, R.L. Huang, R.H. Austin, S.Y. Chou, E.C. Cox, and J.C. Sturm, *Micro- and nanofluidics for DNA analysis.* **Analytical and Bioanalytical Chemistry**, *2004*. 378: p. 1678-1692.

81. Tegenfeldt, J.O., C. Prinz, H. Cao, S. Chou, W.W. Reisner, R. Riehn, Y.M. Wang, E.C. Cox, J.C. Sturm, P. Silberzan, et al., *The dynamics of genomic-length DNA molecules in 100-nm channels.* **Proceedings of the National Academy of Sciences of the United States of America**, *2004*. 101: p. 10979-10983.

82. Tegenfeldt, J.O., H. Cao, W.W. Reisner, C. Prinz, R.H. Austin, S.Y. Chou, E.C. Cox, and J.C. Sturm, *Stretching DNA in nanochannels.* **Biophysical Journal**, *2004*. 86: p. 596A-596A.

83. Tang, J., D.W. Trahan, and P.S. Doyle, *Coil-stretch transition of DNA molecules in slitlike confinement.* **Macromolecules**, *2010*. 43: p. 3081-3089.

84. Balducci, A.G., J. Tang, and P.S. Doyle, *Electrophoretic stretching of DNA molecules in cross-slot nanoslit channels.* **Macromolecules**, *2008*. 41: p. 9914-9918.

85. Balducci, A., C.C. Hsieh, and P.S. Doyle, *Relaxation of stretched DNA in slitlike confinement.* **Physical Review Letters**, *2007*. 99.

86. Cheng, C.M., Y. Kim, J.M. Yang, S.H. Leuba, and P.R. LeDuc, *Dynamics of individual polymers using microfluidic based microcurvilinear flow.* **Lab on a Chip**, *2009*. 9: p. 2339-2347.

87. Ohno, K., K. Tachikawa, and A. Manz, *Microfluidics: Applications for analytical purposes in chemistry and biochemistry.* **Electrophoresis**, *2008*. 29: p. 4443-4453.

CHAPTER 2
BACKGROUND

2.1 Introduction

In this chapter the background knowledge of several fields relevant to this thesis are presented. Polymer physics, in particular polymer relaxation and stretching in confinements are highly relevant to the work presented in Chapters 3 and 4, and are reviewed here. The basic elements of DNA electrophoresis along with the separation mechanism in pulsed field electrophoresis are also presented here in order to facilitate understanding of our discussions in the following chapters.

2.2 Polymer Physics

2.2.1 DNA Conformation in Free Solutions

Deoxyribonucleic acid, DNA is a flexible, linear polymer, which can exist as a single or double stranded molecule. Throughout this thesis, the term DNA corresponds to a double stranded DNA. DNA consists of building units called base pairs (bp), where each base pair is around 0.34 nm long.[1, 2] DNA molecule has a width of around 2 nm. In free solution, sufficiently long DNA assumes a coiled conformation (Figure 2.1a).[3] The simplest model to describe the conformation of DNA in free solution is the random walk or freely-jointed-chain

(FJC), which is a static model.[4] In this model, the DNA is pictured as a chain of N rigid cylinders with a constant length b, also known as the Kuhn length, linked together with freely rotating hinges (Figure 2.1b). Kuhn length is twice the persistence length ($p \sim 50$ nm)[1, 5] of DNA, $b = 2p$. In this model, the chain end-to-end distance R_N, and gyration radius, R_g of DNA chain are given by: [5-9]

$$\left\langle R_N^2 \right\rangle = 6\left\langle R_g^2 \right\rangle = Nb^2 \tag{2.1}$$

According to this relation, the gyration radius of the molecule, R_g scales with the number of segments, N, as:

$$R_g \propto N^{1/2} \tag{2.2}$$

The maximum stretched length of a polymer is known as the contour length, and is represented as $L_{contour} = Nb$.

A dynamic model was introduced by Rouse[10] which is called the Rouse bead-spring model. In this model the DNA chain is pictured as a chain of spheres connected together by springs with root-mean-square length of b as shown in Figure 2.1c.[11, 12]

In both of these models, the self-exclusion interaction between the Kuhn segments (the fact that a position in space cannot be occupied by two segments simultaneously) is ignored. Flory argued that the size of a flexible self-avoiding polymer coil in solution can be obtained by balancing the effect of excluded-volume interactions, which tend to swell the chain, with entropy, which decreases if the coil size is increased and consequently favours smaller coils.[13-15] Taking into account the self-exclusion interactions, Eq. 2.2 is corrected by Flory as:

$$R_g \propto N^{3/5} \tag{2.3}$$

Comparing Eq. 2.2 with Eq. 2.3, one can see that the size of a self-avoiding flexible polymer in a solvent is larger than an ideal chain with no interaction between the monomers.

Using the Rouse model, one can calculate the total friction coefficient of the Rouse chain. Since in the Rouse model, the beads interact with each other through the connecting springs, the total friction coefficient of the Rouse chain, ξ_{total} is the summation of the contribution from each bead; $\xi_{total} = N\xi$, where ξ is the friction coefficient of a bead. Using the Stokes-Einstein relation, one can calculate the diffusion coefficient of the Rouse chain as; $D_{dif} = \frac{k_b T}{\xi_{total}} = \frac{k_b T}{N\xi}$, where k_b is the Boltzmann constant and T is the absolute temperature.[3, 10, 16] Using this equation, the relaxation time of DNA, τ_R can be calculated as:

$$\tau_R \approx \frac{R_N^2}{D_{dif}} \approx \frac{\xi}{k_b T} N R_N^2 \tag{2.4}$$

τ_R has some interesting significance; on time scales shorter than τ_R, the chain shows viscoelastic behaviour, whereas on time scales longer than τ_R, the chain is simply diffusive.[16] Using Eq. 2.1, Eq.2.4 can be modified as:

$$\tau_R \approx \frac{\xi}{k_b T} N R_N^2 \approx \frac{\xi b^2}{k_b T} N^2 \approx \tau_0 N^2 \tag{2.5}$$

where τ_0 is the Kuhn segment relaxation time and is defined as; $\tau_0 \approx \frac{\xi b}{k_b T}$. It is stated in the literature that if DNA is probed on time scales shorter than τ_0, it does

not move but exhibits elastic responses.[3, 16] As described earlier, in calculating the total chain friction coefficient, the Rouse model ignores the hydrodynamic interactions between the beads and assumes they are interacting through connecting springs. Zimm modified this model by adding hydrodynamic interactions between the beads.[17, 18] In the Zimm model, the relaxation time of the chain is defined as:

$$\tau_R \approx \tau_0 N^{3/2} \tag{2.6}$$

Comparing Eq. 2.5 with Eq. 2.6 shows that hydrodynamic interactions between monomers in a polymer chain decreases the relaxation time of the molecule.

2.2.2 DNA Conformation in Confinements

Polymer physics changes dramatically when moving from the case of a polymer in free solutions to the case of a polymer confined in channels.[19] In channels which are smaller than the gyration radius, R_g, but still larger than the persistence length, p, of the polymer, de Gennes[20, 21] demonstrated that self-exclusion divides the polymer into blobs, distributing the length of the molecule along the channel as shown in Figure 2.2a. Using the Flory scaling constant, de Gennes showed:

$$R_N \approx L_{contour} \frac{(pw)^{1/3}}{d_{ch}^{2/3}} \tag{2.7}$$

where w is the DNA width and d_{ch} is the channel diameter. This equation provides an estimate of how much a DNA molecule will stretch in a channel purely due to the self-exclusion effect. The de Gennes theory has been successfully used in the literature to calculate the relaxation time of the polymer in confinement:[21]

$$\tau_R \approx \frac{(pw)^{2/3}}{d_{ch}^{1/3}} \frac{\eta b^2}{k_b T} N^2 \tag{2.8}$$

When the channel size is smaller than the persistence length, $d_{ch} < p$, the DNA conformation is not governed by self-exclusion effects, but by both intrinsic DNA elasticity as well as interactions of DNA with the channel walls. The DNA conformation in the case of polymer in tight confinements ($d_{ch} < p$) was investigated by Odijk and has become known as the Odijk regime.[22, 23] In the Odijk regime, DNA length is stored in the nanochannel in deflections caused by polymer encounters with the channel walls, as shown in Figure 2.2b. These deflections are on the scale of the Odijk segment, $\lambda \approx \left(d_{ch}^2 p\right)^{1/3}$. Using Odijk theory, DNA end-to-end distance in a nanochannel of $d_{ch} < p$ is given by: [21, 24-27]

$$R_N \approx L_{contour}\left[1 - 0.361\left(\frac{d_{ch}}{p}\right)^{2/3}\right] \tag{2.9}$$

In the Odijk regime, DNA friction is caused from the hydrodynamic interaction of the Odijk segments with the channel wall.[21] The relaxation time of the molecule in this regime is calculated as:

$$\tau_R \approx \frac{d_{ch}^a}{p\left(\log\frac{d_{ch}}{w}\right)} \frac{\eta b^2}{k_b T} N^2 \tag{2.10}$$

It should be noted here that there is a controversy over the exponent of the channel size and how the relaxation time scales with the channel size, different values ranging from 1.6 to 2 are suggested for a.[24, 28, 29]

2.3 Electrophoretic Separation of DNA

2.3.1 Electrophoresis

Electrophoresis is the motion of an entity bearing a surface charge in an electrolyte solution under an externally applied electric field.[30] The presence of a charged particle in an electrolyte solution containing free ions polarizes the electrolyte solution surrounding the particle, resulting in formation of an electric double layer (Figure 2.3), where the thickness of the double layer is characterized by the Debye length, κ^{-1}, given by:

$$\kappa^{-1} = \left(\frac{\varepsilon k_b T}{2e^2 z^2 n_\infty} \right)^{1/2} \tag{2.11}$$

for a symmetric electrolyte. Here, e is the charge of an electron, z is the valence of the ions, and n_∞ is the bulk number concentration of ions in the solution. The double layer itself is divided into two layers, as shown in Figure 2.3: i) the immobile Stern layer and ii) the mobile shear layer where the no-slip fluid boundary condition can be applied. The electric potential at this layer is called the zeta potential, ζ, which is different from the surface potential. It is this potential that can be measured by electrophoretic potential measurements techniques.[30, 31]

Once the external electric field is applied, the particle starts to migrate along the applied electric field due to its surface charge. But in addition to this motion, the liquid around the particle that has developed a charge density starts to move in the opposite direction of the particle motion and exerts a drag force on the particle (Figure 2.4). The net velocity of the particle is called the

electrophoretic velocity, U. Electrophoretic mobility, μ is the ratio of velocity of a charged entity, U, with respect to an applied electric field E, $\mu = \frac{U}{E}$. The exact calculation of electrophoretic mobility is complicated, but for a spherical particle, analytical solutions can be found for two limiting cases:

i. $\kappa^{-1} >> a_p$ (Hückle solution)

$$\mu = \frac{Q}{6\pi\eta a_p} \tag{2.12}$$

where Q is the total particle charge, η is the electrolyte viscosity, and a_p is the particle radius.

ii. $\kappa^{-1} << a_p$ (Helmholtz-Smoluchowski solution)

$$\mu = \frac{\varepsilon_0 \varepsilon_r \zeta}{\eta} \tag{2.13}$$

here, ε_0 and ε_r are the vacuum permittivity and relative permittivity of the electrolyte, respectively and ζ is the particle zeta potential, so the mobility is independent of particle size and shape.[30, 31]

2.3.2 Fundamentals of DNA Electrophoresis

In DNA electrophoresis buffers, κ^{-1} is usually of order 1-5 nm and smaller than the intrinsic persistence length of DNA. This means that DNA electrophoresis is performed in the Smoluchowski regime, so DNA electrophoresis mobility in free solution, μ_0, follows an equation similar to Eq. 2.3 and will be independent of DNA size.[32, 33] The thin double layer (small κ^{-1}) means that the hydrodynamic interaction between different segments of DNA is screened

in a very thin cylinder around the molecule, so the free solution mobility of DNA can be written as:

$$\mu_0 = \frac{F_{total}}{\xi_{total} E} = \frac{N(q_k E)}{N \xi_k E} = \frac{q_k}{\xi_k} \tag{2.14}$$

here E is the applied electric field. F_{total} and ξ_{total} are the total force and total friction for the whole molecule, whereas q_k and ξ_k are the effective charge and the friction for the Kuhn length of the molecule, which is independent of size above the Kuhn length.[34, 35]

Equation 2.4 shows the well-known fact that the electrophoretic mobility of DNA in free solutions does not depend on the molecular size. Therefore, size separation in DNA electrophoresis is induced through different mechanisms by adding a porous structure.[36-39] Since DNA is a deformable molecule, the migration mechanism and electrophoretic mobility of DNA in porous structures is strongly affected by the ratio of DNA size relative to pore size of the separation matrix. In DNA electrophoresis literature,[11, 39-41] three different regimes have been proposed for DNA electrophoresis, as shown in Figure 2.5: i) the Ogston regime, where the size of the DNA coil, $2R_g$, is smaller than the pore size of the separation matrix and the DNA molecules remain compact, migrating through the pores as in an electric field driven filtration process, in this regime, DNA mobility, μ, decreases exponentially by increasing DNA size and separation is achieved using electrophoresis methods.[41] ii) Entropic trapping, where the pore size is more or less the same size of the DNA coil. In this regime, there is a competition between the chain staying coiled in larger pores versus deforming and migrating through the smaller pores. In this regime, DNA mobility changes by DNA size as

$\mu \sim 1/M^{1+\gamma}$ (where M is DNA molecular weight and $\gamma > 0$ is the strength of the entropic effect).[42] iii) the Reptation regime, where the pore size is smaller than the size of the DNA coil. At low electric fields or shorter DNA molecules, DNA mobility is a strong function of DNA size and separation can be achieved using DC electrophoresis. For very long DNA molecules or high electric fields, DNA molecule stretches and reptates through the pores in the opposite direction of the electric field, this is called reptation with orientation. In this regime DNA mobility becomes independent of DNA size and different sizes of DNA molecule move with a same velocity under DC electrophoresis so no separation can be achieved.[39, 41] Since in this thesis, all the DNA separation experiments have been conducted in confinements much smaller than the DNA coil size, a more comprehensive description of the DNA migration mechanism in the reptation regime is presented here.

When a long flexible chain such as DNA is placed in a porous structure such as a gel with pore sizes smaller than its gyration radius, DNA threads its way in the gel like a snake by a process called “reptation”. This motion is similar to what was proposed by de Gennes to describe diffusion of a polymer chain in tight confinement.[43-45] Reptation can be described as a curvilinear one-dimensional motion along the chain axis (Figure 2.6a). An alternative to reptation is the formation of loops or hernias when a pore is crossed by the chain twice instead of once, as shown in Figure 2.6b.[20, 45] Upon application of an external electric field, the reptation motion becomes biased in the direction of the electric field, with one head usually leading the chain to thread its way through the porous structure. The

phenomena is called the biased reptation model (BRM) by Slater and Noolandi.[46-48] BRM was later amended to biased reptation with fluctuation (BRF) by Viovy et al.[49] to take into account DNA length fluctuations during migration. BRF successfully predicted the correct field dependence mobility of large DNA molecules. Experimental observations and real-time videomicroscopy of long DNA molecules migrating in gel under DC electric fields also validated BRF. [39, 41] In the next chapter, we explain how a simple theoretical model can be developed to explain the frequency dependent separation of DNA molecules based on biased reptation model.

2.3.3 Separation Mechanism in Pulsed Field Electrophoresis

The pulsed field gel electrophoresis (PFGE) technique was developed to overcome the limitations of constant field, DNA gel electrophoresis (GE) and to increase the size of DNA molecules resolvable by electrophoresis methods.[50] In this method instead of a constant electric field direction, two electric fields of typically the same magnitudes are applied alternately in two directions. Experimental observations suggested that the highest separation resolution can be achieved with an obtuse angle between the directions of the applied fields.[51] Although in this study, angular separation of DNA was achieved using the asymmetric pulsed field electrophoresis (APFE) technique, where the applied electric fields have different magnitudes, the overall separation mechanism is the same for APFE and PFGE. A brief review of the separation mechanism during pulsed field electrophoresis is presented here to help understanding our discussions in the following chapters.

The fundamentals of pulsed field electrophoresis are very similar to those of constant field electrophoresis, with the exception of an added reorientation mechanism for the migration of DNA. Inside the porous structure, DNA molecules travel through the pores in the direction of the electric field, once this direction changes, the molecules reorient themselves to the new direction and continue moving in the new direction. Recent advances in experimental methods for tracking single DNA molecules facilitate the understanding of the reorientation mechanism of the DNA molecules under pulsed electric field.[52] It was observed that the reorientation mechanism is based on head and tail switching of the stretched molecule chain. This means that when the electric field switches its direction, the end of the molecule that was leading the chain along the previous direction is now the tail, so the DNA molecule engages in a chevron type motion, as shown in Figure 2.7.[53, 54] The backtracking motion is caused due to the obtuse angle between the applied electric fields, $\alpha > 90°$. It was observed experimentally that when $\alpha \leq 90°$ the molecule engages in a zigzag type motion (Figure 2.7) which results in poor or no separations.

Pulsed field electrophoresis is usually classified in two categories; i) Crossed field electrophoresis, where the angle between the applied electric fields is $90° < \alpha < 180°$ having a value of 120° or 135° in most of experimental applications. ii) Field inversion electrophoresis, where $\alpha = 180°$. The separation mechanism for both of these categories is based on size-dependent reorientation time of DNA molecules. Short molecules will reorient very rapidly in the direction of the new field and will spend a good fraction of the pulse time

migrating through the pores before the electric field is switched again. On the contrary, long DNA molecules spend most of the pulse time for the reorientation process, thus having only a short time for actual migration as shown in Figure 2.8.[53] This induces a net migration rate in the direction of the average field that is size-dependent. On most circumstances, shorter molecules migrate faster compared to longer molecules.

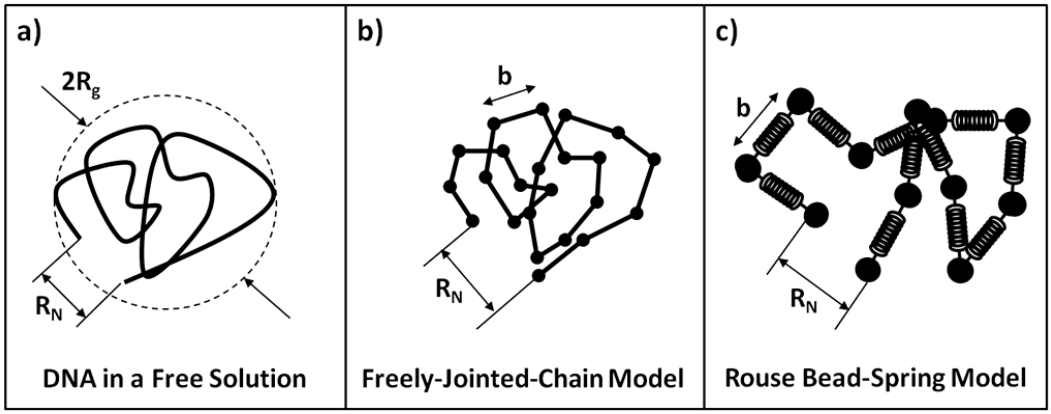

Figure 2.1. Schematic of a) DNA in a free solution as a coiled molecule. b) A freely-jointed-chain model of DNA. Segments have constant length known as the Kuhn length b (~ 100 nm) and are connected by freely rotating hinges. c) The Rouse bead-spring model of DNA. Beads are connected with springs of root-mean-square length of b. R_N is the end-to-end distance of the chain. In all of these cases, the contour length of the DNA molecule is longer than the Kuhn length.

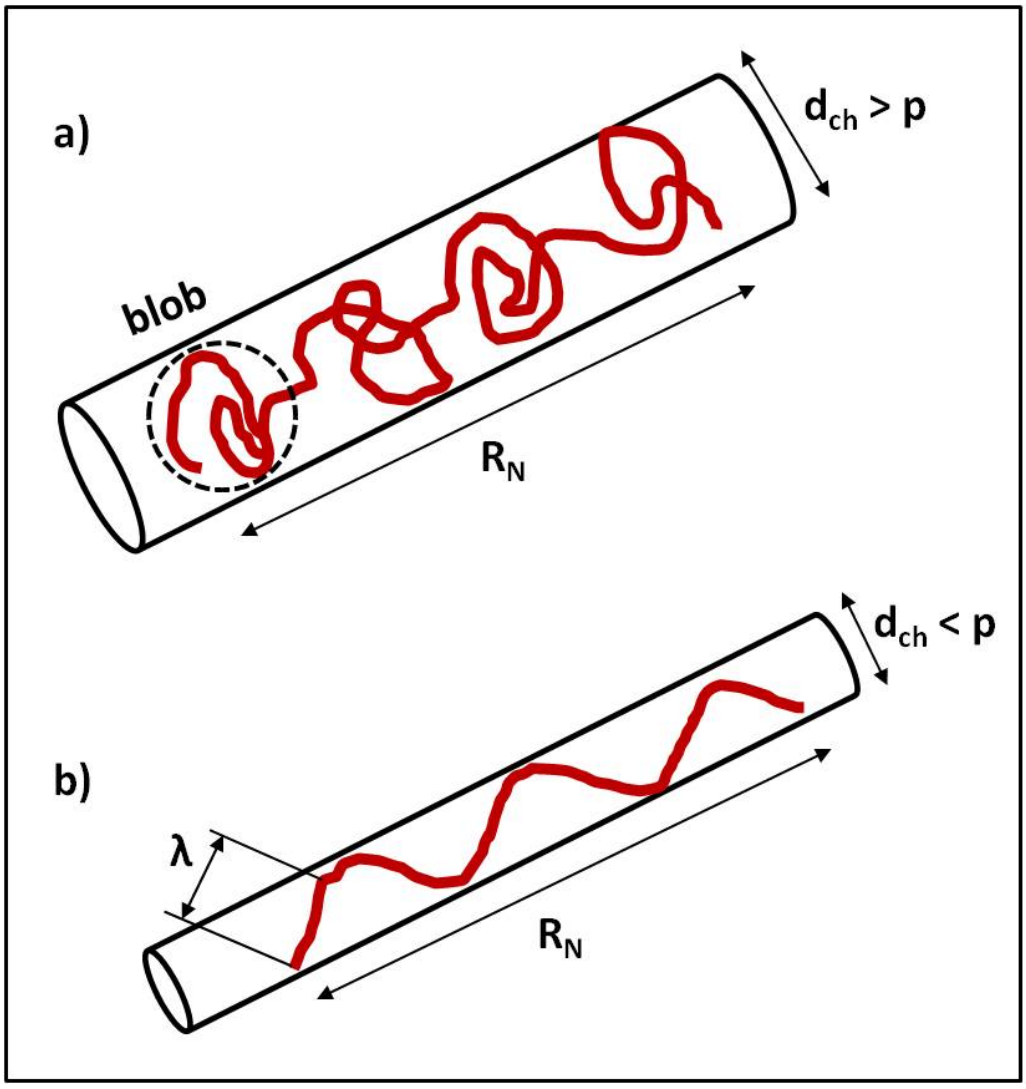

Figure 2.2. a) Conformation of a DNA molecule confined in a channel with a diameter $p < d_{ch} < R_g$ (de Gennes regime). DNA length is distributed along the channel as independent blobs due to self-exclusion interactions between different segments. b) Conformation of a DNA molecule confined in a channel with a diameter $d_{ch} < p$ (Odijk regime). DNA length is distributed along the channel by deflections on the channel wall, due to the interplay between DNA intrinsic elasticity and hydrodynamic interactions with the channel wall.

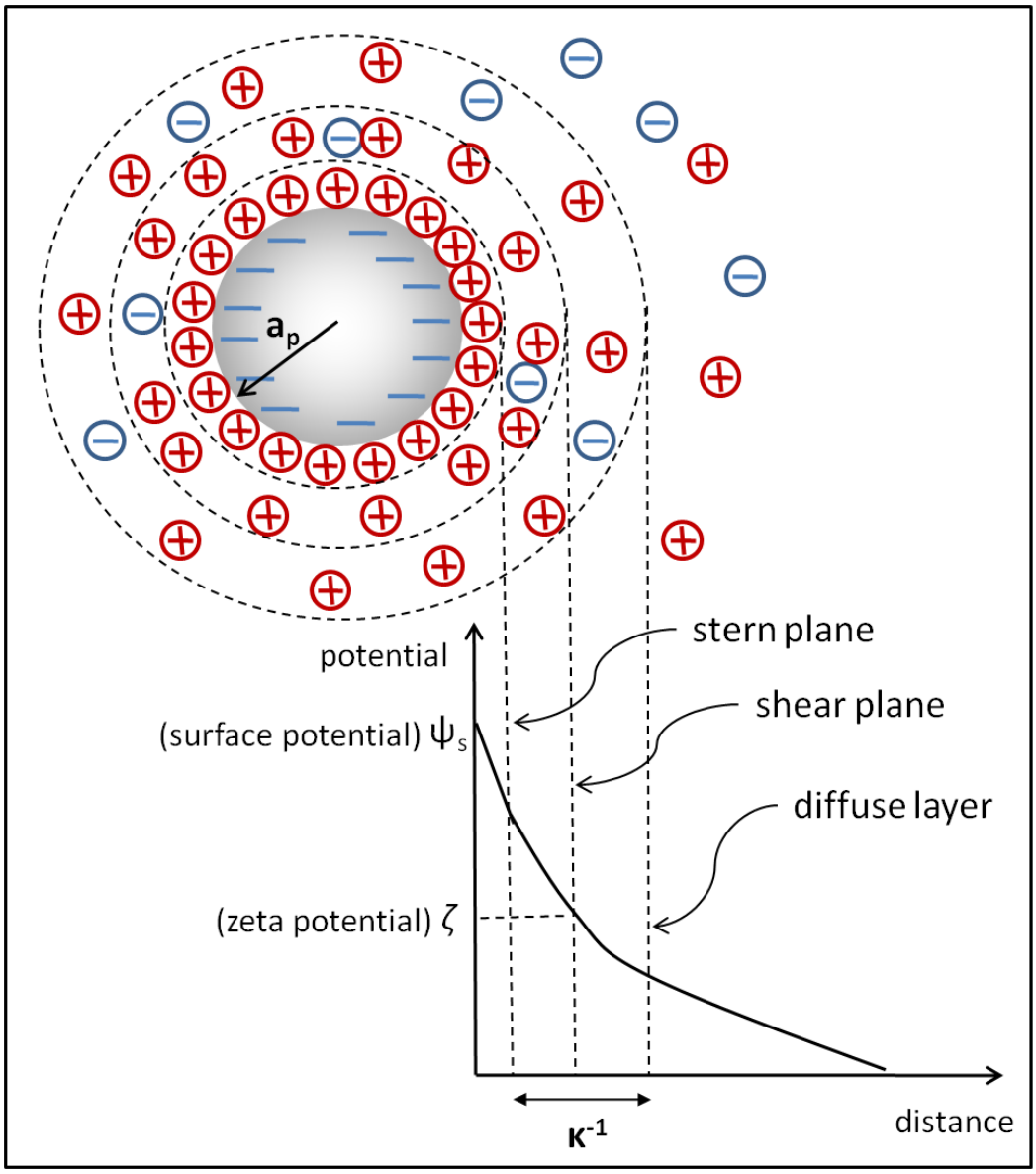

Figure 2.3. Schematic of an electric double layer around a negatively charged particle in an electrolyte solution. κ^{-1} is the Debye length and represents the thickness of the ion cloud surrounding a charged particle in an electrolyte solution.

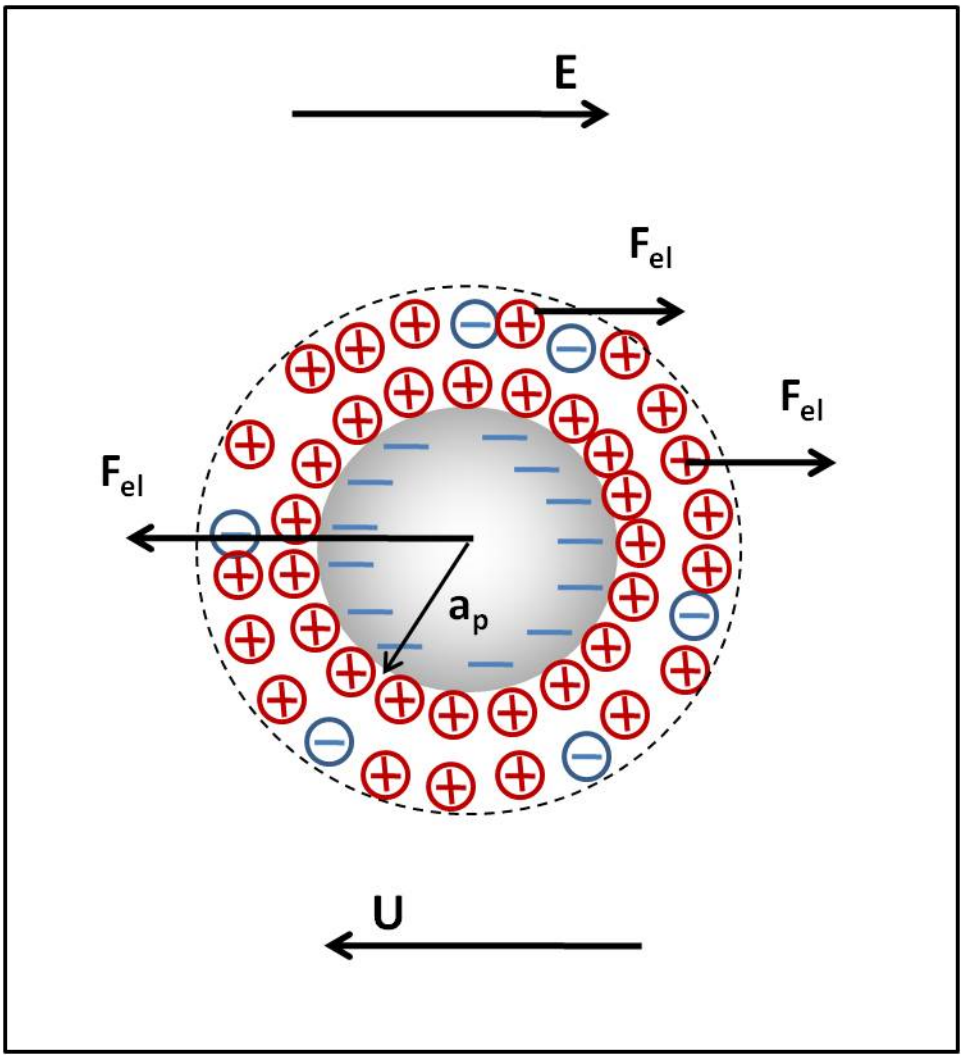

Figure 2.4. Electrophoresis of a negatively charged particle in an electrolyte solution. Both particle and free ions in the electrolyte are subjected to an electric field E. Since the particle is negatively charged, the electric force F_{el} is applied in the opposite direction of the applied electric field, but for the counter ions surrounding the particle, F_{el} is in the direction of the applied field. The net velocity of the particle relative to the media is called the electrophoretic velocity, U, and is the result of electric force and hydrodynamic drag. The viscous shearing is limited in the double layer for the special case defined in Eq. 2.3.

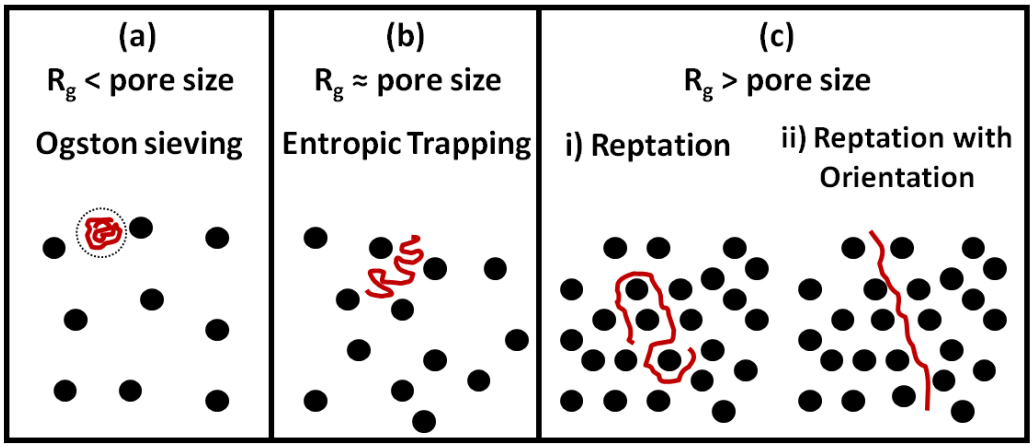

Figure 2.5. Three regimes of DNA electrophoresis; a) Ogston sieving, where the pore size in the separation media is larger than the DNA coil size, R_g. b) Entropic trapping, where the size of pores in the separation media is around the DNA coil size. c) Reptation regime, where the pore size is much smaller than the DNA coil size. Reptation regime can be divided into two categories; i) small DNA molecules or low electric fields, DNA keeps a random coil conformation. ii) longer DNA molecules or higher electric fields, DNA stretches.

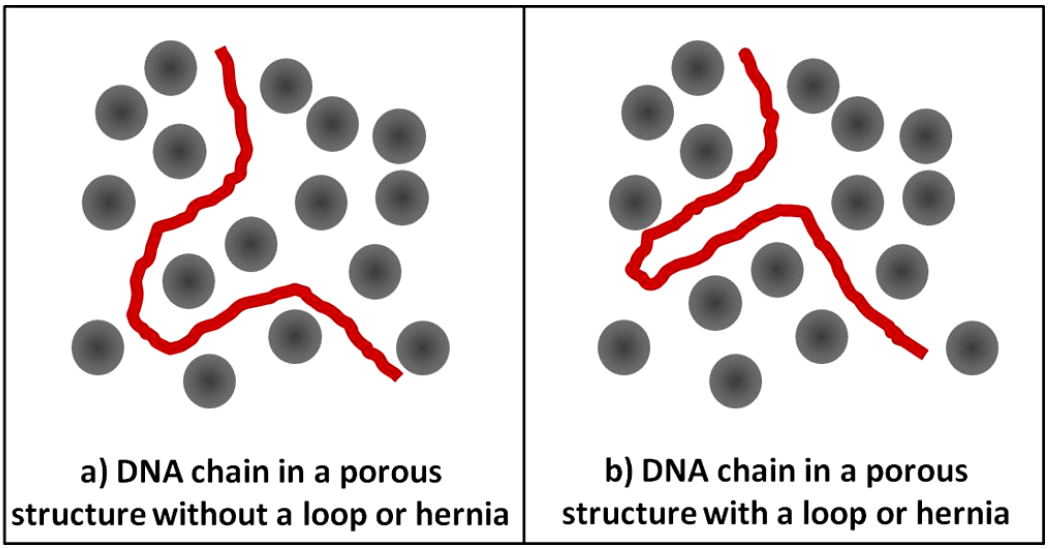

Figure 2.6. Schematic of an unbiased motion of DNA in a separation matrix. a) DNA moves through the pores in a curvilinear one-dimensional motion along the chain axis. Each pore is crossed by the molecule once. b) DNA folds at a point along its length and moves by developing a hernia or loop. Pores are being crossed by the molecule twice.

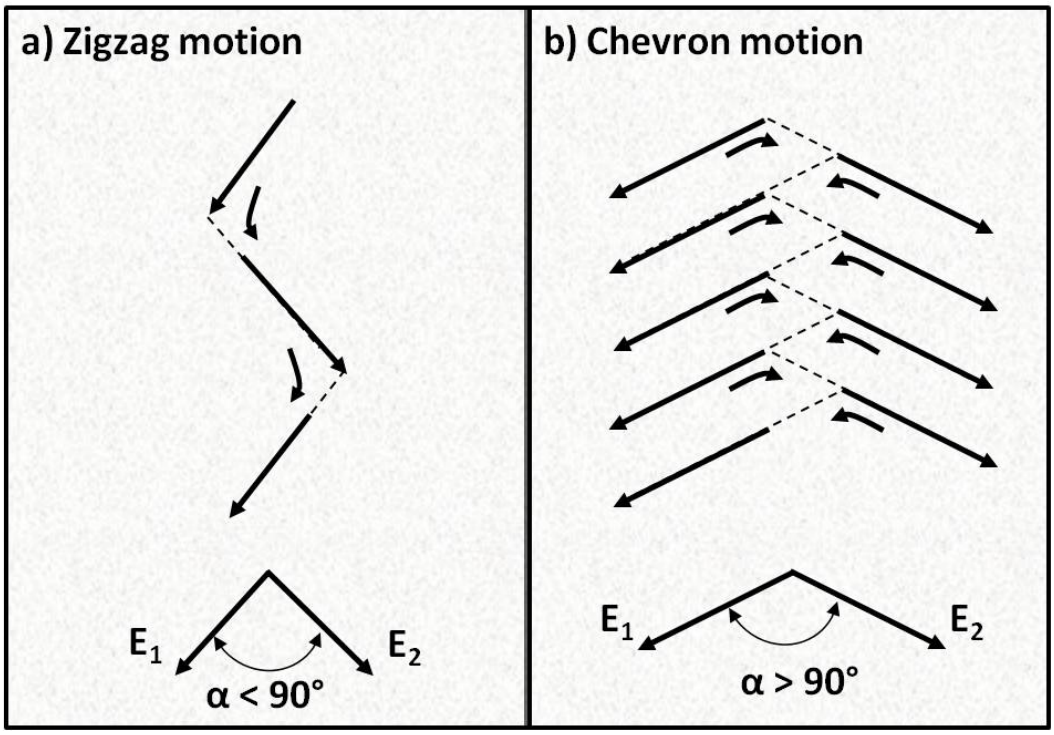

Figure 2.7. Schematic of migration mechanism of DNA in a porous media under a) Pulsed electric fields with an acute angle between the electric fields. DNA moves in a zigzag type motion with one head leading the motion. b) Pulsed electric fields with an obtuse angle between the electric fields. DNA moves in a chevron type motion with head and tail periodically changing (reprinted from Gurrieri S. et al.[54] with permission from Oxford University Press).

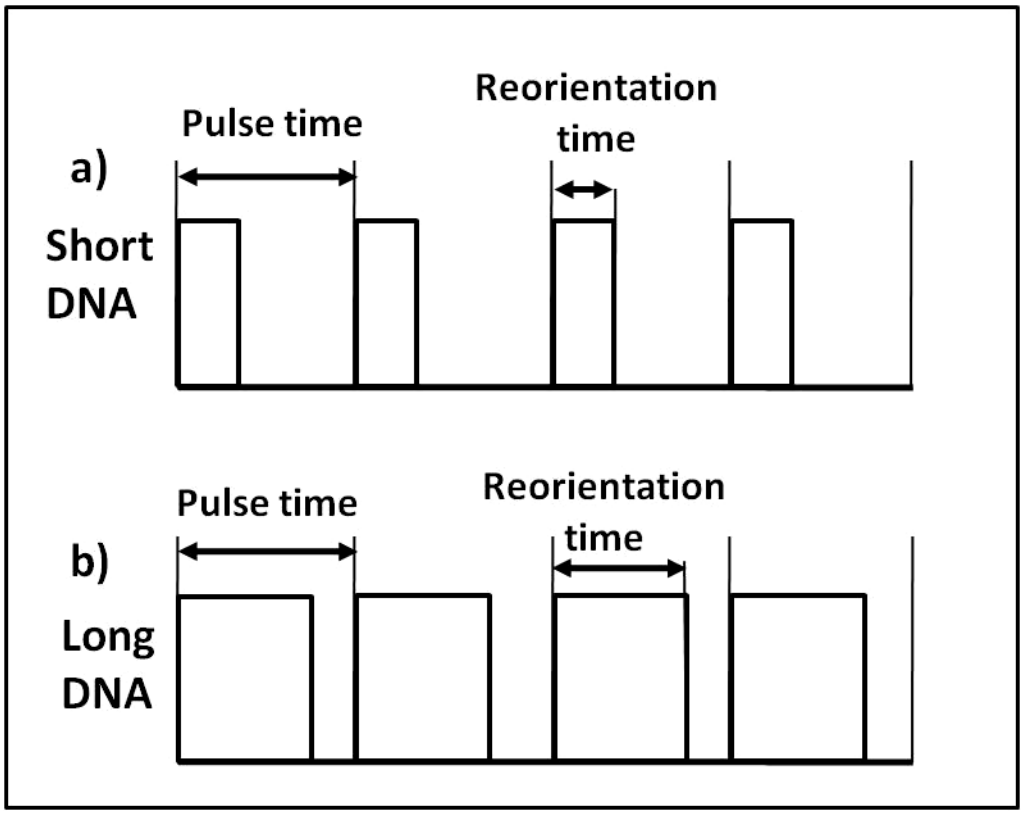

Figure 2.8. Separation mechanism of DNA molecules in obtuse-angle pulsed field electrophoresis. Due to the reorientation mechanism described in Figure 2.7, reorientation time is highly size dependant. Shorter DNA molecules reorient themselves faster, so they spend the majority of the pulse time migrating along the field. Larger DNA molecules have longer reorientation times, so they spend the majority of the pulse time reorienting instead of migrating. This difference induces a migration rate that is size-dependent. Shorter molecules move faster compared to the longer molecules along the direction of the average field in the pulsed field electrophoresis technique (reprinted from Gurrieri S. et al.[54] with permission from Oxford University Press).

2.4 References

1. Hays, J.B., M.E. Magar, and B.H. Zimm, *Persistence length of DNA.* **Biopolymers**, *1969*. 8: p. 531-536.
2. Viovy, J.L., *Electrophoresis of DNA and other polyelectrolytes: Physical mechanisms.* **Reviews of Modern Physics**, *2000*. 72: p. 813-872.
3. Doi, M. and S.F. Edwards, *The theory of polymer dynamics 1986*, New York: Oxford University Press.
4. Fixman, M. and J. Kovac, *Dynamics of stiff chains .2. Freely jointed chain.* **Journal of Chemical Physics**, *1974*. 61: p. 4950-4954.
5. Smith, S.B., L. Finzi, and C. Bustamante, *Direct mechanical measurements of the elasticity of single DNA-molecules by using magnetic beads.* **Science**, *1992*. 258: p. 1122-1126.
6. Baumgartner, A. and K. Binder, *Monte-carlo studies on the freely jointed polymer-chain with excluded volume interaction.* **Journal of Chemical Physics**, *1979*. 71: p. 2541-2545.
7. Baumgartner, A., *Statics and dynamics of the freely jointed polymer-chain with lennard-jones interaction.* **Journal of Chemical Physics**, *1980*. 72: p. 871-879.
8. Livadaru, L., R.R. Netz, and H.J. Kreuzer, *Stretching response of discrete semiflexible polymers.* **Macromolecules**, *2003*. 36: p. 3732-3744.
9. Gratton, Y. and G.W. Slater, *Molecular dynamics study of tethered polymers in shear flow.* **European Physical Journal E**, *2005*. 17: p. 455-465.

10. Rouse, P.E., *A theory of the linear viscoelastic properties of dilute solutions of coiling polymers.* **Journal of Chemical Physics**, *1953*. 21: p. 1272-1280.

11. Slater, G.W. and S.Y. Wu, *Reptation, entropic trapping, percolation, and rouse dynamics of polymers in random-environments.* **Physical Review Letters**, *1995*. 75: p. 164-167.

12. Ferree, S. and H.W. Blanch, *The hydrodynamics of DNA electrophoretic stretch and relaxation in a polymer solution.* **Biophysical Journal**, *2004*. 87: p. 468-475.

13. Huggins, M.L., *Solutions of long chain compounds.* **Journal of Chemical Physics**, *1941*. 9: p. 440-440.

14. Flory, P.I., *Thermodynamics of high polymer solutions.* **Journal of Chemical Physics**, *1942*. 10: p. 51-61.

15. Flory, P.J. and S. Fisk, *Effect of volume exclusion on dimensions of polymer chains.* **Journal of Chemical Physics**, *1966*. 44: p. 2243-2248.

16. Rubinstein, M. and R.H. Colby, *Polymer physics*. *2003*, New York: Oxford University Press.

17. Zimm, B.H., W.H. Stockmayer, and M. Fixman, *Excluded volume in polymer chains.* **Journal of Chemical Physics**, *1953*. 21: p. 1716-1723.

18. Zimm, B.H., *Dynamics of polymer molecules in dilute solution - viscoelasticity, flow birefringence and dielectric loss.* **Journal of Chemical Physics**, *1956*. 24: p. 269-278.

19. Reisner, W., K.J. Morton, R. Riehn, Y.M. Wang, Z.N. Yu, M. Rosen, J.C. Sturm, S.Y. Chou, E. Frey, and R.H. Austin, *Statics and dynamics of single DNA molecules confined in nanochannels.* **Physical Review Letters**, *2005*. 94.

20. Gennes, P.-g.D., *Scaling concepts in polymer physics 1979*, Ithaca, New York: Cornell University Press.

21. Tegenfeldt, J.O., C. Prinz, H. Cao, S. Chou, W.W. Reisner, R. Riehn, Y.M. Wang, E.C. Cox, J.C. Sturm, P. Silberzan, et al., *The dynamics of genomic-length DNA molecules in 100-nm channels.* **Proceedings of the National Academy of Sciences of the United States of America**, *2004*. 101: p. 10979-10983.

22. Odijk, T., *On the statistics and dynamics of confined or entangled stiff polymers.* **Macromolecules**, *1983*. 16: p. 1340-1344.

23. Odijk, T., *Scaling theory of DNA confined in nanochannels and nanoslits.* **Physical Review E**, *2008*. 77.

24. Tegenfeldt, J.O., H. Cao, W.W. Reisner, C. Prinz, R.H. Austin, S.Y. Chou, E.C. Cox, and J.C. Sturm, *Stretching DNA in nanochannels.* **Biophysical Journal**, *2004*. 86: 596A.

25. Tegenfeldt, J.O., C. Prinz, H. Cao, R.L. Huang, R.H. Austin, S.Y. Chou, E.C. Cox, and J.C. Sturm, *Micro- and nanofluidics for DNA analysis.* **Analytical and Bioanalytical Chemistry**, *2004*. 378: p. 1678-1692.

26. Balducci, A., C.C. Hsieh, and P.S. Doyle, *Relaxation of stretched DNA in slitlike confinement.* **Physical Review Letters**, *2007*. 99.

27. Tang, J., D.W. Trahan, and P.S. Doyle, *Coil-stretch transition of DNA molecules in slitlike confinement.* **Macromolecules**, *2010*. 43: p. 3081-3089.

28. Morse, D.C., *Viscoelasticity of concentrated isotropic solutions of semiflexible polymers. 2. Linear response.* **Macromolecules**, *1998*. 31: p. 7044-7067.

29. Maggs, A.C., *Two plateau moduli for actin gels.* **Physical Review E**, *1997*. 55: p. 7396-7400.

30. Russel, W.B., D.A. Saville, and W.K. Schowalter, *Colloidal dispersions*. *1989*, Cambridge, UK: Cambridge University Press.

31. Masliyah, J.H. and S. Bhattacharjee, *Electrokinetic and colloid transport phenomena 2005*, Hobokey, New Jersey: Wiley Interscience.

32. Shafer, R.H., N. Laiken, and B.H. Zimm, *Radial migration of DNA-molecules in cylindrical flow .1. Theory of free-draining model.* **Biophysical Chemistry**, *1974*. 2: p. 180-184.

33. Meagher, R.J., J.I. Won, L.C. McCormick, S. Nedelcu, M.M. Bertrand, J.L. Bertram, G. Drouin, A.E. Barron, and G.W. Slater, *End-labeled free-solution electrophoresis of DNA.* **Electrophoresis**, *2005*. 26: p. 331-350.

34. Stellwagen, N.C., C. Gelfi, and P.G. Righetti, *The free solution mobility of DNA.* **Biopolymers**, *1997*. 42: p. 687-703.

35. Lumpkin, O.J., P. Dejardin, and B.H. Zimm, *Theory of gel-electrophoresis of DNA.* **Biopolymers**, *1985*. 24: p. 1573-1593.

36. Loening, U.E., *Fractionation of high-molecular-weight ribonucleic acid by polyacrylamide-gel electrophoresis.* **Biochemical Journal**, *1967*. 102: p. 251-257.

37. Peacock, A.C. and C.W. Dingman, *Resolution of multiple ribonucleic acid species by polyacrylamide gel electrophoresis.* **Biochemistry**, *1967*. 6: p. 1818-1827.

38. Panyim, S. and R. Chalkley, *High resolution acrylamide gel electrophoresis of histones.* **Archives of Biochemistry and Biophysics**, *1969*. 130: p. 337-346.

39. Slater, G.W., S. Guillouzic, M.G. Gauthier, J.F. Mercier, M. Kenward, L.C. McCormick, and F. Tessier, *Theory of DNA electrophoresis (similar to 1999-2002(1)/(2))*. **Electrophoresis**, *2002*. 23: p. 3791-3816.

40. Slater, G.W., J. Rousseau, J. Noolandi, C. Turmel, and M. Lalande, *Quantitative-analysis of the 3 regimes of DNA electrophoresis in agarose gels.* **Biopolymers**, *1988*. 27: p. 509-524.

41. Slater, G.W., M. Kenward, L.C. McCormick, and M.G. Gauthier, *The theory of DNA separation by capillary electrophoresis.* **Current Opinion in Biotechnology**, *2003*. 14: p. 58-64.

42. Rousseau, J., G. Drouin, and G.W. Slater, *Entropic trapping of DNA during gel electrophoresis: Effect of field intensity and gel concentration.* **Physical Review Letters**, *1997*. 79: p. 1945-1948.

43. Lerman, L.S. and H.L. Frisch, *Why does the electrophoretic mobility of DNA in gels vary with the length of the molecule.* **Biopolymers**, *1982*. 21: p. 995-997.

44. Lumpkin, O.J. and B.H. Zimm, *Mobility of DNA in gel-electrophoresis.* **Biopolymers**, *1982*. 21: p. 2315-2316.

45. de Gennes, P.G., *Reptation of a polymer chain in presence of fixed obstacles.* **Journal of Chemical Physics**, *1971*. 55: p. 572-579.

46. Slater, G.W. and J. Noolandi, *The biased reptation model of DNA gel-electrophoresis - mobility vs molecular-size and gel concentration.* **Biopolymers**, *1989*. 28: p. 1781-1791.

47. Slater, G.W. and J. Noolandi, *On the reptation theory of gel-electrophoresis.* **Biopolymers**, *1986*. 25: p. 431-454.

48. Slater, G.W. and J. Noolandi, *New biased-reptation model for charged polymers.* **Physical Review Letters**, *1985*. 55: p. 1579-1582.

49. Semenov, A.N., T.A.J. Duke, and J.L. Viovy, *Gel-electrophoresis of DNA in moderate fields - the effect of fluctuations.* **Physical Review E**, *1995*. 51: p. 1520-1537.

50. Schwartz, D.C. and C.R. Cantor, *Separation of yeast chromosome-sized dnas by pulsed field gradient gel-electrophoresis.* **Cell**, *1984*. 37: p. 67-75.

51. Bustamante, C., S. Gurrieri, and S.B. Smith, *Towards a molecular description of pulsed-field gel-electrophoresis.* **Trends in Biotechnology**, *1993*. 11: p. 23-30.

52. Duke, T.A.J., R.H. Austin, E.C. Cox, and S.S. Chan, *Pulsed-field electrophoresis in microlithographic arrays.* **Electrophoresis**, *1996*. 17: p. 1075-1079.

53. Akerman, B. and M. Jonsson, *Reorientational dynamics and mobility of DNA during pulsed-field agarose-gel electrophoresis.* **Journal of Physical Chemistry**, *1990*. 94: p. 3828-3838.

54. Gurrieri, S., S.B. Smith, K.S. Wells, I.D. Johnson, and C. Bustamante, *Real-time imaging of the reorientation mechanisms of yoyo-labelled DNA molecules during 90 degrees and 120 degrees pulsed field gel electrophoresis.* **Nucleic Acids Research**, *1996*. 24: p. 4759-4767.

CHAPTER 3

DNA DYNAMICS IN NANOSCALE CONFINEMENT

3.1 Introduction

The difficulty of fabricating ordered nanoscale confinements has limited the understanding of DNA dynamics inside structures with pore sizes smaller than the persistence length (~ 50 nm) of DNA molecules.[1-3] Our group has developed colloidal self assembly (CSA) of crystalline arrays of nanoparticles within microfluidic channels as a powerful tool for the easy fabrication of ordered nanoporous media.[4] Angular separation of DNA has been achieved using asymmetric pulsed field electrophoresis within such crystalline arrays.[5] Here, nanoparticle arrays with particles as small as 100 nm (corresponding to ca. 15 nm pore sizes) were successfully fabricated, and the mechanism of DNA transport in highly confined pores was studied.

3.2 Experimental Section

DNA separation was conducted using a microfluidic chip filled with an array of nanoparticles as a sieving matrix. A schematic of the PDMS

A version of this chapter is published in Angewandte Chemie International Edition, 2010, 49, p. 3326-3329.

(Polydimethylsiloxane) microchip is shown in Figure 3.1a. Aqueous suspensions of monodisperse (particle size CV ~ 10 %) silica colloids (Bangs Laboratories, Fishers, IN) of 100, 330, and 700 nm diameter were used to form self assembled nanoparticle arrays inside the microchips.[4, 5] SEM images of the self assembled structure reveal a closely packed hexagonal array of nanoparticles, where the size of pores (the smallest opening between the particles, d_p) were around 15% of the particle size, i.e., d_p = 15, 50, and 105 nm for 100, 330, and 700 nm particles, respectively. A full description of the packing scheme is provided in Appendix A.

DNA samples, NoLimits™ DNA fragments (6, 10, 20 kbp, Fermentas Life Sciences), λ-DNA (48 kbp, New England Biolabs), and T4 DNA (166 kbp, Nippon Gene) were stained by YOYO-1 (Molecular Probes) with dye-to-base ratio of 1:10. Pulsed field electrophoresis was performed in 4× TBE buffer to suppress electroosmotic flow to ten times lower than DNA electrophoretic mobility.[6] 2-mercaptoethanol was also added with 4% v/v to reduce photobleaching. Angular separation of DNA molecules under a pulsed field was achieved by continuously injecting DNA samples into the separation chamber, as illustrated in Figure 3.1b. The applied pulsed potentials generated asymmetric obtuse-angle pulsed fields across the separation chamber, where the angle between the pulsed fields is $\alpha = 135°$ and $E_1 = 1.4E_2$ in all experiments (Appendix A). Within the separation chamber, different sizes of DNA separate from each other and form individual streams, each stream deflecting an angle θ from the injection angle, as shown in Figure 3.1c.

3.3 Theoretical Section

It was observed that θ was highly dependent on the frequency, electric field strength, and DNA size. We have developed a geometric model that links these operating parameters to molecular size and separation angle, θ. A geometric model was first introduced by Austin et al.[7] to quantify one-dimensional zone electrophoretic separation of DNA within a microfabricated array structure under a pulsed field. Their attempt to fit the model to their observations required a coiling factor,[7, 8] accounting for incomplete stretching of DNA. Here, a similar geometric model was developed for continuous two-dimensional angular separation of DNA under a pulsed field. We have assumed fully stretched DNA, so no fitting coefficient is utilized. The model is based on the known separation mechanism of DNA molecules under obtuse-angle pulse fields.[9, 10] According to this model, DNA reptates along the direction of the electric field as a flexible rod with a constant length (L). Once the direction of the electric field is changed, the molecule backtracks to a new direction as shown in Figure 3.2a–c.

For small frequencies, when the molecule has enough time to reorient itself to the new direction and travel distances larger than its own length, a simple geometric equation can be derived (the description of derivation steps are given in Appendix B). The model relates the net angular distance that the molecule travels at the end of one cycle (deflection angle, θ) to the molecular size (L), electric fields (E_1, E_2), and frequency (f):

$$\tan\theta = 1 - \sqrt{2}\,\frac{\frac{\mu_2 E_2}{2f} - L}{\frac{\sqrt{2}\mu_1 E_2}{2f} - L} \tag{3.1}$$

where μ_1 and μ_2 are DNA mobilities along E_1 and E_2, respectively. According to Eq. 3.1, when the frequency is very small, $\tan\theta = 1 - (\mu_2/\mu_1)$, implying that θ is independent of DNA size. On the other hand, when the frequency increases up to a value of $f = (\mu_2 E_2)/(2L)$, tan θ = 1, giving a θ value of 45°. Here, the net DNA displacement only occurs along the stronger field E_1, since DNA cannot reorient completely along E_2 and θ reaches its maximum value of 45° independent of DNA size. According to this simple model, further increase in the frequency will result in trapping of DNA around a hook, since the DNA cannot align itself completely with either field vector. The model does not include a tortuosity factor. However, the use of experimentally determined mobility values (see below) should compensate for this.

3.4 Results and Discussions

The geometric model assumes DNA migrates along the direction of the electric field, leading with a head. In Figure 3.2a and b, n marks the head of the DNA, whilst in Figure 3.2c, m marks the head. This approach follows the biased reptation model developed by Zimm et al.[11] and Slater et al.[12] According to their model, when an electric field is applied to DNA in a confinement smaller than its gyration radius, migration occurs by one of two mechanisms: i) a sliding motion

in the direction of the electric field led by one of the heads, which was termed reptation by de Gennes[13]; or ii) creation of loops or hernias in the middle of the DNA chain. According to the biased reptation model, the formation of hernias would be improbable as long as external forces applied on the DNA chain are smaller than thermal forces.[14, 15] Viovy et al.[1] introduced a scaled electric force parameter ε, which is the ratio of the electrostatic force to the thermal force applied on a DNA chain:

$$\varepsilon = \frac{\eta d_p^2 \mu_0 E}{k_b T} \tag{3.2}$$

where η is the buffer viscosity, μ_0 is DNA mobility in free solution, k_b is the Boltzmann constant, and T is the absolute temperature. According to the biased reptation model, when $\varepsilon << 1$, hernia formation and therefore DNA length fluctuations are at a minimum inside the pores, whereas they become significant for $\varepsilon \sim 1$. The value of ε in our experiments was calculated by substituting the experimental parameters used, with $\eta = 10^{-3}$ m^2s^{-1}, $\mu_0 = 3.5x\ 10^{-8}$ $m^2\ V^{-1}\ s^{-1}$, $E =$ 28000 Vm^{-1}, giving ε = 0.05, 0.60, and 2.61 for d_p=15, 50, and 105 nm, respectively. Thus, the probability of hernia formation in the larger pore sizes is not negligible, while it should be negligible for 15 nm pores. A key assumption in developing the geometric model was that DNA size fluctuation is negligible and the length is the contour length of the molecule. The effect of confinement on DNA stretching or elongation has been studied.[3, 16-20] Tegenfeldt et al.[18] and Reisner et al.[19] provided empirical equations that relate the ratio of $L/L_{contour}$ to the confinement size, stating:

$$\frac{L}{L_{contour}} = \frac{pw}{d_{ch}^2} \qquad d_{ch} \geq p \tag{3.3a}$$

$$\frac{L}{L_{contour}} = 1 - 0.361\left(\frac{p}{d_{ch}}\right)^{2/3} \qquad d_{ch} \ll p \tag{3.3b}$$

where p is the persistence length of DNA (~ 50 nm), w is the molecule width (~ 2 nm for double stranded DNA), and d_{ch} is the confinement size. Stretching of DNA is assumed to be due to self-exclusion and the interplay of confinement and intrinsic elasticity of DNA, when no external electric force is applied. Substituting the pore sizes used in our experiments as d_{ch} in this equation, $L/L_{contour}$ was calculated for each pore size, giving 0.84, 0.34, and 0.21 for $d_p = d_{ch}$ = 15, 50, and 105 nm, respectively. These results cannot be used in our study to estimate the length of DNA inside the nanoparticle array, since our experiments were conducted under strong electric fields which further stretch DNA molecules. However, according to Eq. 3.3b, mere confinement in pore sizes around 15 nm is sufficient to stretch DNA molecules up to 84% of their contour length. If the additional stretching of DNA under high electric field is considered too, it is obvious that the assumption of fully stretched DNA employed in developing the geometric ratchet model is valid for pore sizes of 15 nm or less.

A comparison between the predicted DNA deflection angle, Eq. 3.1, and those obtained experimentally provides insight into the migration mechanism of DNA molecules in pore sizes ranging around the DNA persistence length (~ 50 nm). In order to calculate the DNA deflection angle θ, predicted by Eq. 3.1, the mobility μ of DNA was determined. Movies of single DNA molecules migrating

inside the nanoparticle arrays were acquired under varying electric fields. The DC electrophoretic mobility of DNA was computed by averaging the velocities of many molecules as they traversed through the array. For each field strength, 10 molecules were studied to calculate mobility, providing an average and a standard deviation. For 20 kbp DNA migrating through 15 nm pores under 280 Vcm^{-1}, the mobility was μ = (3.88 ± 0.62) x10^{-5} $cm^2V^{-1}s^{-1}$. In calculating Eq. 3.1, the molecule length L was assumed to be the contour length of the molecule, $L = L_{contour}$. The results are shown in Figure 3.3, which plots the variation of deflection angle θ for 20 kbp DNA molecules with respect to frequency. The solid line represents θ calculated by Eq. 3.1 while experimental results are shown by symbols. The experiment was conducted for three different pore sizes, 15, 50, and 105 nm. Figure 3.3 shows that the geometric model has the best agreement with experimentally obtained values of θ for a 15 nm pore size, while the observed θ for larger pore sizes do not match the predictions. This behaviour was further investigated for other DNA sizes (48 kbp and 166 kbp) and similar behaviour was observed.

As stated earlier, the simple geometric model predicts a rising curve for DNA deflection angle that reaches a maximum of 45° with increasing frequency, independent of DNA size. Figure 3.4 shows the experimentally observed maximum deflection angle, θ_{max}, corresponding to different DNA sizes ranging from 10 to 166 kbp, in pore sizes ranging from 15 to 105 nm, at an electric field of E_1 = 280 Vcm^{-1}. The frequencies were varied in each study, to determine θ_{max}. It can be seen from Figure 3.4 that for pore sizes of 50 nm and 105 nm, the

maximum deflection angle θ_{max} is strongly dependent on DNA size, contrary to the prediction of the geometric model. We conclude that molecular dynamics of DNA electrophoresis such as size fluctuation and hernia formation significantly affect the deflection behaviour in larger pore sizes. However, for a pore size of 15 nm, θ_{max} is around 45° regardless of DNA size, as predicted by the geometric model.

Our results in Figures 3.3 and 3.4 show that a pore size of 15 nm, which is smaller than the persistence length of DNA and gives ε = 0.05 under our conditions, allows a quantitative fit of the geometric model to the experimental observations when full stretching is assumed. The larger pore sizes do not sufficiently confine DNA and do not prevent the formation of hernias, resulting in the deviation of deflection behaviour of a molecule from the geometric models.

One of the advantages of having an analytical expression to predict the deflection behaviour of DNA is that the effect of different experimental parameters on the separation efficiency can be known a priori. It has been shown experimentally that the effects of field and frequency on DNA separation resolution are coupled.[5, 8, 21, 22] Presently, many exploratory experiments are required to determine the best conditions for resolving different DNA sizes. Figure 3.5a shows the variation of θ with respect to f for three different DNA sizes; 20, 48, and 166 kbp in 15 nm pores. The solid lines represent θ predicted by the geometric model, Eq. 3.1, whereas the symbols represent θ obtained experimentally in 15 nm pores with an electric field of E_1 = 280 Vcm^{-1}. We have found that by rearranging Eq. 3.1 and employing the reorientation time of DNA, it

is possible to normalize these results to provide a predictive model to establish optimal separation conditions. Eq. 3.1 can be reaaranged to yield:

$$\tan\theta = 1 - \frac{\mu_2}{\mu_1}\frac{1 - \dfrac{2fL}{\mu_2 E_2}}{1 - \dfrac{\sqrt{2}\mu_2}{\mu_1}\dfrac{2fL}{\mu_2 E_2}} \tag{3.4}$$

where μ_2/μ_1 can be determined from independent mobility measurement (1.32 in our experiment for d_p = 15 nm). The term $L/(\mu_2 E_2)$ is the time for the molecule to travel its own length under the applied electric field (reorientation time of DNA) and $1/(2f)$ is the pulse time. Hence, the ratio of these two parameters is a dimensionless number which can be considered as the scaled frequency, f^*

$$f^* = \frac{f}{\dfrac{\mu_2 E_2}{2L}} \tag{3.5}$$

Making use of Eq. 3.5, Eq. 3.4 becomes:

$$\tan\theta = 1 - \frac{\mu_2}{\mu_1}\frac{1 - f^*}{1 - \dfrac{\sqrt{2}\mu_2}{\mu_1} f^*} \tag{3.6}$$

The variation of θ with respect to f^* predicted by Eq. 3.6 is shown in Figure 3.5b; the three solid lines of Figure 3.5a have merged into one line by non-dimensionalizing Eq. 3.1. Figure 3.5b shows that in pore sizes smaller than the persistence length of DNA, the frequency response for different sizes of DNA can be normalized to one effective response curve, using the reorientation time of the DNA, which is a size dependent parameter. This result shows that the effects of electric field, frequency, and DNA size on the separation efficiency of DNA

molecules can be integrally linked in one defining parameter. For instance, according to the definition of f^*, Eq. 3.5, if the electric field is increased, in order to preserve the same separation efficiency, the pulse frequency should be increased as well.

3.5 Conclusion

Several authors[23-26] predicted that the migration of DNA in the regime where pore sizes are smaller than the persistence length of DNA, follows the biased reptation mechanism. DNA separation experiments in tight gels supported their predictions. Based on their predictions, we developed a simple geometric model which has a quantitative agreement with our experiments in fabricated, ordered, porous media. Our results show that when the confinement scales are smaller than the persistence length of DNA, the bending elasticity of the molecule prevents formation of hernias and the molecule can be treated as a persistent chain. This allows the use of much simpler deterministic models for simulating DNA dynamics in nanoscale confinement. In contrast, DNA migration through larger pores involves complicated conformations of the molecule such as hernia formation and significant size fluctuation, which necessitate a more sophisticated numerical simulation to model the deflection behaviour of DNA molecules. The present study shows that small ordered confinements achieved by the colloidal self assembly (CSA) approach can provide a reliable tool to study the dynamic behaviour of DNA and to validate the existing theoretical models such as the

reptation model or “lakes-straits” model of Zimm.[27] We have shown that greater confinement, allowed by the CSA fabrication method, leads to fully stretched DNA and more efficient separation of DNA.

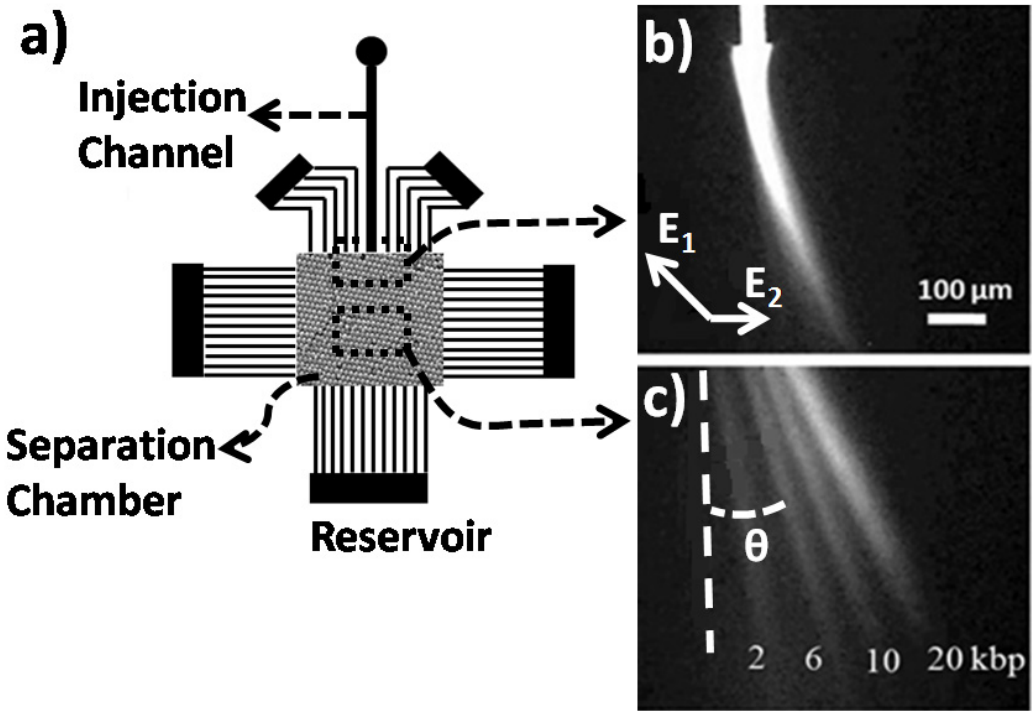

Figure 3.1. a) Schematic of DNA separation microchip. Separation chamber is 4 mm x 4 mm x 0.01 mm. The electric field is applied across the separation chamber by inserting platinum electrodes in buffer reservoirs (Appendix A). b, c) photomicrographs of the DNA separation microchip used in this work. b) DNA solution is injected continuously into the separation chamber. White arrows represent the directions of the applied electric fields. c) The separation chamber is filled with nanoparticle arrays. Different sizes of DNA molecules separate from each other and form individual streams, each deflecting an angle θ from the injection angle.

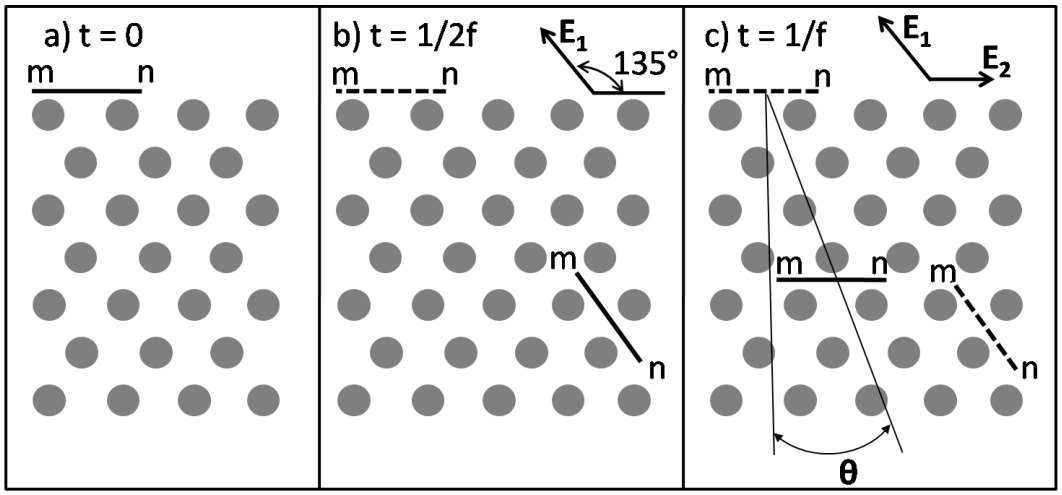

Figure 3.2. Geometric model for angular separation of DNA molecules during one cycle of electric pulses; m and n label the ends of the DNA molecule. a) Initial position of the molecule at the beginning of the cycle. b) Position of the molecule at the end of half cycle. c) Position of the molecule at the end of one cycle.

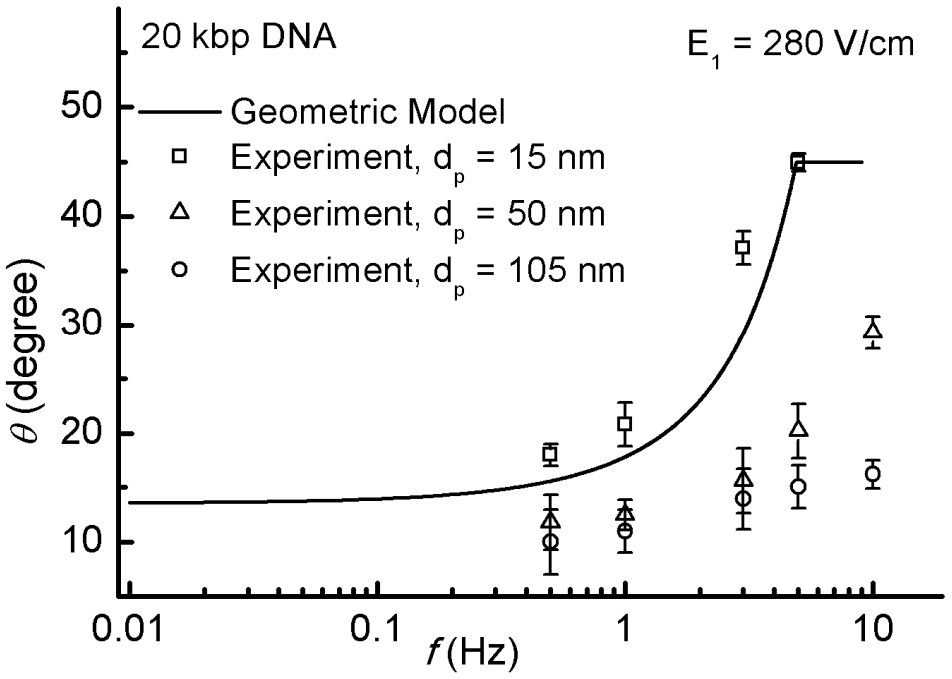

Figure 3.3. Variation of deflection angle θ of 20 kbp DNA with respect to frequency f. Solid line represents the prediction of geometric mode, Eq. 3.1. Symbols represent the experimentally obtained deflection angles of 20 kbp DNA in three different pore sizes (d_p); □: 15 nm, ○: 50 nm, Δ: 105 nm. E_1 = 280 Vcm^{-1} (reproduced from Nazemifard N et al.[28] with permission from Copyright Wiley-VCH Verlag GmbH & Co. KGaA).

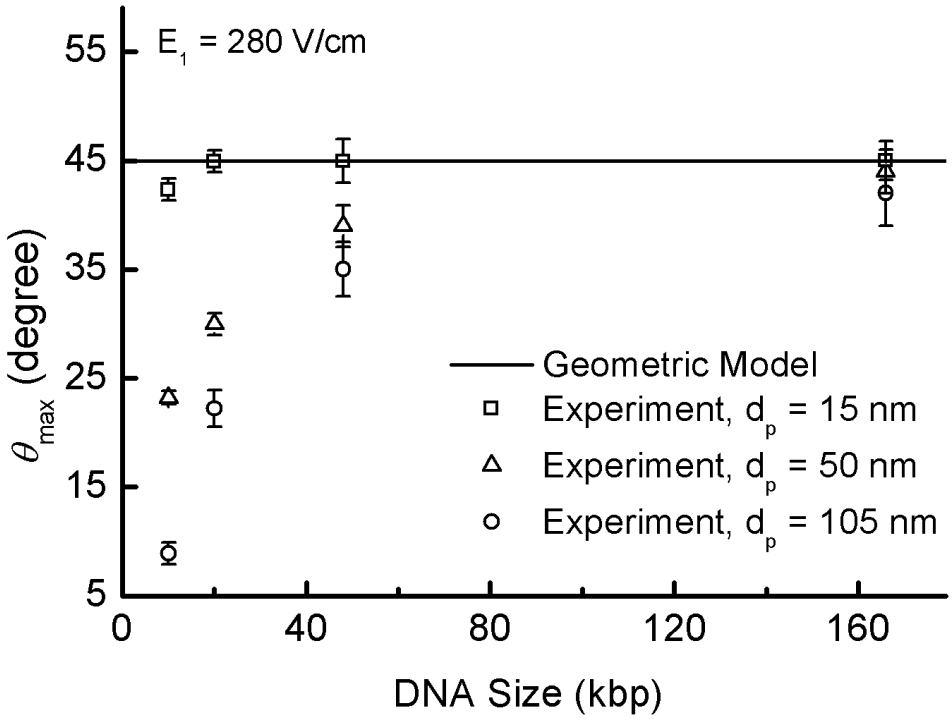

Figure 3.4. Effects of DNA size on maximum deflection angle, θ_{max}. Solid line represents prediction of geometric model as, $\theta_{max} = 45°$, independent of DNA size. Symbols represent experimental values of θ_{max} for three different pore sizes (d_p); □: 15 nm, ○: 50 nm, Δ: 105 nm. $E_1 = 280$ Vcm^{-1} (reproduced from Nazemifard N et al.[28] with permission from Copyright Wiley-VCH Verlag GmbH & Co. KGaA).

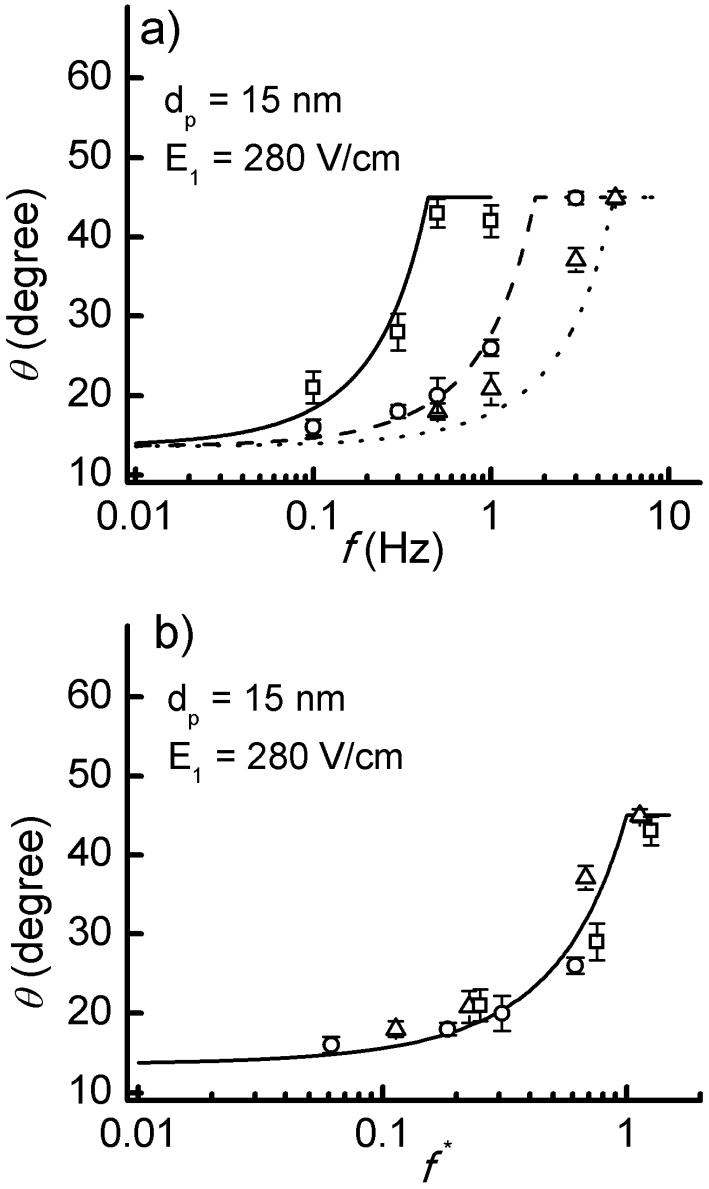

Figure 3.5. a) Frequency dependent behavior of deflection angles of different sizes of DNA molecules (20, 48, 166 kbp) in d_p = 15 nm pores (μ = 3.88, 3.42, and 2.29x10^{-5} cm^{2}V^{-1}s^{-1}, correspondingly). E_1=280 Vcm^{-1}. Lines represent θ predicted by the geometric model, Eq. 3.1, where symbols are the experimental results for θ. Δ and ....: 20 kbp, ○ and ----: 48 kbp, □ and ─: 166 kbp. b) Variation of θ with respect to scaled frequency, f*, for the data set shown in (a). Δ: 20 kbp, ○: 48 kbp, □: 166 kbp, ─: geometric model Eq. 3.6. (reproduced from Nazemifard N et al.[28] with permission from Copyright Wiley-VCH Verlag GmbH & Co. KGaA).

3.6 References

1. Viovy, J.L., *Electrophoresis of DNA and other polyelectrolytes: Physical mechanisms.* **Reviews of Modern Physics**, *2000*. 72: p. 813-872.
2. Austin, R., *Nanopores - the art of sucking spaghetti.* **Nature Materials**, *2003*. 2: p. 567-568.
3. Odijk, T., *DNA confined in nanochannels: Hairpin tightening by entropic depletion.* **Journal of Chemical Physics**, *2006*. 125.
4. Zeng, Y. and D.J. Harrison, *Self-assembled colloidal arrays as three-dimensional nanofluidic sieves for separation of biomolecules on microchips.* **Analytical Chemistry**, *2007*. 79: p. 2289-2295.
5. Zeng, Y., M. He, and D.J. Harrison, *Microfluidic self-patterning of large-scale crystalline nanoarrays for high-throughput continuous DNA fractionation.* **Angewandte Chemie-International Edition**, *2008*. 47: p. 6388-6391.
6. Zeng, Y., *Self assembled nanostructures for biomolecular analysis*. Chemistry. PhD Dissertation. *2007*, Edmonton: Alberta. 158.
7. Duke, T.A.J., R.H. Austin, E.C. Cox, and S.S. Chan, *Pulsed-field electrophoresis in microlithographic arrays.* **Electrophoresis**, *1996*. 17: p. 1075-1079.
8. Huang, L.R., J.O. Tegenfeldt, J.J. Kraeft, J.C. Sturm, R.H. Austin, and E.C. Cox, *A DNA prism for high-speed continuous fractionation of large DNA molecules.* **Nature Biotechnology**, *2002*. 20: p. 1048-1051.

9. Bustamante, C., S. Gurrieri, and S.B. Smith, *Towards a molecular description of pulsed-field gel-electrophoresis.* **Trends in Biotechnology**, *1993*. 11: p. 23-30.

10. Gurrieri, S., S.B. Smith, K.S. Wells, I.D. Johnson, and C. Bustamante, *Real-time imaging of the reorientation mechanisms of yoyo-labelled DNA molecules during 90 degrees and 120 degrees pulsed field gel electrophoresis.* **Nucleic Acids Research**, *1996*. 24: p. 4759-4767.

11. Lumpkin, O.J., P. Dejardin, and B.H. Zimm, *Theory of gel-electrophoresis of DNA*. **Biopolymers**, *1985*. 24: p. 1573-1593.

12. Slater, G.W. and J. Noolandi, *Prediction of chain elongation in the reptation theory of DNA gel-electrophoresis.* **Biopolymers**, *1985*. 24: p. 2181-2184.

13. Degennes, P.G., *Reptation of a polymer chain in presence of fixed obstacles.* **Journal of Chemical Physics**, *1971*. 55: p. 572-&.

14. Akerman, B., *Barriers to DNA loop formation in a porous matrix.* **Progress in Biophysics & Molecular Biology**, *1996*. 65: p. PB144-PB144.

15. Akerman, B., *Tube leakage during electrophoresis retards reptating DNA in unmodified and hydroxyethylated agarose gels.* **Physical Review E**, *1996*. 54: p. 6697-6707.

16. Odijk, T., *Scaling theory of DNA confined in nanochannels and nanoslits.* **Physical Review E**, *2008*. 77.

17. Tegenfeldt, J.O., H. Cao, W.W. Reisner, C. Prinz, R.H. Austin, S.Y. Chou, E.C. Cox, and J.C. Sturm, *Stretching DNA in nanochannels.* **Biophysical Journal**, *2004*. 86: p. 596A-596A.

18. Tegenfeldt, J.O., C. Prinz, H. Cao, S. Chou, W.W. Reisner, R. Riehn, Y.M. Wang, E.C. Cox, J.C. Sturm, P. Silberzan, et al., *The dynamics of genomic-length DNA molecules in 100-nm channels.* **Proceedings of the National Academy of Sciences of the United States of America**, *2004*. 101: p. 10979-10983.

19. Reisner, W., K.J. Morton, R. Riehn, Y.M. Wang, Z.N. Yu, M. Rosen, J.C. Sturm, S.Y. Chou, E. Frey, and R.H. Austin, *Statics and dynamics of single DNA molecules confined in nanochannels.* **Physical Review Letters**, *2005*. 94.

20. Jendrejack, R.M., D.C. Schwartz, M.D. Graham, and J.J. de Pablo, *Effect of confinement on DNA dynamics in microfluidic devices.* **Journal of Chemical Physics**, *2003*. 119: p. 1165-1173.

21. Huang, L.R., P. Silberzan, J.O. Tegenfeldt, E.C. Cox, J.C. Sturm, R.H. Austin, and H. Craighead, *Role of molecular size in ratchet fractionation.* **Physical Review Letters**, *2002*. 89.

22. Chu, G., D. Vollrath, and R.W. Davis, *Separation of large DNA-molecules by contour-clamped homogeneous electric-fields.* **Science**, *1986*. 234: p. 1582-1585.

23. Duke, T.A.J. and J.L. Viovy, *Simulation of megabase DNA undergoing gel-electrophoresis.* **Physical Review Letters**, *1992*. 68: p. 542-545.

24. Heller, C., C. Pakleza, and J.L. Viovy, *DNA separation with field-inversion capillary electrophoresis.* **Electrophoresis**, *1995*. 16: p. 1423-1428.

25. Semenov, A.N., T.A.J. Duke, and J.L. Viovy, *Gel-electrophoresis of DNA in moderate fields - the effect of fluctuations.* **Physical Review E**, *1995*. 51: p. 1520-1537.

26. Slater, G.W. and J. Noolandi, *Effect of nonparallel alternating-fields on the mobility of DNA in the biased reptation model of gel-electrophoresis.* **Electrophoresis**, *1989*. 10: p. 413-428.

27. Zimm, B.H., *Lakes-straits model of field-inversion gel-electrophoresis of DNA.* **Journal of Chemical Physics**, *1991*. 94: p. 2187-2206.

28. Nazemifard, N., S. Bhattacharjee, J.H. Masliyah, and D.J. Harrison, *DNA dynamics in nanoscale confinement under asymmetric pulsed field electrophoresis.* **Angewandte Chemie-International Edition**, *2010*. 49: p. 3326-3329.

CHAPTER 4

FREQUENCY BEHAVIOUR OF DNA ANGULAR SEPARATION

4.1 Introduction

Pulsed field gel electrophoresis or PFGE has been established as the standard method to separate large DNA molecules.[1-3] In this method, electric field is applied periodically in two directions with an obtuse angle ($\alpha > 90°$) [4-6] as shown in Figure 4.1a. A complete description of separation mechanisms in pulsed field electrophoresis has been provided in Section 2.3.3. The major shortcoming of PFGE is its long running times of about 10-200 h.[7-10] In order to overcome this problem, microfluidic devices were developed, where due to the scale of these devices, the separation of DNA molecules was achieved with reported running times of a few seconds.[11-16] However, due to the batch-mode nature of the transverse pulsed field electrophoresis and the small scale of the device, these devices are limited in the amount of material they can analyze.[17] Recently, a microfluidic device was developed by Austin and coworkers[17] which fractionates DNA molecules in different directions based on their molecular sizes, similar to the deflection of different wavelengths of light to different angles in a prism. In their design, asymmetric pulsed field electrophoresis (APFE) was applied to fractionate large DNA molecules inside a microfabricated array as a sieving matrix. Since different sizes of DNA can be directed to different channels (Figure

4.1b), the separation can be operated as a continuous mode, hence, removing the limitation of the amount of sample the device can analyze.[17]

Using a similar asymmetric pulsed field electrophoresis approach, we have developed a microfluidic device for continuous angular separation of DNA molecules.[18, 19] In our device, the microfabricated array of the DNA prism[17] is replaced by self assembled nanoparticle arrays. From the early stages of our experiments, it became clear that the angular separation was highly dependent on the applied frequency,[19] as was observed and reported in the first DNA prism developed by Austin's group. In both of the devices, although the variation of the angular separation with frequency was reproducible, it was complicated and not fully understood. Due to the inherent simplicity of the self assembly approach, our device is significantly easier and faster to fabricate. This provided a unique opportunity to perform a large number of experiments to understand the separation mechanism under asymmetric pulsed field electrophoresis, and the effects of different experimental parameters such as pore size, electric field, and frequency on the separation efficiency of APFE method.

The goal of this chapter is to explain the behavior of angular separation of DNA molecules with respect to frequency under asymmetric pulsed field electrophoresis. High quality real-time movies of DNA migration under different frequencies were used to understand the effect of pulse time on DNA migration mechanism. A simple numerical scheme of DNA migration in a microfabricated array was also developed to further facilitate the understanding of DNA migration. In the analysis presented in this chapter, the goal was to explain the dominant mechanisms dictating the dynamic of DNA molecules under

asymmetric pulsed electric fields, so the effects of Brownian diffusion and DNA size fluctuations, which are responsible for deviations from the averaged results is not considered.

4.2 Experimental Section

4.2.1. DNA Separation Microchip

DNA separation was conducted using a microfluidic chip filled with an array of nanoparticles as a sieving matrix. A schematic of the PDMS microchip is shown in Figure 4.2. PDMS microchips were fabricated using a standard soft lithography technique, then sealed to clean glass slides prior to packing, as described in detail elsewhere.[18] Aqueous suspensions of monodisperse silica colloids (Bangs Laboratories, Fishers, IN) of 100 nm, 330 nm, and 700 nm diameter were used to form the self assembled nanoparticle array inside the microchips. Particle suspension concentrations were optimized for each particle size to achieve crack-free, homogeneous packed structures. SEM images of the self assembled structure revealed a closely packed hexagonal array of nanoparticles,[19] where the size of pores (d_p) were around 15% of the particle size i.e., d_p = 15 nm, 50 nm, and 105 nm for 100 nm, 330 nm, and 700 nm particles, respectively.[20]

4.2.2. DNA Sample Preparation

DNA samples, NoLimits™ DNA fragments (6, 10, 20 kbp, Fermentas Life Sciences), λ-DNA (48 kbp, New England Biolabs), and T4 DNA (166 kbp, Nippon Gene) were stained by YOYO-1 (Molecular Probes) with dye-to-base

ratio of 1:10. Pulsed field electrophoresis was performed in 4× TBE buffer to suppress electroosmotic flow with 4% v/v 2-mercaptoethanol added to reduce photobleaching.

4.2.3. Asymmetric Pulsed Field Electrophoresis

Pulsed electric fields were generated by homebuilt high-voltage amplifiers triggered by square wave signals from a synthesized function generator (Wavetek, San Diego, CA). The separation chamber was connected to reservoirs where pulsed electric potentials were applied using platinum electrodes. The applied pulsed electric potentials generated asymmetric obtuse-angle pulsed fields, E_1 and E_2, across the separation chamber, where the angle between the pulsed fields is ~ 135º and $E_1 = 1.4\ E_2$ in all our experiments (E_2 is the horizontal field shown in Figure 2). Typical electric fields used in our experiments are around 80 - 280 V/cm and the frequencies are between 0.1 to 100 Hz.

4.2.4. Fluorescence Imaging

DNA samples were excited by a 488-nm argon ion laser beam, and the fluorescent emission was collected by a homemade microscope using a 4× objective (0.1 N.A., Olympus, Tokyo, Japan) for separation imaging. For single DNA imaging, a Nikon motorized TIRF (total internal reflection fluorescence microscopy) microscope (Eclipse Ti, Nikon, Tokyo, Japan) was used with either 60× or 100× oil-immersion (1.4 N.A., Nikon, Tokyo, Japan) objectives. TIRF microscopy is specially designed to enable single molecule visualization and dynamic observation with a high signal to noise ratio. A complete description of DNA visualization using TIRF techniques can be found in literature. [21-23]

4.3 Results and Discussion

4.3.1. Angular Separation

Angular separation of DNA molecules was conducted by continuously injecting DNA samples into the separation chamber by applying a DC electric field in the DNA sample reservoir. Once the pulsed electric field is applied, different streams of DNA are formed which corresponds to different DNA sizes. Each stream then proceeds to one of the collecting channels in the bottom of the microchip. The migration mechanism of DNA in our microchip is similar to the typical mechanism of DNA migration under pulsed electric field in gel or microfabricated array.[24] Once the pulsed electric field is applied, DNA molecules stretch and undergo a chevron type motion with the head and tail repeatedly switching. As a result, larger DNA molecules deviate from the average field direction (vertical line) more, compared to the smaller DNA molecules. We called this deflection angle θ, as shown in Figure 4.2. The fluorescence image in Figure 4.2 shows three distinct streams of DNA corresponding to three different sizes of DNA molecules; 20, 48, and 166 kbp. The packed structure was made with 700 nm silica particles. The electric fields were E_1 = 120 and E_2 = 86 V/cm and f = 2 Hz.

4.3.2. Frequency Dependence of Angular Separation

Angular separation of DNA molecules was performed for different pulse frequencies as explained in Section 4.2 and the values of θ were recorded for each DNA molecule at each frequency. Figure 4.3a shows the variation of deflection angle, θ, with respect to frequency, f, for two different DNA sizes; 48 and 166

kbp. It can be seen in Figure 4.3a that for either DNA molecule, θ changes with frequency in a non-monotonic way; θ increases initially with increasing frequency, reaches a plateau, and then declines with further increasing the frequency. Finally it assumes a constant value independent of the pulse frequency. Similar separation experiments were conducted for DNA sizes ranging from 6 to 166 kbp in pore sizes ranging from 15 to 105 nm, at different electric fields and frequencies. For all of these different scenarios, the variation of θ with f was similar to that shown in Figure 4.3a, although the maximum value of θ, and the frequency of θ_{max} varied with DNA size and separation conditions.

The fact that angular separation is highly dependent on pulse frequency is not surprising,[3, 25, 26] since pulse frequency is one of the key parameters controlling separation efficiency in traditional PFGE. However, the non-monotonic behavior of θ with f is rather complicated.[17, 19]. As discussed in Chapter 3, in addition to pulse time, another critical time scale in any pulsed field electrophoresis scheme either in gel[26-28] or microfabricated array[24, 29] is the reorientation time of DNA, t_{or}. In pulsed field electrophoresis, the reorientation time of DNA has been defined as the time it takes DNA to completely align itself to the newly applied electric field, once the direction of the electric field changes.[3] In other words, it is the time it takes the molecule to travel its own length;[24] $t_{or} = \frac{L}{\mu E}$, where L is a fraction of the contour length of the molecule; $L = cL_{contour}$ (c is a coefficient between zero and one depending on pore size, electric field angle, and buffer viscosity), μ is the electrophoretic mobility of DNA, and E is the applied electric field.

In PFGE, the ratio of pulse time (T_p) to reorientation time (t_{or}), $\frac{t_{or}}{T_p}$, is used to develop universal mobility curves in order to characterize the separation behavior of different DNA sizes in one single curve. As shown in Chapter 3, a similar approach can be taken for APFE for graphs such as the ones in Figures 3.5a and 4.3a, once the reorientation times of the molecules are known. Using high quality real-time movies of DNA migrating in our nanoparticle array structures, the reorientation times for 48 and 166 kbp DNA molecules were calculated in 105 nm pores under a DC electric field of 114 V/cm (the experimental conditions in Figure 4.3a). The reorientation times were 0.10 ± 0.02 s and 0.28 ± 0.06 s for 48 and 166 kbp DNA molecules, respectively. As described in Chapter 3, Section 3.4, using the reorientation times, a scaled frequency can be defined using Eq. 3.5 ($f^* = \frac{f}{1/2t_{or2}}$, since 114 V/cm is named E_2, its associated reorientation time is named t_{or_2}). Figure 4.3b shows the variation of θ with f^* for the same experimental parameters as in Figure 4.3a. It can be seen from Figure 4.3b that by normalizing the horizontal axis using f^*, the four regimes (rise, plateau, fall, and the second plateau) in Figure 4.3a seen at different frequencies for 48 and 166 kbp DNA molecules, actually occur around the same values of f * for the two DNA sizes. According to Figure 4.3b, for both DNA sizes, at low frequencies, where $f < 1/2t_{or_2}$, θ increases with increasing frequency (regime I). Once the frequency reaches a value around $f \approx 1/2t_{or_2}$, θ reaches its maximum value and remains constant until $f \approx 2 \times (1/2t_{or_2})$ (regime

II). At higher frequencies, where $f > 2 \times (1/2t_{or_2})$, θ decreases with increasing frequency (regime III). At very high frequencies, where $f > 10 \times (1/2t_{or_2})$, θ reaches a constant value close to the average field direction and becomes independent of frequency (regime IV).

In order to understand the frequency behavior of angular separation of DNA molecules, real-time movies of 166 kbp DNA were obtained using TIRF microscopy. The results for four different frequencies corresponding to four regimes in Figure 3b will be discussed in detail in the next four sections.

Regime I, $\frac{f}{1/2t_{or_2}} < 1$. According to Figure 4.3, when frequency is smaller than the frequency associated with the reorientation time ($\frac{1}{2t_{or_2}}$) of the molecule, θ increases with increasing frequency. In order to understand the molecular details of the electromigration in this regime, movies of 166 kbp DNA molecules migrating under asymmetric pulsed electric fields at f = 0.5 Hz and E_2 = 114 V/cm were obtained in 105 nm pores. Figure 4.4 shows sequential fluorescence images associated with this movie. The white arrows in Figure 4.4 represent the directions of the applied electric fields at each snapshot.

It can be seen from the images in Figure 4.4 that the DNA molecules under asymmetric pulsed field electrophoresis follow the same migration mechanism reported for PFGE. As described in Chapter 3, due to the ratchet effects of asymmetric pulsed electric fields, DNA molecules backtrack to different positions based on their molecular size; larger DNA molecules deflect more

compared to the smaller molecules with respect to the direction of the averaged electric field.

Based on this migration mechanism, a simple geometric model (Eq. 3.1) was developed to explain the frequency behavior of DNA in this regime as described in Chapter 3.[19, 30] In this model, it was assumed that DNA is a flexible rod with a length L which is a fraction of its contour length. One can relate θ to the reorientation times of the molecule using Eq. 3.1, to give:

$$\tan\theta = 1 - \sqrt{2}\,\frac{\dfrac{1}{2t_{or_2}} - f}{\dfrac{1}{2t_{or_1}} - f} \qquad (4.1)$$

where t_{or_1} and t_{or_2} are the reorientation times associated with E_1 and E_2, respectively. ($t_{or_1} = \dfrac{L}{\mu_1 E_1}$ and $t_{or_2} = \dfrac{L}{\mu_2 E_2}$).

The variation of θ with respect to f can be calculated using Eq. 4.1, if the values of μ_1, μ_2, and L are known. A more detailed description of the geometric model and the range of its validity have been discussed in Chapter 3.[30] It can be seen in Figure 3.3 that by increasing the frequency, θ increases as long as $f < 1/2t_{or_2}$. Although a quantitative fit between the geometric model and the experiment was only achieved in the smallest pore size of 15 nm, but even in the larger pores, this simple model still predicted the trend of changing θ with f.

Regime II, $1 < \dfrac{f}{1/2t_{or_2}} < 2$. According to Figure 4.3b, once the frequency is around the frequency associated with DNA's reorientation time ($\dfrac{1}{2t_{or_2}}$),

deflection angle, θ, reaches its maximum and remains constant up to $\frac{f}{1/2t_{or_2}} \approx 2$.

Movies of 166 kbp DNA molecules migrating at a frequency of 2 Hz (associated with regime II) through 105 nm pores were obtained to facilitate understanding of the migration mechanism. Time-lapse images are shown in Figure 4.5. Following DNA motion through the images in Figure 4.5, one can see that DNA molecules follow the same backtracking motion as in regime I. However, since the frequency is around or higher than $\frac{1}{2t_{or_2}}$, the instant DNA backtracks and realigns itself in the direction of E_2, the field direction changes to E_1, so the molecule does not have time to migrate along E_2, but tends to retrace the same path it just followed. This means that there will be no net displacement in the direction of the smaller field (E_2), and the molecule follows the direction of the higher field (E_1) all through the separation chamber. As a result, θ assumes the same angle as E_1 (= 45°) with respect to the vertical direction.

According to Eq. 4.1, for $f = \frac{1}{2t_{or_2}}$, θ reaches 45° independent of DNA size. The maximum deflection angle, θ_{max}, for different DNA sizes were measured and the results were presented in Chapter 3, Figure 3.4. It can be seen in Figure 3.4 that although there exists a θ_{max} for all DNA sizes in all pore sizes in our experiments, the value of θ_{max} is not always 45°. A reduced value of θ_{max} relative to 45° can also be seen in Figure 4.3b, where, although 48 kbp DNA reaches its maximum deflection angle at $f \approx 1/2t_{or_2}$ (regime II) its corresponding $\theta_{max} < 45°$. Our observations indicate that θ_{max} follows the prediction of the geometric model

for molecules that do not have time to relax from their extended conformations during their reorientations, $t_{or_2} < \tau_r$, where τ_r is the relaxation time of the molecule. Since DNA molecules in our experiments are confined in pores smaller than their gyration radius, their relaxation time (τ_r) can be calculated by de Gennes theory as:[31, 32]

$$\tau_r \approx \left(\frac{\eta (pw)^{2/3}}{k_b T} \right) \frac{{L_{contour}}^2}{d_{ch}^{1/3}} \tag{4.2}$$

where η is the buffer viscosity, p is the persistence length of DNA, w is the width of the molecule, k_b is the Boltzmann constant, T is the absolute temperature, $L_{contour}$ is the contour length of molecule, and d_{ch} is the confinement size. The schematics in Figure 4.6 show the difference in migration mechanism between a molecule with $t_{or_2} < \tau_r$ and a molecule with $t_{or_2} > \tau_r$ at a frequency of $f \approx 1/2t_{or_2}$. The left column shows migration of a molecule with a relaxation time longer than the reorientation time, meaning that the molecule remains stretched throughout the reorientation. The right column shows migration of a molecule with a relaxation time shorter than the reorientation time, meaning that the molecule has time to relax from its stretched conformation during the reorientation time. The solid lines in panel i show the position of the molecules after E_1 is applied. The dashed lines are the initial positions of the molecules. Panel ii shows the molecules after E_2 is applied and panel iii shows the positions of the molecules after E_1 is applied again. The migration of the two molecules in panel i is similar. The difference in the migration of the two molecules is in panels ii and iii. It can be seen from panel ii, while the molecule in the left column ($t_{or_2} < \tau_r$) remains

stretched, the molecule in the right column ($t_{or_2} > \tau_r$) relaxes from its extended conformation at some point in time after E_2 is applied. As a result, once the electric field directions change to E_1 again (panel iii), the molecule in the left column, slides off the same obstacle and backtracks to the same path in panel iii as in panel i whereas, the molecule in the right column slides off a different obstacle and backtracks to a different path in panel iii from that of panel i.

Movies of 48 kbp DNA moving under pulsed electric fields of 160 and 114 V/cm in 105 nm pores were captured at a frequency of 5 Hz (regime II). Time-lapse images of this movie are shown in Figure 4.7. A comparison between the images in Figures 4.5 and 4.7 shows the difference between migrations of the two different sizes of DNA (48 and 166 kbp) in regime II. Tracking the 48 kbp DNA through the images in Figure 4.7, one can see that, similar to the 166 kbp DNA, upon applying the field in E_1 direction, the molecule stretches and moves in the opposite direction. Once the electric field changes to E_2, the molecule backtracks and reorients itself to the new field direction, and this process repeats itself with each change in field direction. Examining Figure 4.5, 166 kbp retraces the same path in the direction of E_1 as in previous cycle, so there will be no displacement in E_2 direction. In contrast, 48 kbp DNA relaxes from its highly extended conformation, and then backtracks in the direction of E_1 in a different path from the previous cycle due to its change in extended length. As a result, although the molecule does not have sufficient time to fully travel its length, L in the direction of E_2, due to its relaxation there is a net displacement in the direction of E_1. As a result, the net deflection angle θ_{max} will be the summation of displacements in both E_1 and E_2 direction and smaller than 45°. Other effects such

as Brownian diffusion and U-shape formation contribute to the dispersion of angular separation around θ_{max} and are the reason for the presence of error bars in Figure 3.4.

As shown in Figure 4.3, the angular separation of DNA under asymmetric pulse field electrophoresis varies between the minimum value equal to the angle of the average field and a maximum value equal to the angle of the larger field (angle of average field < θ < angle of larger field). So the difference between the angle of the average field (0°, in our experiments) and the larger electric field (45°, in our experiments) defines the separation window. It is important to know which range of DNA sizes can be resolved within the maximum separation window. Comparing the definition of the relaxation time, Eq. 4.2, with the definition of reorientation time of the molecule, one can define a criterion for which maximum deflection angle reaches 45°. As stated earlier, for θ_{max} = 45°, $\tau_r > t_{or_2}$, substituting the equations for τ_r and t_{or}, the criterion for having θ_{max} = 45° can be defined as:

$$L > \frac{cD^{1/3}}{c_r \mu E} \tag{4.3}$$

here, $c_r = \left(\frac{\eta (pw)^{2/3}}{k_b T} \right)$ and $c = \frac{L_{contour}}{L}$. According to Eq. 4.3, for DNA sizes larger than a critical size, relaxation time will always be longer than the reorientation time, meaning that DNA stays stretched throughout the pulsed electric fields. It can also be seen from Eq. 4.3 that the critical size decreases by decreasing pore size and increasing electric field. This indicates that by having

smaller pore sizes or higher electric fields, more DNA sizes would reach the maximum deflection angle of 45°, as shown in Figure 3.4.

Another interesting feature of regime II that can be observed in Figure 4.3 is that the maximum deflection angle is not just a point, but it is a plateau. θ reaches its maximum at $f = \frac{1}{2t_{or_2}}$ and remains constant while increasing the frequency. For instance, according to the frequency curve in Figure 4.3a, 166 kbp DNA reaches its maximum deflection angle at $f \sim 2$ Hz and remains constant up to $f \sim 4$ Hz. Movies of 166 kbp DNA molecules migrating through 105 nm pores under asymmetric pulsed electric fields of 160 and 114 V/cm were obtained at frequencies of 2, 3, and 4 Hz to understand the reason behind this plateau. As presented in Figure 4.5 and described in detail earlier, at a frequency of 2 Hz, 166 kbp DNA has enough time to completely reorient itself to the direction of E_2, but does not have time to migrate in this direction. At a frequency of 3 Hz, 166 kbp DNA does not have time to either reorient itself completely or migrate in the direction of E_2, so it is just partially reoriented to E_2 when the direction of field changes to E_1. The same migration mechanism was observed at higher frequencies, so long as DNA has enough time to reorient completely in the direction of E_1. This means the plateau in regime II has an upper limit as $f < \frac{1}{2t_{or_1}}$, where t_{or_1} is the reorientation time in the direction of E_1. The ratio between the upper and lower limit for regime II can then be defined as:

$$\frac{1/2t_{or_1}}{1/2t_{or2}} \approx \frac{\mu_1}{\mu_2}\frac{E_1}{E_2} \tag{4.4}$$

In all of our experiments, $\frac{E_1}{E_2} = 1.4$ and the mobility ratio is measured to be around $\frac{\mu_1}{\mu_2} = 1.2$, so $\frac{1/2t_{or1}}{1/2t_{or2}} \approx 1.7$ which is close to the upper limit of regime II in Figure 4.3b. This result means that the plateau observed in the frequency behavior of deflection angle is caused by the asymmetric nature of the applied electric fields ($E_1 > E_2$). As can be seen from Eq. 4.4, if the two electric fields have the same magnitudes, ($E_1 = E_2$), the maximum in Figure 4.3 would be a point instead of a plateau. On the other hand, the plateau can be extended to higher frequencies, by increasing the ratio of the two electric fields ($E_1 >> E_2$).

Regime III, 2 < $\frac{f}{1/2t_{or_2}}$ < 10. At higher frequencies, when the molecule does not have time to reorient completely in the directions of either E_1 or E_2 ($f < \frac{1}{2t_{or1}}$), the migration mechanism changes compared to regime I and II. As was observed in real-time movies of DNA migration, at smaller frequencies, one of the two ends of the molecule usually lead the migration in the separation media. One can imagine that if this was the dominant migration mechanism at higher frequencies, DNA molecules would stop moving and would go back and forth in the directions of E_1 and E_2 around a particle in the separation chamber, similar to what is called "dynamic trapping" in the literature.[24] However, our real-time movies of 166 kbp DNA migrating at f = 10 Hz (associated with regime III in Figure 4.3) reveal a different migration mechanism. Time-lapse images of such a movie are shown in

Figure 4.8. This figure shows migration of 166 kbp DNA molecules at f = 10 Hz in pores of 105 nm at asymmetric pulsed electric fields of 160 and 114 V/cm.

Following DNA molecules in the images of Figure 4.8, it can be seen that they are not trapped around any particle, rather they move towards the collection channels in the separation chamber. The direction of this migration is observed to be a combination of directions of E_1 and E_2. Contrary to the migration mechanism in regimes I and II, where one of the two ends of the molecule typically lead the migration, in regime III, for large pore sizes, a random point along the DNA chain can lead the motion, with the molecule assuming a hairpin conformation. Our observations of DNA motion in regime III show that in this regime, DNA migration is a complicated combination of hernia formations, prolonged migration in one direction for multiple cycles, and moving with the same head in a zigzag fashion. As a result, the net deflection angle is reduced from the angle of the larger field E_1 (45°), and comes closer to the direction of the average electric field (0°). This is consistent with the behavior of DNA during pulsed field gel electrophoresis, where the formation of hernias significantly and qualitatively changes the separation behavior, as reported in the literature.[33-36]

Regime IV, $\frac{f}{1/2t_{or_2}} > 10$. According to Figure 4.3, the decline of deflection angle by increasing frequency (regime III) is followed by a second plateau in the frequency dependent curve. As can be seen in Figure 4.3a, around a frequency of 50 Hz, θ reaches a value close to the angle of the average electric field (0°) and remains relatively constant, with little frequency dependence for both 48 and 166 kbp DNA molecules. The same behavior was observed for DNA sizes of 6, 10,

and 20 kbp. Real-time movies of 166 kbp DNA were captured at a frequency of 50 Hz, associated with regime IV, to help understand the migration mechanism of DNA in this regime. Three sequential images are shown in Figure 4.9a (i, ii, iii). Figure 4.9a shows migration of 166 kbp DNA molecules at a frequency of 50 Hz through pores of 105 nm, under asymmetric electric fields of 160 and 114 V/cm. Our real-time videos of single DNA molecules migrating under high frequency pulsed electric field show the migration mechanism changes significantly. The molecule reptates along the average direction of the two electric fields (Figure 4.9a) and no backtracking is observed.

Since the angle between the two electric fields (α) is an obtuse angle, there is a component of E_1 that is always in the opposite direction of E_2 (in our experiments, since α = 135°, the horizontal component of E_1 has the same magnitude as E_2). This means that during one cycle, in the horizontal direction, the electric field changes between two equal but inverse electric fields. In the vertical direction, the electric field changes between zero and the normal component of E_1. From real-time videos of DNA migration, it appears that the effect of the two inverse fields in the horizontal directions is insignificant at high frequencies, so the molecule just follows the normal electric field component. In order to verify this observation, two experiments with different configurations of electric field were conducted, as shown in Figures 4.9b and c. In the first experiment, the electric field was pulsed between zero and a vertical field equal to the normal component of E_1 (Figure 4.9b). The frequency of the pulsed field was 50 Hz, the same as in Figure 4.9a. In the second experiment, a DC electric field (f = 0 Hz) equal to the normal component of E_1 was applied (Figure 4.9c). The

migration and configurations of 166 kbp DNA molecules under these three conditions were observed to be significantly similar. In all of these experiments, the DNA molecules were stretched and migrated along the vertical direction, leading with a head (Figures 4.9a, b, and c) with occasional hooking and pulling-free cycles.

One possible way of explaining the behavior of DNA molecules under asymmetric pulsed electric fields at high frequencies is by considering the Kuhn segment relaxation time, τ_0 (also known as shortest relaxation time of a polymer).[24, 32, 37] Polymer size scales with the number of segments in the chain, so their relaxation time (τ_r) can be written as the product of time scale for the motion of individual Kuhn segments and a power law in the number of segments in the chain:[37]

$$\tau_r \approx \left(\frac{\eta}{k_b T} \frac{(pw)^{2/3} b^2}{d_{ch}^{1/3}} \right) N^2 \approx \tau_0 N^2 \qquad (4.5a)$$

$$\tau_0 \approx \left(\frac{\eta}{k_b T} \frac{(pw)^{2/3}}{d_{ch}^{1/3}} \right) b^2 \qquad (4.5b)$$

here, N is the number of Kuhn segments in the chain and b is the size of Kuhn segments (~ 2 x persistence length), so $L_{contour} = Nb$. Substituting $L_{contour}$ by Nb in Eq. 4.2, one can derive Eq. 4.5a. The importance of the Kuhn segment relaxation time (τ_0), as explicitly stated in the literature,[37] is that "if polymer is probed on time scales around τ_0, the polymer will not move but shows elastic responses". This may be the reason why, at high frequencies in pulsed field electrophoresis, DNA molecules do not undergo the backtracking (chevron type) motion they exhibited at lower frequencies.

According to Eq. 4.5b, $\tau_0 \approx 10^{-3} s$ for b = 100 nm, which corresponds to a frequency of 500 Hz. As can be seen in Eq. 4.5b, in contrast to τ_r which is dependent on $L_{contour}{}^2$, τ_0 is independent of DNA size. The relaxation time, τ_r, provided by Eq. 4.5a, known as the longest relaxation time of a molecule, is around $\tau_r \approx 19.7 s$ (~ 0.02 Hz) for a 166 Kbp DNA molecule in a 100 nm channel. The deflection angle for different DNA sizes reaches a plateau in regime IV between these frequencies, consistent with the behavior of DNA in this frequency regime being related to the Kuhn segment relaxation time. Between the shortest and the longest relaxation times, τ_0 and τ_r, there are different modes of relaxation, τ_P, which correspond to the coherent motion of a section of a chain consisting of P Kuhn segments, where $1 < P < N$ and $\tau_0 < \tau_P < \tau_r$. Since DNA is a self similar object, τ_P is similar to the longest relaxation time of a chain with P Kuhn segments, $\tau_P \approx \tau_0 P^2$.[37] Substituting the pulse time corresponding to f = 50 Hz in this equation as τ_P, the number of Kuhn segments associated with this relaxation mode is calculated to be $P \sim 3$ Kuhn segments, or ~ 300 nm. It is interesting to see that the equivalent length of three Kuhn segments is very close to the radius of 700 nm silica particles used to make the self assembled array in this experiment. This implies that at pulse times larger than $\tau_{P=3}$, the head of the molecule corresponding to $P \sim 3$ Kuhn segments has time to react to the change in the direction of the applied electric fields. At shorter pulse times, the molecule has insufficient time to respond, and simply reptates along the direction of the average field.

Another possible reason for the behavior of DNA molecules at high frequency might be found by considering the dynamic of backtracking motion under obtuse angle pulsed electrophoresis. As observed in the previous three frequency regimes, once the direction of the electric field changes, the molecule backtracks to the direction of the new field. If the frequency of pulsed field is high enough so that the molecule does not have time to backtrack, then it is reasonable to assume that it would just move in the direction of the average field. The time scale of this phenomenon can be calculated by calculating the time it takes for the head of the molecule to travel one column in the horizontal direction in the nanoparticle array structure, t_p:

$$t_p = \frac{a_p}{\mu_2 E_2} \tag{4.6}$$

where a_p is the particle radius. Substituting the values of a_p, μ_2, and E_2 as; 350×10^{-9} m, 5×10^{-9} m^2 V^{-1} s^{-1}, and 11400 Vm^{-1}, respectively, t_p is calculated to be 0.006 s, which corresponds to the frequency of around 80 Hz. This means that at pulse frequencies around 80 Hz, once the direction of the field changes, the molecule does not have time to backtracks even by one column, so it continues to move with the same head in the direction of the average field. The difference between the two time scales, τ_p and t_p discussed here is that although both are independent of the DNA size, but τ_p is also independent of the applied field, whereas, t_p is dependent on the applied electric field. This might provide the key to answer the question of which one of these two time scales are dominant factor in defining the behavior of DNA at high frequencies. Our experimental results for this frequency regime do not show a strong electric field dependence of the frequency at which θ

reaches a plateau. However, the values of the electric fields used in this study where not orders of magnitude different. A more comprehensive parametric study is needed to investigate the dependency of this frequency regime on electric field and to verify which of the two above time scales are responsible for the behavior of DNA in this regime.

4.3.3. Mobility Minima in Pulsed Field Gel Electrophoresis

As described earlier, in transverse pulsed field electrophoresis, the two electric fields are applied in two directions with an obtuse angle and have the same magnitude. Due to the backtracking mechanism, different molecules move in the direction of the average electric field with different mobilities, as shown in Figure 4.1a, which means DNA mobility in the direction of the average field is representative of DNA separation. From the early years of pulsed field gel electrophoresis, it became clear that DNA mobility under transverse pulsed electrophoresis is highly affected by the pulse time or frequency. The variation of mobility with frequency showed the presence of mobility minima at pulse times close to the reorientation time of molecules for a wide range of DNA sizes at different electric fields and gel concentrations. A similar behavior of mobility with frequency was also observed for field inversion electrophoresis (α = 180°). The phenomenon was called “anomalous mobility” or “mobility minima” in the pulsed field electrophoresis literature.[29, 36, 38, 39] Numerous experimental and theoretical studies were conducted to explain the anomalous mobility. It was stated that DNA size fluctuation, along with hairpin or hernia conformations are

responsible for the presence of mobility minima during pulsed field gel electrophoresis.[36, 40]

In asymmetric pulsed field electrophoresis, the deflection angle or θ is representative of DNA separation. In order to probe the existence of mobility minima in asymmetric pulsed field electrophoresis, the DNA mobility in the direction of the average field (vertical direction) was measured. Figure 4.10 shows the variation of mobility, μ, along the vertical direction (dashed line) and the deflection angle, θ, (solid line) for 166 kbp DNA under asymmetric pulsed electric fields of 160 and 114 V/cm. The pore size was 105 nm. It can be seen from Figure 4.10 that DNA mobility decreases with increasing frequency, reaches a minimum, and then increases with further increasing frequency. It can also be seen that the mobility reaches its minimum at exactly the same frequency as deflection angle reaches its maximum. At low frequencies, when the pulse time is larger than the reorientation time of DNA molecules (regimes I and II), the head and tail switching mechanism is dominant for both asymmetric pulse field electrophoresis (APFE) and transverse pulsed field gel electrophoresis (PFGE). This results in a rise and a maximum in the $\theta - f$ curve in APFE, while corresponding to a decline followed by a minimum in the $\mu - f$ curve in PFGE. At higher frequencies, the migration mechanism is dominated by hernia formations (regime III), and migration in the direction of the average field (regime IV). These migration mechanisms are known to cause the PFGE frequency response of the separation mobility (a decline, plateau, and a rise in the $\mu - f$ curve).[26, 28, 36, 38] The same mechanisms give the frequency response observed in APFE (a rise, plateau, and a fall in the $\theta - f$ curve). These comparisons lead us to the conclusion

that the basic polymer physics in the nanoparticle array, microfabricated posts, and gel devices is clearly correlated and the presence of minima or maxima as a function frequency are related to the same basic physics.

4.4 Theoretical Section

In this section, the frequency behavior of DNA angular separation under asymmetric pulsed field electrophoresis is modeled numerically. A Langevin type of simulation, similar to the simulations of Deutsch,[24, 41, 42] is developed to investigate the frequency behavior of DNA chains. The DNA molecule is modeled as a series of freely-jointed-chains (FJC) with a fixed segment size of the Kuhn length b.[43-45] A detailed description of the numerical scheme and the parameters used in our simulation is presented in Appendix B. The separation matrix is modeled as a network of hexagonally oriented posts, where the distance between any consecutive posts is equal to the segment size. The chain moves through the posts in the presence of a pulsed external force applied on each segment of the chain. The external force is pulsed between two directions (F_1 and F_2) separated by $\alpha = 135°$, with a ratio of $F_1 = 1.4\ F_2$, similar to our experiments. No thermal force is present. The simulation is conducted using Working Model 2D software (Design Simulation Technologies, Inc., Canton, MI, USA).

Deflection angles, θ, of two chains of different size; $N = 12$ and $N = 6$ (where N is the number of segments) are calculated using our numerical model. The simulation is conducted for the two chains at the same frequency and pulsed force magnitude. Once the chains reach the end of the hexagonal network, the

deflection angles of the two chains are measured. The result is shown in Figures 4.11a and b. Figure 4.11 shows the deflection angles of the smaller (a) and larger (b) chains at the end of the separation matrix. It can be seen that similar to what we observed in our experiments, here also the larger chain deviates farther from the normal direction compared to the smaller chain.

The frequency behavior of the longer chain (N = 12) was investigated numerically by conducting the simulation at different frequencies and measuring the deflection angle at the end of the hexagonal network for each frequency. The reorientation time, t_{or} of the chain (the time it takes a chain to travel its own length) was also measured and used to define the scaled frequency, $f^* = \frac{f}{1/2t_{or}}$, as described in Section 4.3.2. The result is shown in Figures 4.12. Figures 4.12a-d are snapshots of the migration of the freely-jointed-chain in the hexagonal network under asymmetric pulsed force at three different scaled frequencies; f^* = 0.3, 1, 2.4 and 40. It can be seen from Figures 4.12a, b, and c that the dynamics of the chain in a hexagonal array is very similar to what is observed in fluorescence images of DNA molecules moving in a packed structure. Figure 4.12a corresponds to the migration of a freely-jointed-chain at a frequency smaller than the inverse of the chain's reorientation time, f^* = 0.3. Figure 4.12a shows a backtracking motion for a chain when the direction of the applied external force is changed, similar to what was observed for DNA molecules under pulsed electric fields. It can be seen from this figure that when $f^* < 1$, the chain has enough time to reorient and move in the direction of the applied force. Figure 4.12b shows migration of a freely-jointed-chain at a frequency equal to the inverse of chain's

reorientation time, $f^* = 1$. The snapshots in Figure 4.12b show that at $f^* = 1$, once the chain reorients itself to the direction of the smaller force, F_2, the direction of the force is changed, so the chain has no time to move in the direction of the smaller force and all the displacement occurs in the direction of the larger force, F_1. As a result, the net displacement of the chain will be in the direction of the larger force, $\theta = 45°$.

Figure 4.12c corresponds to the migration of a freely-jointed-chain at a frequency higher than the inverse of the chain's reorientation time, $f^* = 2.3$. It can be seen from Figure 4.12c that in contrast to Figures 4.12 a and b, where the motion of the chain was typically led by one of the two ends of the chain, at high frequencies, the chain is folded and the motion is led by a segment along the chain length. The conformation of the chain in Figure 4.12c is very similar to the conformation of DNA in Figure 4.8. Figure 4.12d corresponds to the migration of a freely-jointed-chain at a frequency much higher than the inverse of the chain's reorientation time, $f^* = 40$. It can be seen from Figure 4.12d that at high frequencies, the backtracking and head and tail switching (chevron type) motion of the chain, which was observed at lower frequencies does not happen. Instead, the chain moves in the direction of the average force more or less with the same end. This migration mechanism is similar to what was observed in real-time movies of DNA molecules under pulsed fields at high frequencies. As mentioned earlier, in this simulation the DNA diffusion is not considered, which means there is no relaxation time similar to what is given by Eq. 4.5 for this freely-jointed-chain. However, as seen in Figure 4.12d, similar to the behavior of DNA molecule at high frequency regime, the FJC chain in this simulation also stops backtracking

and moves in the direction of the average field. This might indicate that the time scale associated with fourth frequency regime is dictated by the time it take the chain to backtracks one column in the hexagonal array as given by Eq. 4.6.

The frequency behavior of this chain ($N = 12$) was studied by measuring θ at the end of hexagonal array for each frequency and the results are summarized in Figure 4.12e, showing the variation of θ with respect to f^*. The plot illustrates a rise, plateau, and fall in deflection angle curve, once frequency is increased. A comparison between Figure 4.12e and Figure 4.3b shows that the frequency behavior of θ for a freely-jointed-chain in a hexagonal array network under pulsed external forces is very similar to the frequency behavior of θ for a DNA molecule under pulsed electric fields. As explained above, this model is a mechanical model which does not consider thermal noises and its subsequent effects, such as molecular diffusion. The similarity between the predictions of our model and our experimental results suggests that different regimes in the θ-f curve are caused predominantly by the mechanics of a flexible chain in a network of obstacles reacting to a pulsed external force field. As shown in Sections 4.3.2 and 4.3.3, the frequency response of DNA separation (either μ-f curve or θ-f curve) under pulsed electrophoresis either in gel, microfabricated array, or self assembled nanoparticle array can be characterized using the reorientation time of DNA. Here we have shown the separation behavior of a freely-jointed-chain under pulsed force field can also be characterized using the chain reorientation time. The way reorientation time of a DNA molecule or a freely-jointed-chain varies with separation parameters such as pore size, electric field, chain length, and geometry of obstacles is significantly different and is specific to each separation method.

However, the fact that for all of these pulsed-based separation methods the separation behavior can be characterized primarily using its associated reorientation time, further confirms our understanding that the observed frequency behavior in our separation system is a natural response of a flexible chain to a pulsed external force field.

4.5 Conclusions

Frequency dependence of angular separation of DNA molecules under asymmetric pulsed field electrophoresis was studied both experimentally and numerically. It was observed that there are four different regimes present in the frequency response curve. Using real-time movies of DNA molecules, the migration mechanism of DNA molecules in each frequency domain was investigated. When frequency was less than the inverse of the molecular reorientation time, the molecules follow the backtracking, chevron type motion that was described in the literature for DNA pulsed field electrophoresis. At frequencies around the inverse of the molecular reorientation time, the angular separation reaches its highest value. However, at higher frequencies, we observe that DNA migration becomes a complicated combination of chevron and zigzag type motions, where the probability of backtracking decreases with increasing frequency. The backtracking motion completely stops at higher frequencies. The frequency dependant angular separation of DNA was verified theoretically as well as by using a simple mechanical model of a freely-jointed-chain under an asymmetric pulsed force applied on each segment. The same frequency dependant

behavior was observed for the chain through a hexagonally arranged array network.

Given the similarity between the mobility minima in gel and the deflection angle maxima in a microfabricated array, the variation of deflection angle with frequency in a self assembled nanoparticle structure undergoing APFE seems to be intrinsic to DNA migration in porous media under pulsed electric field. The definition of reorientation time of DNA molecules may vary in gel, microfabricated arrays, or self assembled nanoparticle structures, depending on the DNA migration mechanism and conformations in different porous structures. However, in all of these structures, the ratio of pulse time with corresponding reorientation time of DNA along with relaxation time of the molecule dictates the separation efficiency of pulsed field electrophoresis of DNA.

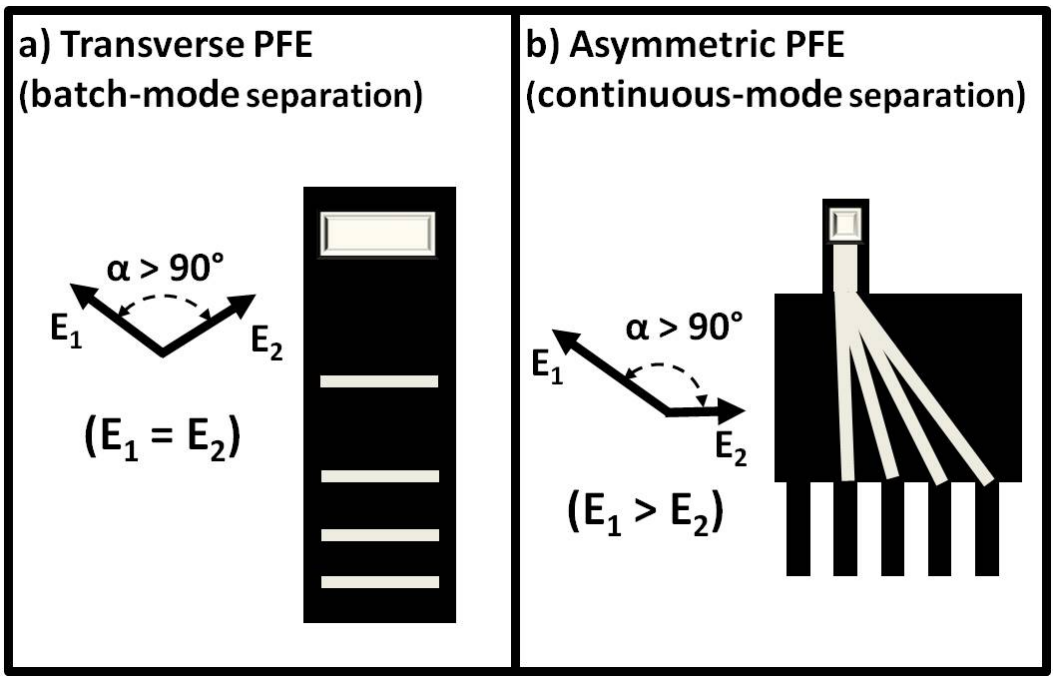

Figure 4.1. Schematics of a) Transverse pulsed field electrophoresis (PFE). The electric field is applied alternately between two directions with an obtuse angle where the magnitude of the field remains constant. The separation is achieved in the direction of the average electric field. b) Asymmetric pulsed field electrophoresis (APFE). The electric field is applied alternately between two directions where the field magnitude is larger in one direction compared to the other one. The separation is achieved in different directions compared to the average electric field.

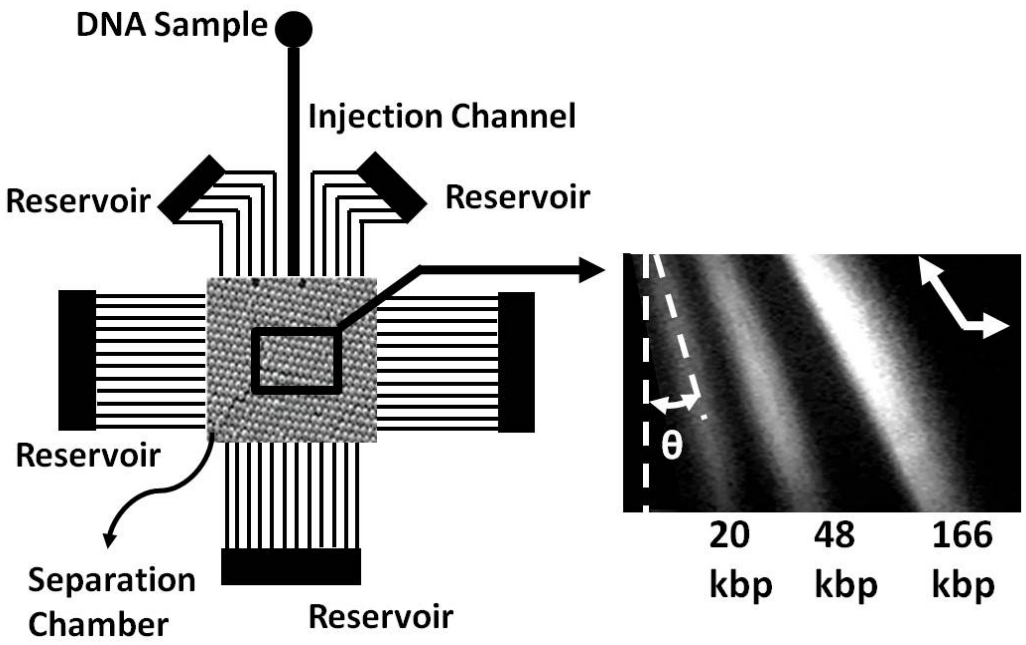

Figure 4.2. Left: Schematic of the microfluidic chip for angular separation of DNA molecules. DNA samples are injected continuously into the separation chamber which is filled by hexagonal packed arrays of silica nanoparticles. Using the buffer reservoirs, the pulsed electric field is applied across the separation chamber in the directions as shown by the white arrows in the right image. Right: fluorescence image of three separated DNA sizes. Each stream of DNA deviates from the vertical line with a deflection angle (θ) depending on their size. Larger DNA molecules have larger θ compared to the smaller molecules. This experiment is conducted in 105 nm pore size with E_1 = 120 V/cm, f = 2 Hz.

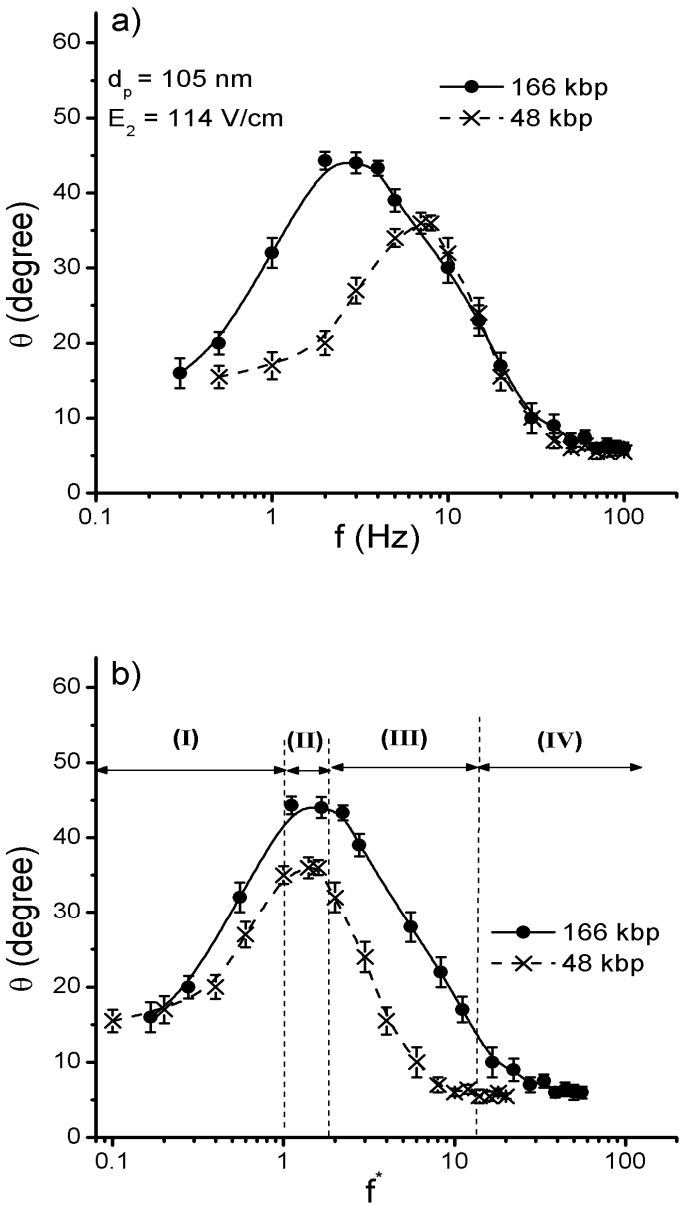

Figure 4.3. a) Variation of θ with respect to frequency for two different DNA sizes; 48 and 166 kbp in 105 nm pore size where the electric field is pulsed between 160 and 114 V/cm. b) Variation of θ with respect to the scaled frequency for the same DNA sizes under identical experimental conditions as in part (a). The frequency behavior can be divided into four distinct regimes: (I) $\frac{f}{1/2t_{or2}} < 1$, (II) $1 < \frac{f}{1/2t_{or_2}} < 2$, (III) $2 < \frac{f}{1/2t_{or_2}} < 10$, and (IV) $\frac{f}{1/2t_{or_2}} > 10$.

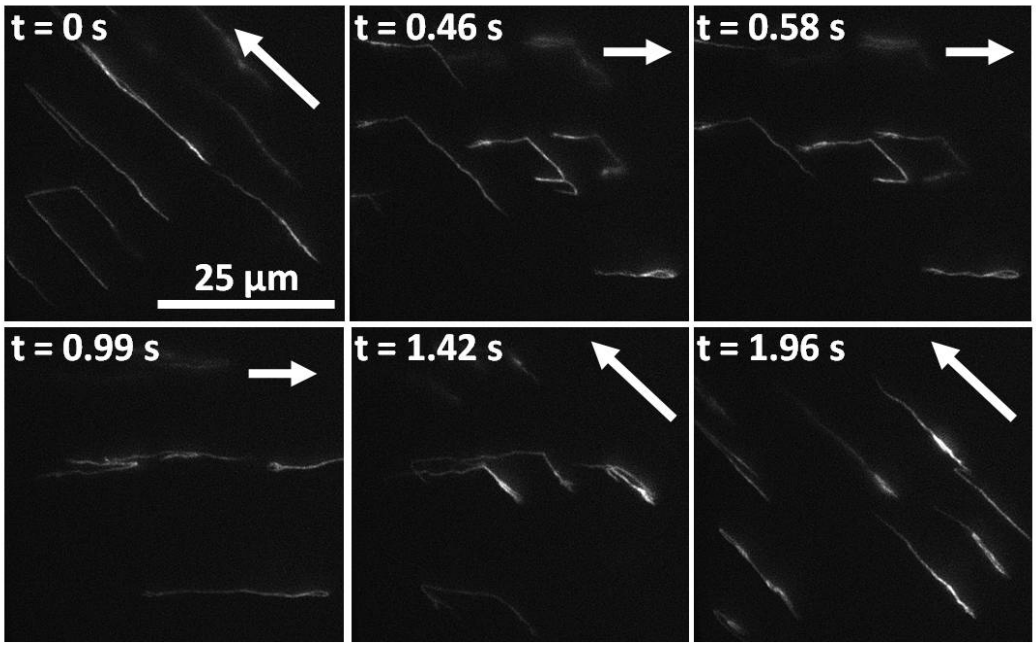

Figure 4.4. Sequential images of 166 kbp DNA migrating under asymmetric pulsed electric fields of 160 and 114 V/cm at the frequency of f = 0.5 Hz. This frequency corresponds to regime I in Figure 4.3. The pore size in this experiment is 105 nm.

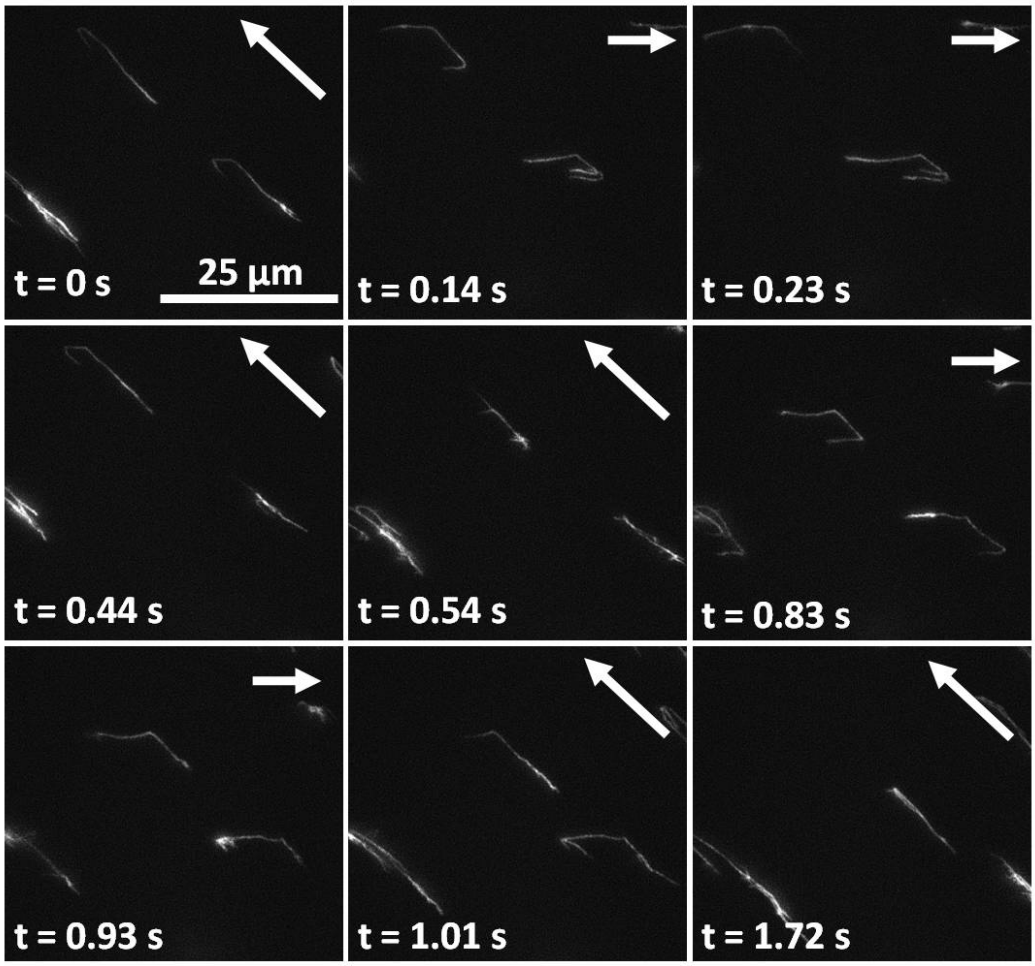

Figure 4.5. Time-lapse images of 166 kbp DNA moving in 105 nm pores at frequency of 2 Hz under asymmetric pulsed electric fields of 160 and 114 V/cm as E_1 and E_2. White arrows show the direction of the electric fields for each image.

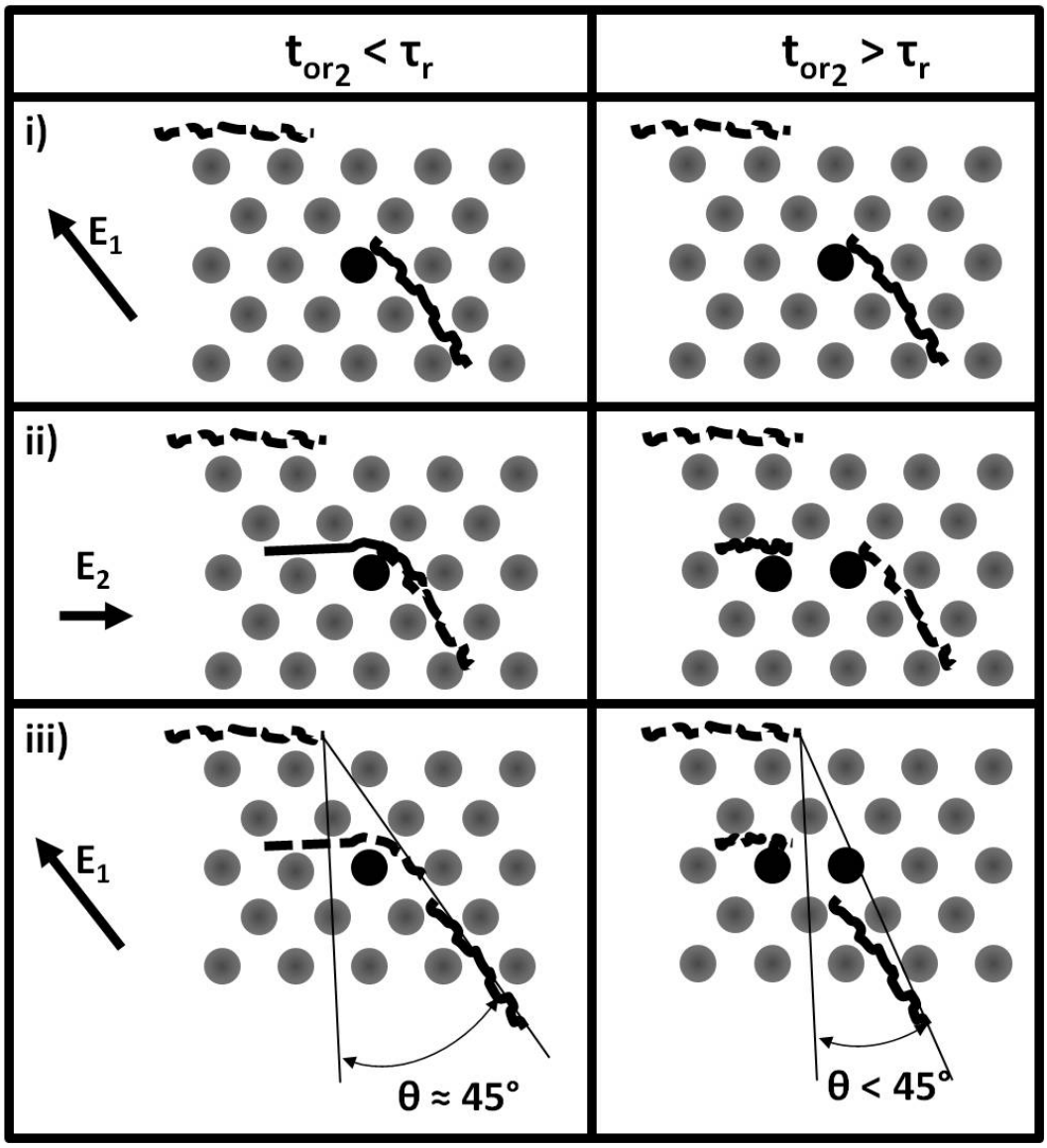

Figure 4.6. Schematic presenting the migration of two DNA chains under asymmetric pulsed electric field. Left column presents migration of DNA chain where its relaxation time is longer than its reorientation time. Right column presents migration of DNA chain where its relaxation time is shorter than its reorientation time. Three panels; i, ii, and iii show the positions of DNA chains after the electric field in each panel is applied.

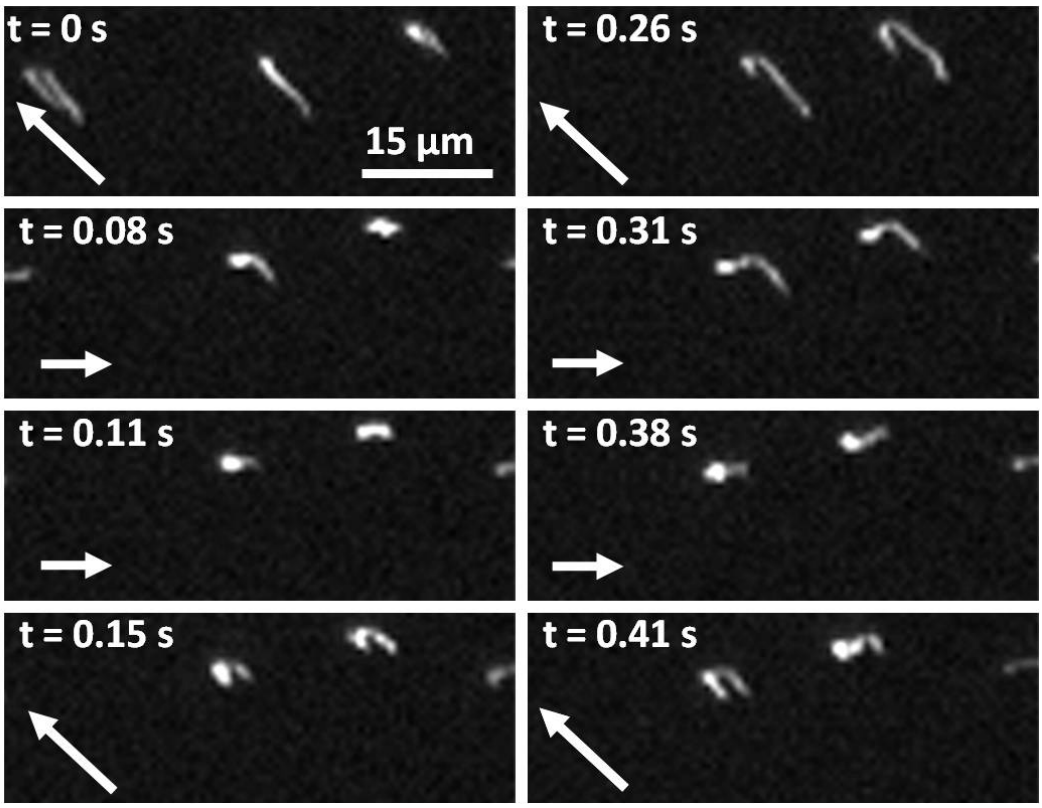

Figure 4.7. Time-lapse images of 48 kbp DNA moving at frequency of 5 Hz under asymmetric pulsed electric fields of 160 and 114 V/cm as E_1 and E_2. White arrows show the direction of the electric fields for each image.

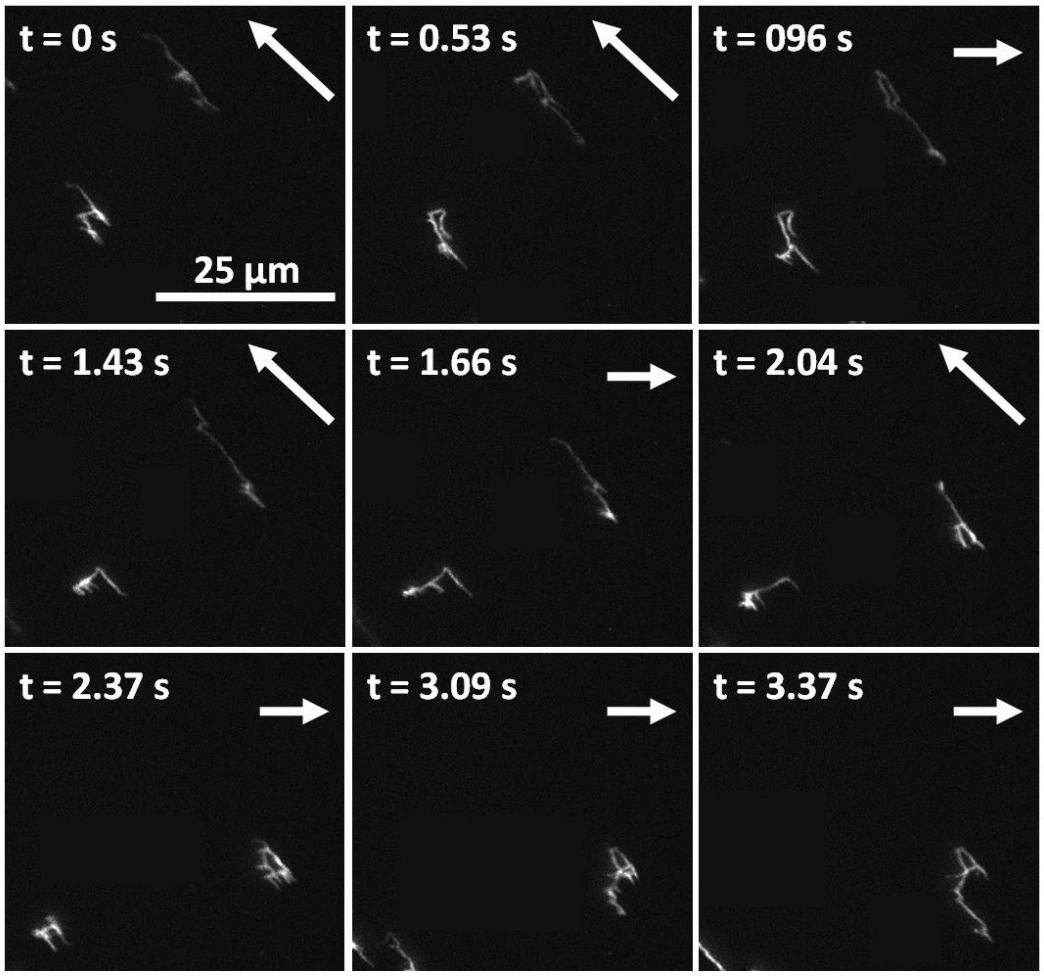

Figure 4.8. Sequential images of 166 kbp DNA migrating through 105 nm pores at frequency of 10 Hz associated with regime III. The applied electric fields are 160 and 114 V/cm. White arrows represent the direction of the applied electric fields.

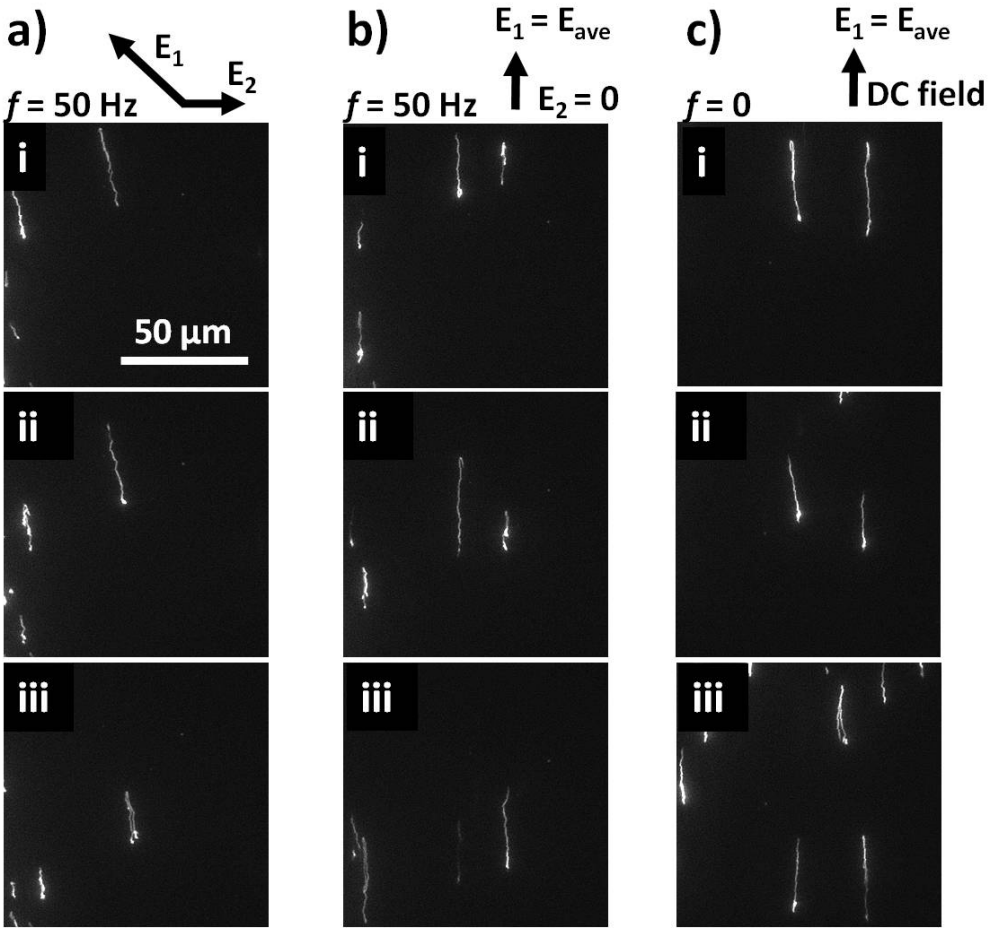

Figure 4.9. Panels i, ii, iii: sequential fluorescence images of 166 kbp DNA migrating in 105 nm pores a) under asymmetric pulsed electric fields of 160 and 114 V/cm at frequency of 50 Hz. b) under pulsed electric fields of zero and 114 V/cm at frequency of 50 Hz. c) under a DC field of 114V/cm in vertical direction. The corresponding electric field configurations are shown at the top of each column.

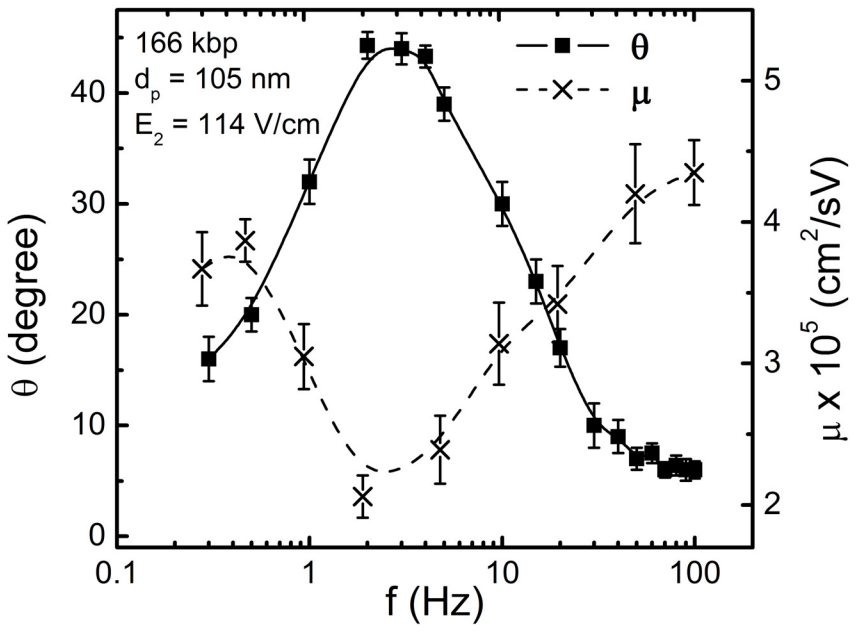

Figure 4.10. Frequency behavior of deflection angle, θ (solid line) and electrophoretic mobility, μ (dashed line) for 166 kbp DNA molecules under asymmetric pulsed field electrophoresis. The electric fields are 160 and 114 V/cm, the pore size is 105 nm.

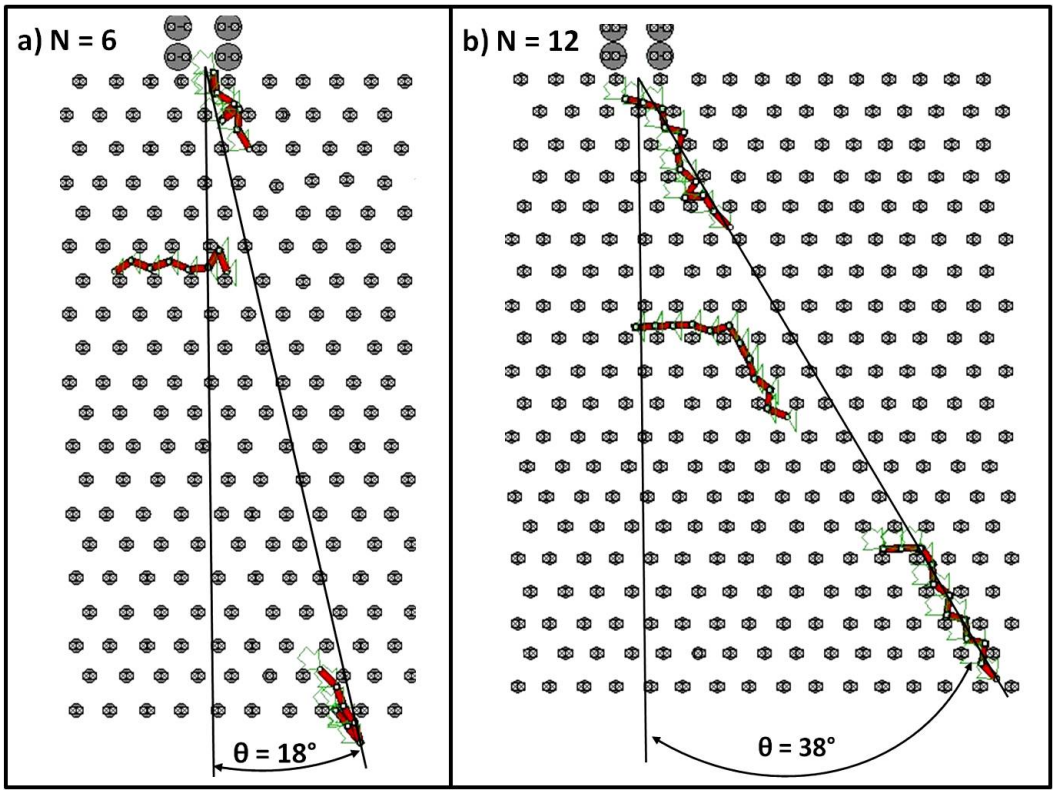

Figure 4.11. Simulation of asymmetric pulse field electrophoresis of two freely-jointed-chains with a) $N = 6$ and b) $N = 12$ in a hexagonal array. A time sequence of the conformations is shown during three pulses; from the top $E_1 \rightarrow E_2 \rightarrow E_1$. The longer chain deflects farther from the injection angle compared to the smaller chain, similar to the experimental observation.

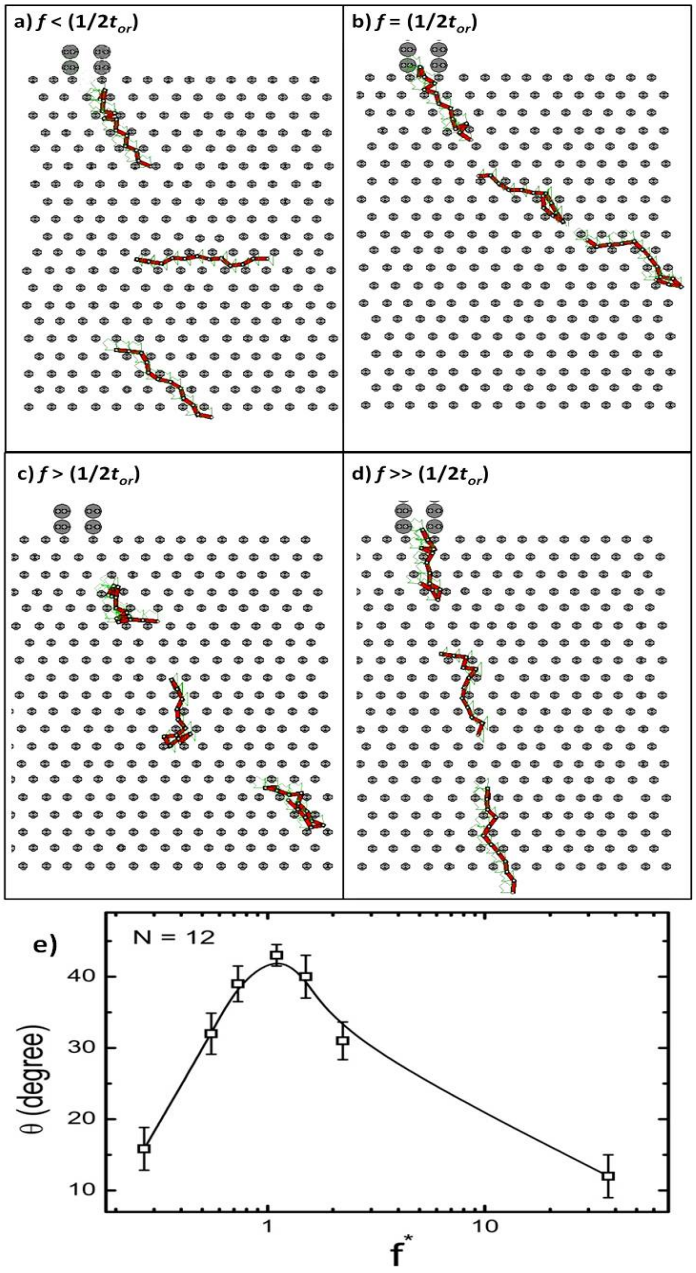

Figure 4.12. Frequency behavior of angular separation, θ verified numerically for a freely-jointed-chain of $N = 12$, at three different frequencies; a) $f^* = 0.3$, b) $f^* = 1$, c) $f^* = 2.3$, and d) $f^* = 40$. A time sequence of the conformations is shown during three pulses; from the top $E_1 \rightarrow E_2 \rightarrow E_1$. e) Variation of θ with f^* for the same chain calculated numerically.

4.6 References

1. Schwartz, D.C. and C.R. Cantor, *Separation of yeast chromosome-sized dnas by pulsed field gradient gel-electrophoresis.* **Cell**, *1984*. 37: p. 67-75.
2. Carle, G.F. and M.V. Olson, *Separation of chromosomal DNA-molecules from yeast by orthogonal-field-alternation gel-electrophoresis.* **Nucleic Acids Research**, *1984*. 12: p. 5647-5664.
3. Viovy, J.L., *Electrophoresis of DNA and other polyelectrolytes: Physical mechanisms.* **Reviews of Modern Physics**, *2000*. 72: p. 813-872.
4. Chu, G., D. Vollrath, and R.W. Davis, *Separation of large DNA-molecules by contour-clamped homogeneous electric-fields.* **Science**, *1986*. 234: p. 1582-1585.
5. Smith, C.L. and C.R. Cantor, *Purification, specific fragmentation, and separation of large DNA-molecules.* **Methods in Enzymology**, *1987*. 155: p. 449-467.
6. Mathew, M.K., C.L. Smith, and C.R. Cantor, *High-resolution separation and accurate size determination in pulsed-field gel-electrophoresis of DNA .1. DNA size standards and the effect of agarose and temperature.* **Biochemistry**, *1988*. 27: p. 9204-9210.
7. Schmalzing, D., A. Adourian, L. Koutny, L. Ziaugra, P. Matsudaira, and D. Ehrlich, *DNA sequencing on microfabricated electrophoretic devices.* **Analytical Chemistry**, *1998*. 70: p. 2303-2310.
8. Cheng, J., E.L. Sheldon, L. Wu, A. Uribe, L.O. Gerrue, J. Carrino, M.J. Heller, and J.P. O'Connell, *Preparation and hybridization analysis of*

DNA/rna from e-coli on microfabricated bioelectronic chips. **Nature Biotechnology**, *1998*. 16: p. 541-546.

9. Bruin, G.J.M., *Recent developments in electrokinetically driven analysis on microfabricated devices.* **Electrophoresis**, *2000*. 21: p. 3931-3951.

10. Khandurina, J. and A. Guttman, *Bioanalysis in microfluidic devices.* **Journal of Chromatography A**, *2002*. 943: p. 159-183.

11. Liu, L., P.S. Li, and S.A. Asher, *Entropic trapping of macromolecules by mesoscopic periodic voids in a polymer hydrogel.* **Nature**, *1999*. 397: p. 141-144.

12. Kaji, N., Y. Tezuka, Y. Takamura, M. Ueda, T. Nishimoto, H. Nakanishi, Y. Horiike, and Y. Baba, *Separation of long DNA molecules by quartz nanopillar chips under a direct current electric field.* **Analytical Chemistry**, *2004*. 76: p. 15-22.

13. Han, J. and H.G. Craighead, *Separation of long DNA molecules in a microfabricated entropic trap array.* **Science**, *2000*. 288: p. 1026-1029.

14. Lagally, E.T., C.A. Emrich, and R.A. Mathies, *Fully integrated pcr-capillary electrophoresis microsystem for DNA analysis.* **Lab on a Chip**, *2001*. 1: p. 102-107.

15. Doyle, P.S., J. Bibette, A. Bancaud, and J.L. Viovy, *Self-assembled magnetic matrices for DNA separation chips.* **Science**, *2002*. 295: p. 2237-2237.

16. Chou, H.P., C. Spence, A. Scherer, and S. Quake, *A microfabricated device for sizing and sorting DNA molecules.* **Proceedings of the**

National Academy of Sciences of the United States of America, *1999*. 96: p. 11-13.

17. Huang, L.R., J.O. Tegenfeldt, J.J. Kraeft, J.C. Sturm, R.H. Austin, and E.C. Cox, *A DNA prism for high-speed continuous fractionation of large DNA molecules.* **Nature Biotechnology**, *2002*. 20: p. 1048-1051.
18. Zeng, Y. and D.J. Harrison, *Self-assembled colloidal arrays as three-dimensional nanofluidic sieves for separation of biomolecules on microchips.* **Analytical Chemistry**, *2007*. 79: p. 2289-2295.
19. Zeng, Y., M. He, and D.J. Harrison, *Microfluidic self-patterning of large-scale crystalline nanoarrays for high-throughput continuous DNA fractionation.* **Angewandte Chemie-International Edition**, *2008*. 47: p. 6388-6391.
20. Zhang, H. and M.J. Wirth, *Electromigration of single molecules of DNA in a crystalline array of 300-nm silica colloids.* **Analytical Chemistry**, *2005*. 77: p. 1237-1242.
21. Garland, P.B., *Optical evanescent wave methods for the study of biomolecular interactions.* **Quarterly Reviews of Biophysics**, *1996*. 29: p. 91-117.
22. Kang, S.H., M.R. Shortreed, and E.S. Yeung, *Real-time dynamics of single-DNA molecules undergoing adsorption and desorption at liquid-solid interfaces.* **Analytical Chemistry**, *2001*. 73: p. 1091-1099.
23. Krichevsky, O. and G. Bonnet, *Fluorescence correlation spectroscopy: The technique and its applications.* **Reports on Progress in Physics**, *2002*. 65: p. 251-297.

24. Duke, T.A.J., R.H. Austin, E.C. Cox, and S.S. Chan, *Pulsed-field electrophoresis in microlithographic arrays.* **Electrophoresis**, *1996*. 17: p. 1075-1079.

25. Sudor, J. and M.V. Novotny, *Pulsed-field capillary electrophoresis - optimizing separation parameters with model mixtures of sulfonated polystyrenes.* **Analytical Chemistry**, *1994*. 66: p. 2139-2147.

26. Bustamante, C., S. Gurrieri, and S.B. Smith, *Towards a molecular description of pulsed-field gel-electrophoresis.* **Trends in Biotechnology**, *1993*. 11: p. 23-30.

27. Slater, G.W., J. Noolandi, J. Rousseau, C. Turmel, and M. Lalande, *Understanding and improving DNA pulsed field electrophoresis using the biased reptation model.* **Biophysical Journal**, *1988*. 53: p. A475-A475.

28. Chu, G., *Bag model for DNA migration during pulsed-field electrophoresis.* **Proceedings of the National Academy of Sciences of the United States of America**, *1991*. 88: p. 11071-11075.

29. Duke, T.A.J., *Monte-carlo reptation model of gel-electrophoresis - response to field pulses.* **Journal of Chemical Physics**, *1990*. 93: p. 9055-9061.

30. Nazemifard, N., S. Bhattacharjee, J.H. Masliyah, and D.J. Harrison, *DNA dynamics in nanoscale confinement under asymmetric pulsed field electrophoresis.* **Angewandte Chemie-International Edition**, *2010*. 49: p. 3326-3329.

31. Tegenfeldt, J.O., C. Prinz, H. Cao, S. Chou, W.W. Reisner, R. Riehn, Y.M. Wang, E.C. Cox, J.C. Sturm, P. Silberzan, et al., *The dynamics of*

genomic-length DNA molecules in 100-nm channels. **Proceedings of the National Academy of Sciences of the United States of America**, *2004*. 101: p. 10979-10983.

32. de Gennes, P.G., *Scaling concepts in polymer physics 1979*, Ithaca, N. Y.: Cornell University Press.

33. Akerman, B., *Barriers against DNA-loop formation in a porous matrix.* **Physical Review E**, *1996*. 54: p. 6685-6696.

34. Jonsson, M., B. Akerman, and B. Norden, *Orientation of DNA during gel-electrophoresis studied with linear dichroism spectroscopy.* **Biopolymers**, *1988*. 27: p. 381-414.

35. Mayer, P., J. Sturm, and G. Weill, *Stretching and overstretching of DNA in pulsed-field gel-electrophoresis .1. A quantitative study from the steady-state birefringence decay.* **Biopolymers**, *1993*. 33: p. 1347-1357.

36. Zimm, B.H., *Size fluctuations can explain anomalous mobility in field-inversion electrophoresis of DNA.* **Physical Review Letters**, *1988*. 61: p. 2965-2968.

37. Rubinstein, M. and R.H. Colby, *Polymer physics 2003*, New York: Oxford University Press.

38. Kobayashi, T., M. Doi, Y. Makino, and M. Ogawa, *Mobility minima in field-inversion gel-electrophoresis.* **Macromolecules**, *1990*. 23: p. 4480-4481.

39. Stellwagen, A. and N.C. Stellwagen, *Anomalously slow electrophoretic mobilities of DNA restriction fragments in polyacrylamide gels are not*

eliminated by increasing the gel pore-size. **Biopolymers**, *1990*. 30: p. 309-324.

40. Deutsch, J.M., *Explanation of anomalous mobility and birefringence measurements found in pulsed field electrophoresis.* **Journal of Chemical Physics**, *1989*. 90: p. 7436-7441.

41. Deutsch, J.M., *Theoretical studies of DNA during gel-electrophoresis.* **Science**, *1988*. 240: p. 922-924.

42. Slater, G.W., C. Holm, M.V. Chubynsky, H.W. de Haan, A. Dube, K. Grass, O.A. Hickey, C. Kingsburry, D. Sean, T.N. Shendruk, et al., *Modeling the separation of macromolecules: A review of current computer simulation methods.* **Electrophoresis**, *2009*. 30: p. 792-818.

43. Baumgartner, A., *Statics and dynamics of the freely jointed polymer-chain with lennard-jones interaction.* **Journal of Chemical Physics**, *1980*. 72: p. 871-879.

44. Baumgartner, A. and K. Binder, *Monte-carlo studies on the freely jointed polymer-chain with excluded volume interaction.* **Journal of Chemical Physics**, *1979*. 71: p. 2541-2545.

45. Doi, M. and S.F. Edwards, *The theory of polymer dynamics*. *1986*, New York: Oxford University Press.

CHAPTER 5

ROLE OF CRYSTALLINE ORDER ON DNA SEPARATION

5.1 Introduction

The separation of DNA molecules by size is essential in molecular biology. Microfabrication techniques have led to implementation of new separation mechanisms for DNA, which essentially arise from the high level of order that can be fabricated within the porous structure that makes up the separation matrix. In other microfluidic separation devices, such as the work of Baba and colleagues,[1] that replicate gel separation mechanisms, the random geometry of the gel has been replaced by a highly ordered microarray of pillars, with well controlled pore sizes. In contrast, conventional DNA separations are performed in a gel made of Agarose or polyacrylamide, with a highly random structure exhibiting a wide distribution of pore sizes.[2, 3] The opportunity to fabricate porous structures with varying degrees of order, raises the interesting question as to how an ordered, coherently repetitive structure will influence the separation of large biomolecules. In this report, we examine the impact of order

A version of this chapter has been submitted for publication to Analytical Chemistry. The work was done in collaboration with co-authors, Ledi Wang and Wenmin Ye. A version of the submitted manuscript will appear in their thesis as well.

of the porous matrix on the quality of DNA separation, an issue which has not yet been addressed experimentally, despite the opportunities presented by microfabrication to control order in a porous matrix. Some modeling works[4-6] have suggested there can be important differences between ordered and disordered porous materials, highlighting the importance of an experimental evaluation.

Pulsed field gel electrophoresis (PFGE) has been the conventional method of separating long DNA molecules (≥ 10 kbp).[7-9] In this method the electric field is switched between two directions with an obtuse angle, allowing the negatively charged DNA molecules to reorient themselves to the new field direction each cycle. The separation mechanism in PFGE depends upon head and tail switching (reorientation) of DNA molecules,[10, 11] as larger molecules have a longer reorientation time compared to smaller molecules,[12] and involves substantial collisions with the polymer matrix that makes up the separation media as described in Section 2.3.3. The use of two-dimensional separation mechanisms in a microfabricated array structure for DNA separation was pioneered by Austin,[13] who employed soft lithography to fabricate microarrays in silicon, and separated DNA molecules with obtuse-angle pulsed fields. Separation arises from the pulsed electric field causing DNA molecules to stretch and reorient periodically, with their head and tail repeatedly switched (Figure 5.1a). Due to this periodic head and tail switching of the molecule, the net migration of DNA molecules of different lengths is biased into different angles by the asymmetric fields; larger molecules are deflected farther from the injection angle compared to smaller ones as shown in Figure 5.1. The separation matrix provides the lanes for the DNA to

travel and the narrow pores confine the DNA to remain significantly stretched for the majority of the time.

Recently, we developed a microfluidic chip packed with self assembled nanoparticle arrays for two-dimensional pulsed field DNA separation,[14, 15] following the ratchet mechanism explored by Austin and coworkers.[16] An evaporation induced self assembly technique was employed to form hexagonal close packed nanoparticles, known as colloidal self assembly (CSA), as has been described elsewhere.[15, 17, 18] Interestingly, Wirth and colleagues[17] have speculated that they achieved high efficiencies in CSA devices as a result of the high degree of order, while Ahn and coworkers[18] felt defects had prevented them from achieving high efficiencies. The self assembly approach provides an opportunity to systematically study the effect of order of the separation matrix on DNA separation resolution and band broadening. Monodisperse particle suspensions form uniform, ordered structures similar to microfabricated arrays, while bidisperse particle suspensions, exhibit disorder as a function of the particle ratio, and have some similarity to the disordered structure of gel. By changing the ratio of the particle concentrations in bidisperse solution, structures with different degrees of disorder can be fabricated. Using this scheme, structures varying from highly ordered to essentially random structures, along with states in between, can be reproducibly fabricated and used to probe the role of order on DNA separation in a pulsed electric field.

Viovy[19] developed microarrays comprising randomly ordered self assembled columns of magnetic beads, formed upon imposition of magnetic field.

Several researchers[4, 5] developed numerical simulations to study the effects of order on DNA electrophoresis within these one-dimensional, sparse (dilute) arrays of obstacles where the spacing between the obstacles (~ 1-4 μm) was orders of magnitude larger than the persistence length of DNA (~ 50 nm). The separation of DNA in a sparse post array such as these magnetic bead arrays is based on collision frequency of DNA molecules with the obstacles.[20, 21] Patel and Shaqfeh[4] concluded that fully random post arrays would give better separation than fully ordered post arrays. Mohan and Doyle[5] refined this model, calculating that a post array with local order, but no long range order, would give better separation than a disordered array, which would be better than a fully ordered array. Hickey and Slater[6] calculated the diffusion coefficient of DNA in an ordered porous matrix. They observed significant, non-monotonic changes in diffusion with order. These intriguing calculations have not been tested experimentally. While the head to tail switching-based ratchet mechanism used in our study is not the same as in the sparse array models, the devices we have fabricated provide a powerful tool to experimentally explore the importance of order in a porous structure on large molecule separation.

5.2 Experimental Section

5.2.1. DNA Separation

DNA separation was conducted using a microfluidic chip filled with an array of nanoparticles as a sieving matrix. A schematic of the PDMS microchip is

shown in Figure 5.1b. PDMS microchips were fabricated using a standard soft lithography technique, then sealed to clean glass slides prior to packing, as described in detail elsewhere.[15, 22] Aqueous suspensions of silica colloids (Bangs Laboratories, Fishers, IN) of 330 and 700 nm diameter were used to form the self assembled nanoparticle array inside the microchips. DNA fragments (6, 10, 20 kbp, Fermentas Life Sciences) were stained with YOYO-1 (Molecular Probes) using a dye-to-base ratio of 1:10. Pulsed field electrophoresis was performed in 4× TBE buffer to suppress electroosmotic flow, with 4% v/v 2-mercaptoethanol added to reduce photobleaching. Pulsed electric fields were generated by a homebuilt high-voltage amplifier triggered by square wave signals from a synthesized function generator.[15] DNA samples were excited with a 488-nm argon ion laser beam, and the fluorescent emission was collected using a homemade microscope using a 4× objective (0.1 N.A., Olympus). Digitized images were analyzed using ImageJ (NIH, http://rsb.info.nih.gov/ij/).

Separation of DNA molecules was conducted by continuously injecting DNA samples into the separation chamber inside the microchip, as described previously.[15] The fluorescence image shown in Figure 5.1c represents the junction of the injection channel and separation chamber. The applied pulsed electric potentials generate asymmetric obtuse-angle pulsed fields, E_1 and E_2 across the separation chamber, where the angle between the pulsed fields is ~ 135º and $E_1 = 1.4E_2$ (as shown in Figure 5.1a) in all our experiments. The variance for each DNA stream was calculated at a distance of 2.6 mm from the injection channel. A description of the statistical procedure to calculate variances is provided in

Appendix A. Differences in observed mean variances, or separation distances, or resolution were evaluated for statistical significance at the 95% confidence level.

5.2.2. Self assembled Nanoparticle Array Structures

Monodisperse suspensions of silica particles (Bangs Laboratories, Fishers, IN) of 320 and 700 nm or mixtures of the two were used to fabricate ordered packed structures inside the separation chamber in the microfluidic device. Particle suspensions have known volume fractions, so simple volumetric mixing gives various volume fractions in the packed beds. SEM images of these structures revealed homogenous, ordered, packed structures, where the pore size is around 15% of the particle size for monodisperse arrays.[23, 24]

5.3 Results and Discussions

In order to introduce defects and disrupt the regular crystalline geometry of self assembled opal structures, bidisperse suspensions of 320 and 700 nm silica beads with different volume fractions of the 700 nm particles (χ_{700}) were fabricated. This mixture produced packed structures with different degrees of defects, with $\chi_{700} = 0$ and $\chi_{700} = 1$ representing the most ordered structures, whereas $0 < \chi_{700} < 1$ produced less ordered structures. These two particle sizes were used because the mixtures exhibit a small difference in porosity across the range of χ_{700}. The porosity of binary packed structures of two particles with size ratios around 0.45 (d/D = 320/700 = 0.45) is known to have a maximum 10%

difference compared to the porosity of the monodisperse packed structures of either particle.[25-27] This relative uniformity means that the addition of the second particle to the packed structure of the primary particle will affect degree of order far more than the average porosity.

5.3.1. Characterization of the Packed Structures

Colloidal structures with different χ_{700} were characterized by SEM images, as shown in Figure 5.2a, panels II to V. Panel I shows an image of ideal hexagonally packed spheres, which represents the highest degree of order. Using image analysis techniques, the center of all the particles in the images were located, and the location of the centers relative to each other was then analyzed.

Colloidal order in two-dimensional images can be evaluated by the radial distribution function, g(r), where the number and magnitude of the peaks in the plot of g(r) with respect to *r* represent the degree of order in the structures.[28-30] Figure 5.2b shows plots of g(r) calculated for the particle centers determined for each corresponding SEM image. A single parameter is more useful for characterizing two-dimensional order, and is provided by a global bond orientational order parameter given as $\psi = \frac{1}{N_p}\sum_{N_p}\frac{\exp(6i\beta)}{6}$ where i is the imaginary unit, β is the angle between a line joining nearest neighbors and an arbitrary reference axis, and N_p is the total number of particles (Appendix A). ψ approaches unity for perfect hexagonal order and approaches zero for fully random configurations.[29, 31]

Using the particle center coordinates, ψ was calculated for each structure, as shown in Figure 5.2c. Panels I and II show that the self assembled array of 320 nm particles is highly ordered, $\psi = 0.93$, however, defects are present in the long range order. Figure 5.2d shows the variation of ψ with respect to χ_{700}. The highest degree of order is seen for monodisperse particles, while $\chi_{700} = 0.5$ represents the packed structure with the highest degree of disorder.

An important difference between mono and binary packed structures is their pore size distribution. In mono-packed structures, the pore size distribution is very sharp, whereas in binary packed structures, there is a broad pore size distribution, which is strongly dependent on the size ratio of the two particles.[32] Assuming that each pore is formed by four adjacent particles in a hexagonal lattice, there are five different possibilities for pore formation in a binary packed structure of small (d) and large (D) particles as illustrated in Figure 5.3, taken from Andrade.[32] Also shown is the pore size frequency distribution, *P*, as a function of volume fraction of the larger particle (χ_D) for a particle size ratio around 0.45. While for mono-packed structures there is only one pore size present, in binary packed structures Figure 5.3 shows there can be up to five different pore sizes present, at certain volume fractions (e.g., $\chi_D = 0.75$).

5.3.2. DNA Separation

In order to study the effect of disorder on DNA separation performance, experiments were conducted in structures with χ_{700}varying from zero to unity. Fluorescence intensity profiles were acquired at various distances from the

injection channel, as shown in Figure 5.1e and f, from which DNA band positions and band variances were calculated. The separation between band positions, the band broadening or variance, and the resolution between bands provide a full characterization of separation performance. As illustrated in Figures 5.4 to 5.7, each of these performance parameters varies in a non-monotonic fashion with the crystalline order, with some subtle variations modifying the overall trends. In interpreting the results, several structural parameters illustrated in Figures 5.2 and 5.3 must be considered. Maximum order is observed at χ_{700} = 0 and 1, with maximum disorder at χ_{700} = 0.5. The pore sizes increase steadily on going from χ_{700} = 0 to 1, while the range in pore sizes is maximum at χ_{700} = 0.75.

Figure 5.4 shows the difference in separation distance of DNA bands with respect to χ_{700} for 6-10 kbp and 10-20 kbp at a) E_1 = 160 V/cm, f = 15 Hz and b) E_1 = 280 V/cm, f = 20 Hz. The frequencies for each electric field were adjusted to maximize the separation. The average values and error bars were determined from three chips prepared at each χ_{700} value. Figure 5.4 shows that, as a general trend, increasing the degree of disorder decreases the band separation distances between DNA sizes. This effect is more pronounced at higher electric field. The minimum band separation distance was observed at χ_{700} = 0.75 for all cases, though the difference relative to χ_{700} = 0.5 is statistically significant for higher field only. It is noteworthy that the smallest separation distances are seen where the highest pore size distribution is present.[32] It is also striking that the peak separation

distance reached a maximum at $\chi_{700} = 0.1$, with $\psi = 0.47$, rather than at $\chi_{700} = 0$, where the lattice is maximally ordered.

The smaller band separation distance in disordered structures can be explained based on the separation mechanism. When DNA molecules are subjected to an electric field, they stretch and move in the direction of the applied electric field, once the direction of the electric field changes with an obtuse angle, the molecules backtrack to the new direction of the electric field, with the tail in the previous half cycle becoming the head. Due to this backtracking motion, the overall distance that the molecule migrates in each cycle becomes strongly dependent on the DNA size. This distance varies linearly with the fully stretched DNA length in ordered structures such as microfabricated arrays.[12, 33] In disordered structures such as gels, the DNA dynamics is more complicated. The higher collision frequency of DNA molecules with the structure in disordered matrices[4, 5] results in complicated conformations of DNA, so that the distance traveled by the molecules will no longer be a linear function of DNA size.[12]

Figure 5.5 shows that the observed band broadening, or variance, of the DNA bands exhibits a mirror image response to the volume fraction (and hence order) compared to the band separation distances. Here, band width is defined as $w_b = 4\sigma$, where σ^2 is the variance of the fluorescence intensity profile. The variance for each DNA stream was calculated at a distance of 2.6 mm from the injection channel. The variance due to injection (σ^2_{inj}) can be calculated using the fluorescence intensity profiles at the injection channel (Figure 5.1e), allowing estimation of the variance due to other contributions (σ^2_{bed}) [34]:

$$\sigma_{total}^2 = \sigma_{inj}^2 + \sigma_{bed}^2 \quad (5.1a)$$

$$\sigma_{bed} = \sqrt{\sigma_{total}^2 - \sigma_{inj}^2} \quad (5.1b)$$

σ_{bed} is the band broadening due to DNA size fluctuations, Brownian diffusion, electric field gradients, pore size distribution, and other components.

Figure 5.5 shows the variation of σ^2_{bed} with respect to χ_{700} for three different DNA sizes: 6, 10, and 20 kbp at two field strengths. The band broadening is highest for χ_{700} = 0.5, the structure with the maximum degree of disorder. Local minima, with similar values of band broadening are seen for χ_{700} = 0.25 and χ_{700} = 0.75 (which have very different pore size distributions). Surprisingly, band broadening increases again for maximum ordered states, χ_{700} = 0 and 1 in a statistically significant manner, except at high fields and low value of χ_{700}. These results show that band broadening is greatly affected by strong disorder in the pore structure, and that this effect is much more dominant than the effect of different pore sizes on variance in binary packed structures.

The non-monotonic behavior of variance around χ_{700} = 0.1 and 0.75 is not understood, however it is consistent with Doyle[5] and Slater's[6] calculations, that show some form of non-monotonic response of DNA to order. Hickey and Slater[6] predicted by Monte Carlo simulations that DNA diffusion coefficients in an array of obstacles show non-monotonic behavior. They suggested that increasing order favored reptation, while decreasing order favored entropic trapping, and that these two models of molecular behavior exhibited diffusion coefficients with opposite

dependence on order. In electromigration of DNA, Brownian diffusion is often a minor contributor to band broadening, whereas other molecular dynamics play a larger role.[35-38] By analogy, increasing order will increase reptation like motion and decrease hooking, entanglement, hernia formation, and entropic trapping, while decreasing order will increase the latter effects. The net result will be a competition between band broadening effects that could also lead to non-monotonic behavior. It should be noted that at χ_{700} = 0.1, where we observe a minimum in band broadening, corresponds to a condition of short range, local order, with longer range disorder. Mohan and Doyle[5] have modeled DNA separation in sparse magnetic particle arrays in which a different separation mechanism is operative. They concluded that a non-monotonic dependence on order should arise, with short range order providing the best separation. They also agreed with the Patel and Shaqfeh[4] model that suggested disorder was better for separation than order, contrasting strongly with our observation. Given the difference in separation mechanism in our experimental study versus these theoretical analyses, it is hard to interpret this discrepancy. However, our report is consistent in identifying a non-monotonic dependence.

Separation resolution is a key performance parameter, and is defined as the quotient of the band separation distance over the average standard deviation (square root of band broadening) for two consecutive DNA bands; effectively convoluting the data in Figures 5.5 and 5.6.

$$Rs_{6-10} = \frac{PD_{6-10}}{\frac{w_{b6} + w_{b10}}{2}} = \frac{PD_{6-10}}{2\left(\sigma_6 + \sigma_{10}\right)} \tag{5.2}$$

where $Rs_{6\text{-}10}$ is the separation resolution between 6 and 10 kbp DNA, PD is the band separation distance, and σ_6 and σ_{10} are the standard deviations for 6 and 10 kbp DNA, respectively. The separation resolution Rs, is shown in Figure 5.6 as a function of the degree of order, ψ, for χ_{700} = 0 to 0.5. Figure 5.6 shows the separation resolution increases significantly as the order increases. On the other hand, comparing ψ = 0.47 and ψ = 0.93 shows that small scale, scattered defects or disorder have either no significant or sometimes even positive effects on separation resolution, so long as the local order in the structure is preserved. Once the degree of disorder is increased such that the local order of the structure is affected, the separation resolution decreases significantly.

The injection band broadening width contributes significantly to the observed resolution in Figure 5.6. Using Eq. 5.1 to isolate σ^2_{bed}, then substituting these corrected values into Eq. 5.2 allows evaluation of the resolution arising solely from the separation bed. Figure 5.7 shows the variation of the scaled "bed-resolution", $Rs^*_{bed} = Rs_{bed}/Rs_{bed,x_{700}=0}$, with respect to χ_{700}, illustrating the variation of separation resolution with the degree of disorder is more pronounced for larger electric fields and longer DNA molecules. For a field of 280 V/cm, the separation resolution between 10 and 20 kbp DNA molecules in a structure with χ_{700} = 0.5 drops to around one third of the resolution in ordered structures with χ_{700} = 0. This is particularly important, since most of the new DNA separation devices perform in strong electric fields to accelerate the separation process.

A comparison between the resolution for ordered (χ_{700} = 0 and 1) and highly disordered (χ_{700} = 0.5) arrays shows that regardless of the pore size (~ 50 nm for χ_{700} = 0 and 105 nm for χ_{700} = 1), the resolution in ordered structures is higher compared to disordered structures. The change in resolution is not symmetric around χ_{700} = 0.5. This may be caused by the asymmetric pore size distribution around χ_{700} = 0.5. Between χ_{700} = 0 to 0.5, pore sizes introduced to the structure are all larger than the initial pore size (dddd ~ 50 nm). Between χ_{700} = 1 to 0.5, the pore sizes introduced to the structure are all smaller than the initial pore size (DDDD ~ 105 nm). As stated in the literature[7], and shown in Figure 5.7, separation resolution decreases by increasing the pore size. By changing the structure from χ_{700} = 0 to χ_{700} = 0.5, both the greater disorder and greater pore sizes could contribute to decreasing the separation resolution. On doping the structure from χ_{700} = 1 to χ_{700} = 0.5, the pore sizes decrease while the order decreases too. The observations show that the effect of order must dominate, since the resolution decreases with increasing disorder, overcoming the effect of decreasing pore size on separation resolution.

5.4 Conclusions

Our results clearly demonstrate that extended range order within a nanoporous matrix has a significant effect on the separation performance parameters for DNA. Further, doping self assembled colloids of monodisperse

particles with a different sized particle provides a powerful and readily controllable tool for exploring the role of order, by allowing the ready fabrication of nanoporous arrays with varying degrees of order. In general, microfabrication and nanolithography, as well as colloidal self assembly offer a unique opportunity to examine the impact of coherent, reproducible separation processes. This feature stands in contrast to the random structures that are in common use today in separation science. Already, unique ratchet effects and methods such as entropic trapping, that would not be available in random gel-based matrices, have been demonstrated in lithography fabricated devices. The work presented here illustrates that there is a potentially even richer impact on performance in separation science, arising from the ability to create ordered separation matrices.

The separation mechanism employed in this work relies on highly stretched DNA and on well defined transport pathways for DNA. In contrast, the mechanisms modeled to date, in terms of the impact of order of the porous structure, rely upon hooking, hernias, and specific collisions and interactions with the separation matrix, which are enhanced by disorder. This difference in mechanism may account for the disagreement between our observation that an ordered matrix is up to 3 times more efficient than a disordered matrix, while the modeling work predicts separation performance will be better in a disordered matrix compared to a fully ordered matrix. Of greater importance though, is the conclusion of both experiment and theory that the degree of order does impact the separation efficiency, and that short range order does appear to offer somewhat better efficiency than complete order. Our results demonstrate that controlling the

order with a separation matrix should provide a fruitful means to improve separation performance.

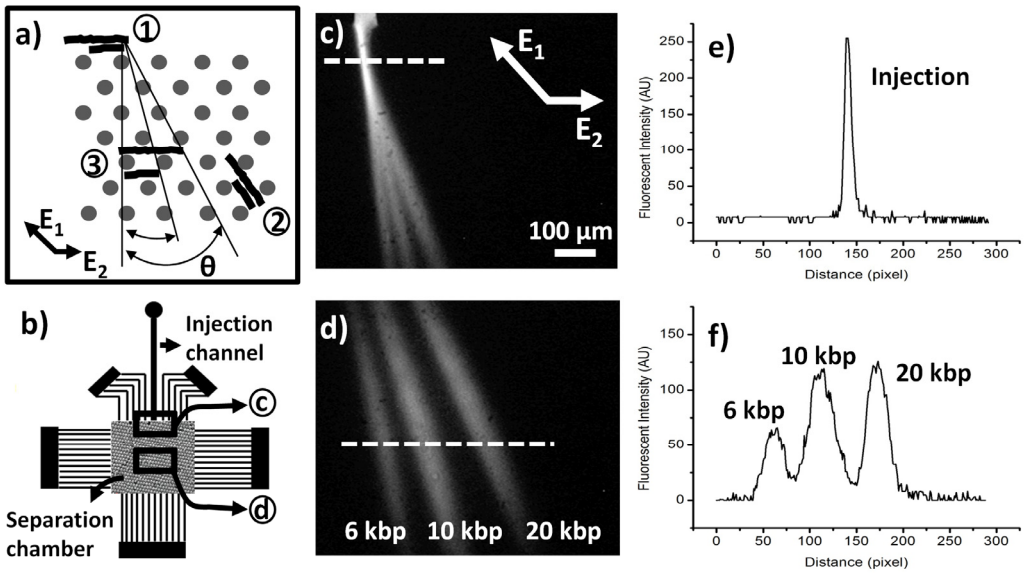

Figure 5.1. (a) Separation mechanism under pulsed electric field is shown schematically in a hexagonal array, where (1) is the initial position of two molecules with different lengths (2) is the position of the molecules just before the field direction changes from E_1 to E_2, and (3) is the position of the molecules at the end of one cycle. (b) Schematic of the DNA separation microchip. (c) Fluorescent image of the junction of the separation chamber and injection channel. A mixture of three different sizes of DNA: 6, 10, and 20 kbp is continuously injected into the separation chamber. (d) Fluorescent image of the separated DNA molecules in the middle of the separation chamber. (e) and (f) fluorescent intensity profiles at the injection and the middle of the separation chamber along the dashed lines in (c) and (d), respectively.

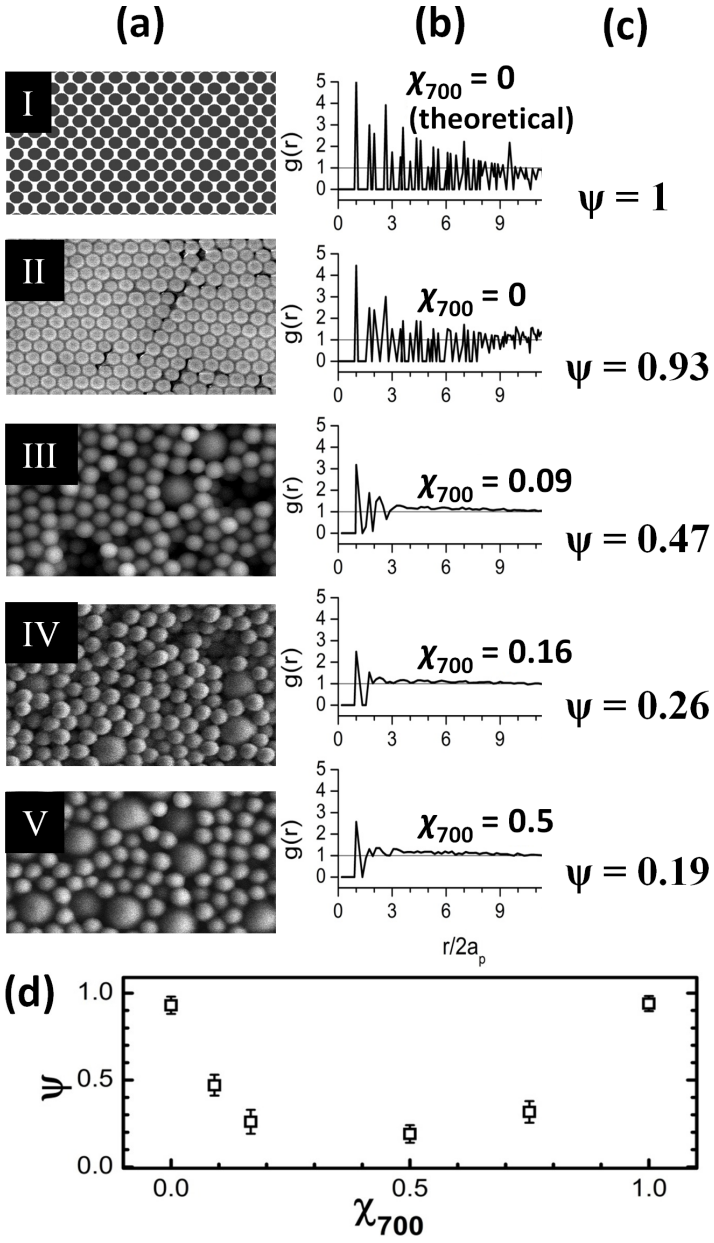

Figure 5.2. (a) SEM images of the self assembled packed structures of 320 and 700 nm silica particles with different volume fractions, χ_{700} from the top: χ_{700} = 0, 0.09, 0.16, and 0.5. The top image I is an ideal hexagonal lattice of spheres generated by image analysis software. (b) Radial distribution function calculated for each structure shown in (a), where a_p is the particle radius and r is the radial distance from the particle center. (c) Global orientational order parameter, ψ,

calculated for each structure shown in (a). (d) Experimentally determined variation of global orientational order parameter, ψ, with respect to χ_{700}.

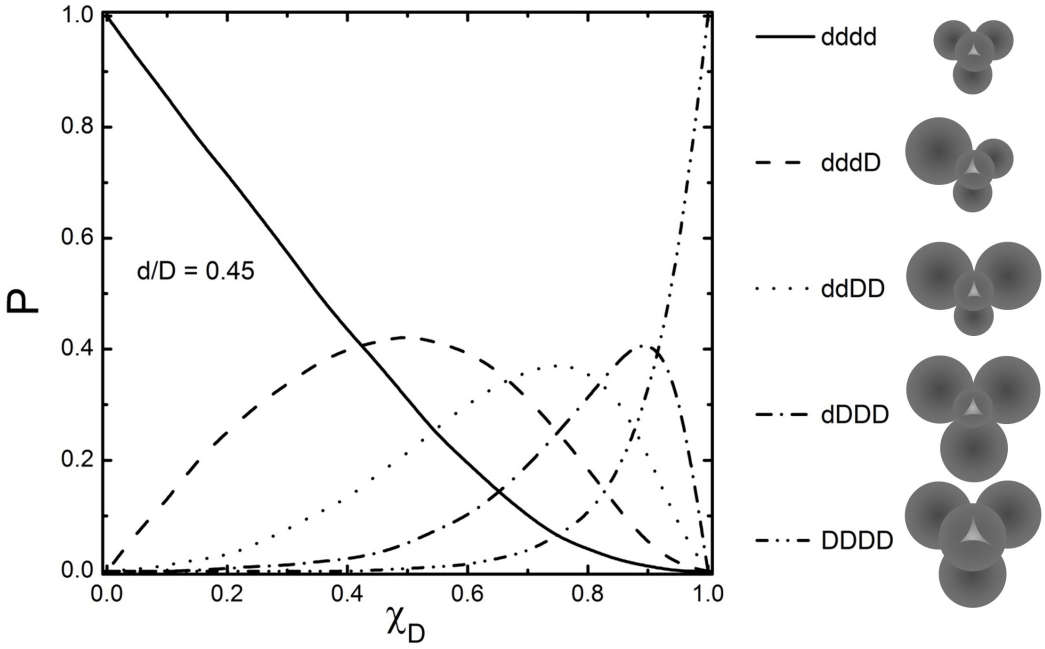

Figure 5.3. Theoretical probability of the presence of five different pore sizes as a function of the volume fraction of the larger particle, χ_D, in the 3D binary packing of spheres with size ratio of 0.45 (reprinted from Andrade JS[32] with permission from Elsevier).

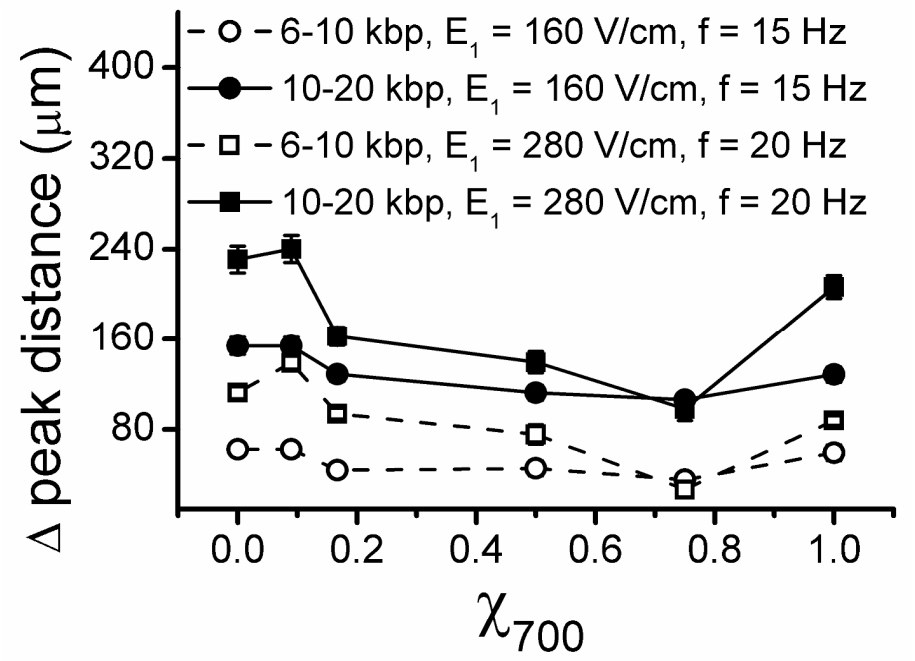

Figure 5.4. Variation of band separation distance between (open) 6-10 kbp and (filled) 10-20 kbp DNA molecules with respect to χ_{700} for (circles) E_1 = 160 V/cm, f = 15 Hz and (squares) E_1 = 280 V/cm, f = 20 Hz.

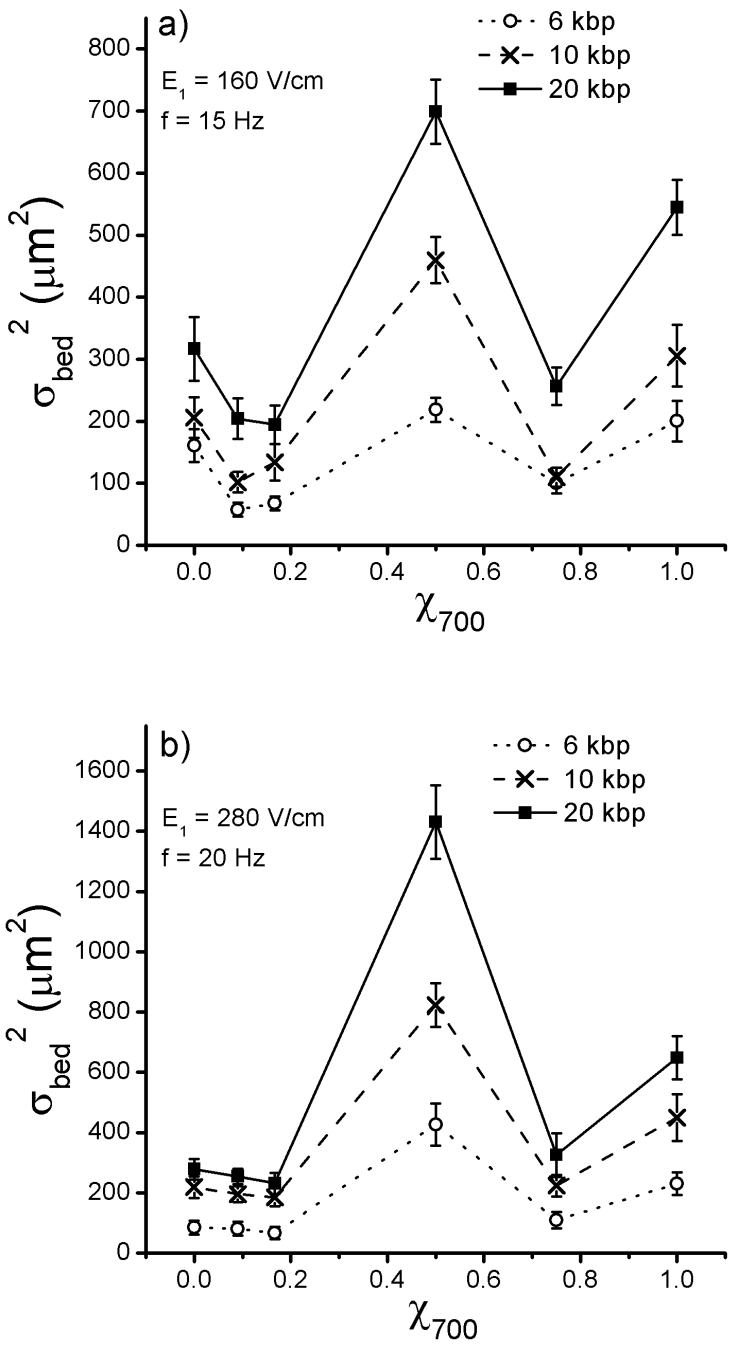

Figure 5.5. Variation of band broadening, $\sigma^2_{bed,}$ calculated using Eq. 5.1b, for 6, 10, and 20 kbp DNA molecules with respect to χ_{700} for (a) E_1 = 160 V/cm, f = 15 Hz and (b) E_1 = 280 V/cm, f = 20 Hz.

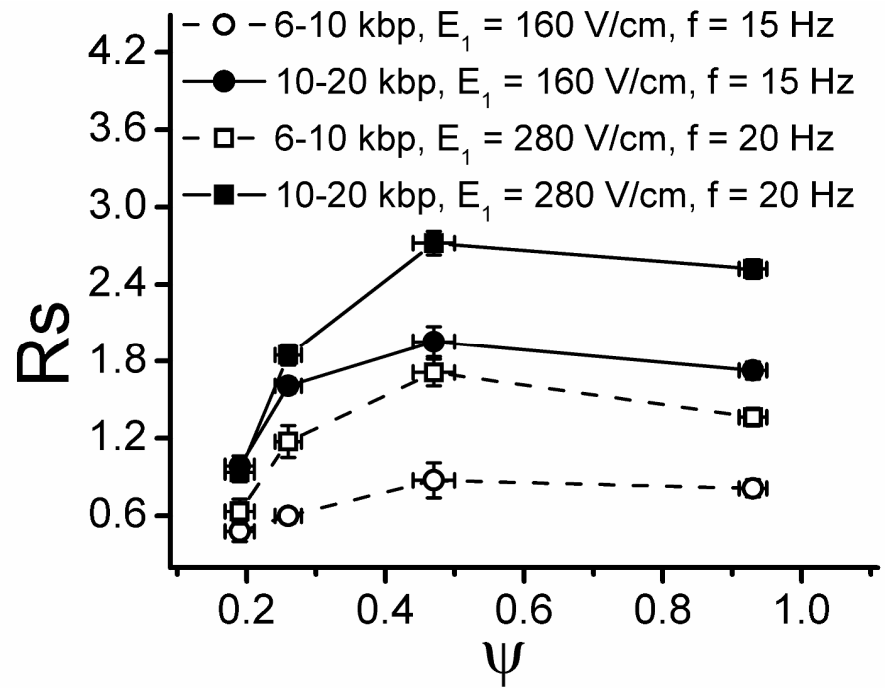

Figure 5.6. Variation of separation resolution, Rs calculated using Eq. 5.2, between 6-10 kbp and 10-20 kbp DNA molecules with respect to Ψ for E_1 = 160 V/cm, f = 15 Hz and E_1 = 280 V/cm, f = 20 Hz. These results correspond to χ_{700} = 0-0.5. Error bars are standard deviations and in most cases, they are smaller than the data symbols.

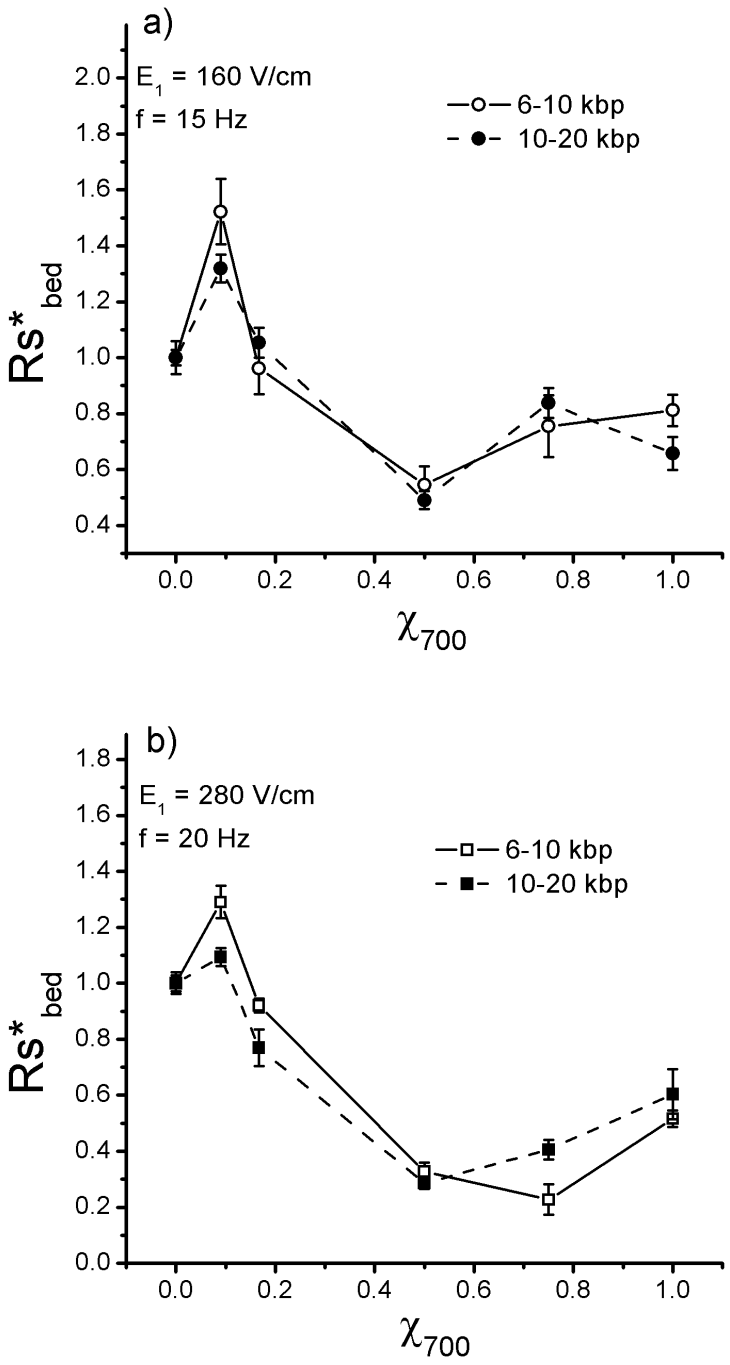

Figure 5.7. Variation of scaled resolution corrected for band broadening due to injection, $Rs^*_{other} = Rs_{bed}/Rs_{bed,\chi_{700}=0}$ with respect to χ_{700} for (a) E_1 = 160 V/cm, f = 15 Hz and (b) E_1 = 280 V/cm, f = 20 Hz.

5.5 References

1. Kaji, N., Y. Tezuka, Y. Takamura, M. Ueda, T. Nishimoto, H. Nakanishi, Y. Horiike, and Y. Baba, *Separation of long DNA molecules by quartz nanopillar chips under a direct current electric field.* **Analytical Chemistry**, *2004*. 76: p. 15-22.
2. Chui, M.M., R.J. Phillips, and M.J. McCarthy, *Measurement of the porous microstructure of hydrogels by nuclear-magnetic-resonance.* **Journal of Colloid and Interface Science**, *1995*. 174: p. 336-344.
3. Pernodet, N., M. Maaloum, and B. Tinland, *Pore size of agarose gels by atomic force microscopy.* **Electrophoresis**, *1997*. 18: p. 55-58.
4. Patel, P.D. and E.S.G. Shaqfeh, *A computational study of DNA separations in sparse disordered and periodic arrays of posts.* **Journal of Chemical Physics**, *2003*. 118: p. 2941-2951.
5. Mohan, A. and P.S. Doyle, *Effect of disorder on DNA electrophoresis in a microfluidic array of obstacles.* **Physical Review E**, *2007*. 76.
6. Hickey, O.A. and G.W. Slater, *The diffusion coefficient of a polymer in an array of obstacles is a non-monotonic function of the degree of disorder in the medium.* **Physics Letters A**, *2007*. 364: p. 448-452.
7. Viovy, J.L., *Electrophoresis of DNA and other polyelectrolytes: Physical mechanisms.* **Reviews of Modern Physics**, *2000*. 72: p. 813-872.
8. Schwartz, D.C. and C.R. Cantor, *Separation of yeast chromosome-sized dnas by pulsed field gradient gel-electrophoresis.* **Cell**, *1984*. 37: p. 67-75.

9. Gunderson, K. and G. Chu, *Pulsed-field electrophoresis of megabase-sized DNA.* **Molecular and Cellular Biology**, *1991*. 11: p. 3348-3354.

10. Volkmuth, W.D. and R.H. Austin, *DNA electrophoresis in microlithographic arrays.* **Nature**, *1992*. 358: p. 600-602.

11. Bustamante, C., S. Gurrieri, and S.B. Smith, *Towards a molecular description of pulsed-field gel-electrophoresis.* **Trends in Biotechnology**, *1993*. 11: p. 23-30.

12. Duke, T.A.J., R.H. Austin, E.C. Cox, and S.S. Chan, *Pulsed-field electrophoresis in microlithographic arrays.* **Electrophoresis**, *1996*. 17: p. 1075-1079.

13. Volkmuth, W.D., T. Duke, M.C. Wu, R.H. Austin, and A. Szabo, *DNA electrodiffusion in a 2d array of posts.* **Physical Review Letters**, *1994*. 72: p. 2117-2120.

14. Zeng, Y. and D.J. Harrison, *Self-assembled colloidal arrays as three-dimensional nanofluidic sieves for separation of biomolecules on microchips.* **Analytical Chemistry**, *2007*. 79: p. 2289-2295.

15. Zeng, Y., M. He, and D.J. Harrison, *Microfluidic self-patterning of large-scale crystalline nanoarrays for high-throughput continuous DNA fractionation.* **Angewandte Chemie-International Edition**, *2008*. 47: p. 6388-6391.

16. Huang, L.R., J.O. Tegenfeldt, J.J. Kraeft, J.C. Sturm, R.H. Austin, and E.C. Cox, *A DNA prism for high-speed continuous fractionation of large DNA molecules.* **Nature Biotechnology**, *2002*. 20: p. 1048-1051.

17. Zhang, H. and M.J. Wirth, *Electromigration of single molecules of DNA in a crystalline array of 300-nm silica colloids.* **Analytical Chemistry**, *2005*. 77: p. 1237-1242.

18. Park, J., D. Lee, W. Kim, S. Horiike, T. Nishimoto, S.H. Lee, and C.H. Ahn, *Fully packed capillary electrochromatographic microchip with self-assembly colloidal silica beads.* **Analytical Chemistry**, *2007*. 79: p. 3214-3219.

19. Minc, N., C. Futterer, K. Dorfman, A. Bancaud, C. Gosse, C. Goubault, and J.L. Viovy, *Quantitative microfluidic separation of DNA in self-assembled magnetic matrixes.* **Analytical Chemistry**, *2004*. 76: p. 3770-3776.

20. Dorfman, K.D., *DNA electrophoresis in microfluidic post arrays under moderate electric fields (vol 73, art no 061922, 2006).* **Physical Review E**, *2008*. 77.

21. Ou, J., J. Cho, D.W. Olson, and K.D. Dorfman, *DNA electrophoresis in a sparse ordered post array.* **Physical Review E**, *2009*. 79.

22. Nazemifard, N., S. Bhattacharjee, J.H. Masliyah, and D.J. Harrison, *DNA dynamics in nanoscale confinement under asymmetric pulsed field electrophoresis.* **Angewandte Chemie-International Edition**, *2010*. 49: p. 3326-3329.

23. Dufresne, E.R., E.I. Corwin, N.A. Greenblatt, J. Ashmore, D.Y. Wang, A.D. Dinsmore, J.X. Cheng, X.S. Xie, J.W. Hutchinson, and D.A. Weitz,

Flow and fracture in drying nanoparticle suspensions. **Physical Review Letters**, *2003*. 91.

24. Wang, S.H., S. Sato, and K. Kimura, *Preparation of hexagonal-close-packed colloidal crystals of hydrophilic monodisperse gold nanoparticles in bulk aqueous solution.* **Chemistry of Materials**, *2003*. 15: p. 2445-2448.

25. Dias, R.P., J.A. Teixeira, M.G. Mota, and A.I. Yelshin, *Particulate binary mixtures: Dependence of packing porosity on particle size ratio.* **Industrial & Engineering Chemistry Research**, *2004*. 43: p. 7912-7919.

26. Dias, R., J.A. Teixeira, M. Mota, and A. Yelshin, *Tortuosity variation in a low density binary particulate bed.* **Separation and Purification Technology**, *2006*. 51: p. 180-184.

27. Song, M., K.T. Chuang, and K. Nandakumar, *A theoretical correction of the ouchiyama and tanaka formula for predicting average porosity of packed beds consisting of nonuniform spheres.* **Industrial & Engineering Chemistry Research**, *1998*. 37: p. 3490-3496.

28. Aste, T., *Variations around disordered close packing.* **Journal of Physics-Condensed Matter**, *2005*. 17: p. S2361-S2390.

29. Bevan, M.A., J.A. Lewis, P.V. Braun, and P. Wiltzius, *Structural evolution of colloidal crystals with increasing ionic strength.* **Langmuir**, *2004*. 20: p. 7045-7052.

30. Clarke, A.S. and H. Jonsson, *Structural-changes accompanying densification of random hard-sphere packings.* **Physical Review E**, *1993*. 47: p. 3975-3984.

31. Halperin, B.I. and D.R. Nelson, *Theory of 2-dimensional melting.* **Physical Review Letters**, *1978*. 41: p. 121-124.

32. Andrade, J.S., *Hydrodynamic dispersion in binary packings of spheres.* **Physica A**, *1993*. 199: p. 431-444.

33. Gurrieri, S., S.B. Smith, K.S. Wells, I.D. Johnson, and C. Bustamante, *Real-time imaging of the reorientation mechanisms of yoyo-labelled DNA molecules during 90 degrees and 120 degrees pulsed field gel electrophoresis.* **Nucleic Acids Research**, *1996*. 24: p. 4759-4767.

34. Lucy, C.A., L.L.M. Glavina, and F.F. Cantwell, *A laboratory experiment on extracolumn band broadening in liquid-chromatography.* **Journal of Chemical Education**, *1995*. 72: p. 367-374.

35. Mercier, J.F. and G.W. Slater, *Universal interpolating function for the dispersion coefficient of DNA fragments in sieving matrices.* **Electrophoresis**, *2006*. 27: p. 1453-1461.

36. Tinland, B., N. Pernodet, and A. Pluen, *Band broadening in gel electrophoresis: Scaling laws for the dispersion coefficient measured by frap.* **Biopolymers**, *1998*. 46: p. 201-214.

37. Meistermann, L. and B. Tinland, *Band broadening in gel electrophoresis of DNA: Measurements of longitudinal and transverse dispersion coefficients.* **Physical Review E**, *1998*. 58: p. 4801-4806.

38. Popelka, S., Z. Kabatek, J.L. Viovy, and B. Gas, *Peak dispersion due to geometration motion in gel electrophoresis of macromolecules*. **Journal of Chromatography A**, *1999*. 838: p. 45-53.

CHAPTER 6
CONCLUSION AND FUTURE WORK

6.1 Concluding Remarks

The focus of the study presented in this thesis is to analyze and investigate the separation of DNA molecules in self assembled nanoparticle arrays and the key parameters affecting separation efficiency in a microfluidic platform. The important conclusions based on the work described in this thesis are summarized below.

- Using the colloidal self assembly approach, crack-free, large scale structures of nanoparticle arrays were formed in a microfluidic chip for DNA separation. By tuning the concentrations of particle suspensions, ordered arrays with pore sizes as small as a few nanometres were fabricated, which is hard to achieve using conventional nanolithography techniques.
- Angular separation of DNA molecules in nanoparticle arrays under asymmetric pulsed field electrophoresis (APFE) was studied by developing a simple geometric model. The geometric model was developed by modeling DNA as a flexible rod moving opposite to the direction of applied fields with one of its heads. It was observed that in confinements smaller than the persistence length of DNA, there is an

agreement between the experimental results and predictions of geometric model.

- Our experimental results show that in nanoscale confinement, where pore sizes are smaller than the persistence length of DNA molecule: i) mere confinement is sufficient to stretch the molecule close to a substantial fraction of its contour length and ii) the bending elasticity of the molecule lowers the probability of hernia formations so that the molecule can be treated as a persistent chain following the biased reptation mechanism for its migration.
- Frequency behaviour of DNA angular separation during asymmetric pulsed field electrophoresis was investigated for a variety of DNA sizes, pore sizes, and electric fields. In all of these experimental conditions, four distinct regimes were observed in the frequency response of angular separation; a rise, plateau, fall, and a second plateau. Using high resolution real time movies of DNA acquired by TIRF microscopy, DNA migration corresponding to each regime was studied.
- Inspired by conventional pulsed field gel electrophoresis, DNA reorientation time was measured and employed to define a scaled frequency. It was observed that a universal curve can be defined based on this scaled frequency, where different frequency responses for different sizes of DNA can be normalized to one effective response curve.
- In addition to angular separation, DNA mobility under asymmetric pulsed field electrophoresis in the direction of the average electric field was

measured. It was observed that similar to angular separation, DNA mobility also varied in a non-monotonic fashion with pulse frequency. The contrast was that, at the same frequency that angular separation reached its maximum, mobility reached its minimum value. This shows that physics behind the anomalous mobility minimum in PFGE and angular separation maximum in APFE is directly related.

- Variation of angular separation with frequency was also verified numerically, using a freely-jointed-chain model of DNA. The nanoparticle structure was modeled as an array of hexagonal posts. The chain migration through the array was calculated under a pulsed external force applying on all segments of the chain, while no thermal noise was taken into account. According to this model, the angular separation of a freely-jointed-chain exhibit a frequency dependant behaviour similar to what was observed in our experiments for the same four regimes.
- Using the self assembly approach (CSA), a new experimental procedure was developed to fabricate nanoporous structures with different degrees of crystalline order. Using electron micrograph images of the structures, the degree of order was characterized in each structure by a radial distribution function, as well as an orientation order parameter. It was observed that the structures made with monodisperse particle suspensions have the highest degree of order, while structures made with bidisperse particle suspensions have different degrees of order, depending on the volume fractions of the particles in the suspension.

- The ability of CSA to provide reproducible structures, where the degree of order can systematically be tuned, provided an opportunity to investigate the effect of order in a separation matrix on DNA separation efficiency. Peak separation distance, band width, and resolution were calculated for different sizes of DNA in structures with different degrees of order. It was observed that all three separation parameters are strongly affected by the degree of order and vary in a non-monotonic fashion with degree of order in separation media. To our knowledge, this is the first experimental evaluation of the effect of order on separation efficiency.

6.2 Future Work

Based on the observations and experience from this study, a few suggestions and recommendations are presented here for future research in this field.

- Although a wide range of particle sizes was used, in all of our experiments self assembled nanoparticle arrays were made with plain silica particles. The feasibility of forming large scale, crack-free self assembled structures with particles other than plain silica can be investigated since particles with a variety of functional groups and surface chemistry are available commercially. These structures can then be used for separation of DNA or other biomolecules to study the effect of surface chemistry of the porous structures on separation efficiency. Since surface chemistry affects the

particle surface charge significantly, the interactions of DNA and particles might have a significant effect on DNA mobility and conformations. The result of such a study might benefit the problem of trapping large DNA molecules at high electric fields by investigating the variation of trapping probability with particle surface chemistry.

- As observed in Chapter 3, a certain pore size provides a good separation only for a certain range of DNA sizes. On the other hand, our experimental results in Chapter 5 showed that DNA separation is lower in disordered structures compared to ordered structures. This means that having a random structure consisting of different pore sizes would not serve as a good separation media to address both separation resolution and peak capacity (the number of DNA sizes resolvable by a structure). In order to introduce different pore sizes without disturbing the crystalline order of our nanoparticle array structure, different particles can be introduced to the separation chamber individually. This way, sequential stacks of arrays would be formed, where each section has a different pore size from the rest, and since each section is made with a monodisperse suspension, the separation quality has been preserved as well.
- DNA size fluctuation and relaxations under pulsed electric fields can also be investigated in nanoparticle array structure. The effects of pore size and electric fields on DNA relaxation times can be studied. This would help understanding the behaviour of DNA molecules under high frequency

pulsed electric fields and the time scales associated with the plateau regime discussed in Chapter 4.

- Due to the robustness of the self assembled structure in providing reproducible DNA separation results, and the simplicity of our fabrication process, our device has great potential to serve as a reliable tool for producing a comprehensive dataset for DNA mobility and dispersion. An extensive parametric study can be developed to measure mobility and dispersion for a wide range of DNA sizes, in a variety of pore sizes, and for a broad range of electric fields and frequency. This would provide a much needed dataset, which can serve as a basis for developing universal functions for DNA mobility and dispersion under electrophoretic forces.
- As described in Chapter 5, DNA separation parameters all show a non-monotonic behaviour with respect to the degree of order in the separation matrix. A complete understanding of this behaviour might be achieved by a numerical model of DNA separation in structures with varying degrees of order under pulsed field electrophoresis. Such simulations exist for DNA diffusion and DNA separation in sparse array structures, but the separation mechanism in our experiments is different. Such a simulation might provide an insight into the reasons behind the non-monotonic variation of separation parameters with order.
- Following the success of our microchip in separation of a wide range of DNA molecules, our separation device can be further developed to serve as an integrated, stand-alone, lab-on-a-chip device for DNA analysis. It

has been shown in the literature that colloidal self assemblies can serve as sample pre-concentrators. Other elements of DNA analysis experiment such as polymerase chain reaction (PCR) and DNA sequencing can also be integrated with our DNA separation microchip to form an integrated bio-analytical microsystem.

APPENDIX A

Experimental Procedures

A.1 Colloidal Self-Assembly

Colloidal self-assembled structures were formed within a microfluidic device using an evaporation self-assembly technique. Aqueous suspensions of silica colloids (Bangs Laboratories, Fishers, IN) of 100, 330, and 700 nm diameter (10 % CV) were used to form the self assembled nanoparticle array inside the microchips. Figure A.1 shows the steps taken for fabrication of the self-assembled structures schematically. Particle suspensions were ultrasonicated for 10-15 minutes prior to packing. Once the PDMS microchip was sealed to a clean glass slides, the device was filled with the particle suspension. All the reservoirs except than one were covered by PDMS pieces to prevent the solvent evaporation, so that the evaporation would take place only in open reservoir. Solvent evaporation induced the crystal nucleation in the channels connected to the open reservoir and the packed structure started to grow until the whole microchip was packed by silica nanoparticle. The packing can be stopped at any time by replacing the particle suspension with buffer solution in the reservoirs. It was observed that fabrication of large scale, crack free structures depends on packing time (the time it takes for colloidal crystal to form all through the microchip). A higher probability of crack formation was observed when the packing was fast (less than

an hour). On the other hand, when the packing was slow (around 24 h), the interface of the reservoir and the channels would get dried, which prevented the flow of the buffer into the separation chamber.

Since the packing relied on solvent evaporation, the packing time could be controlled by tuning the temperature and humidity. However, since the fabrication was conducted in room condition, controlling the temperature and humidity would complicate the fabrication process. A simpler parameter to tune in order to control the packing speed was found to be the particle concentration. For each particle size, different particle concentrations ranging from 2.5 to 20 % w/v were used to fabricate the packed structures. It was observed that optimum packing can be achieved by using higher concentrations for smaller particles and lower concentrations for larger particles. The optimized particle concentrations along with corresponding packing times were presented in Table A.1 for three particle sizes used in this study.

A.2 Generating Pulsed Electric Field

Pulsed electric fields were generated across the separation chamber by applying alternating DC voltages to buffer reservoirs using platinum electrodes as shown in Figure A.2. A four-channel function generator (TGA 1244, Thurlby Thandar Instruments Limited, Cambridgeshire, UK) was used to generate square wave signals. The outputs of the function generator were connected to two dual channel high voltage linear amplifiers (F20AD, FLC Electronics AB, Partille,

Sweden) to form the high voltage alternating signals shown in Figure A.2. The signals were monitored continuously using a four-channel oscilloscope with sampling rate of 1 Gs/s (TDS2004C, Tektronics Inc., Beaverton, OR, USA).

A.3 Calculation of Variance

Separation peak distances and band broadening for each DNA band can be calculated using fluorescent intensity profiles extracted from fluorescent images captured during separation experiments. The intensity profiles were captured at a distance of 2.6 mm from the injection channel along a horizontal axis. Since the DNA separation in our experiment is an angular separation, the intensity profiles can also be captured along a cord for each DNA stream perpendicular to the stream which would be another approximation. But in this study, we used the intensity profiles along a horizontal axis (x) similar to conventional 1D DNA separation. For each intensity curve, the average of the intensity signal can be recognized as the peak location, and the variance, or the standard deviation σ, reflects the peak broadening. The peak location PD and variance σ^2 of an intensity curve I(x) can be calculated as:

$$PD = \frac{\int I(x)xdx}{\int I(x)dx}$$
$$\sigma^2 = \frac{\int I(x)(x-PD)^2 dx}{\int I(x)dx} \quad \text{(A1)}$$

Since the actual intensity curve is formed by discrete data points, the trapezoidal rule is used to evaluate all the above integrals using MATLAB software (MathWorks, Natick, MA, USA):

$$\int I(x)dx = \sum_{i=1}^{n} \frac{I(x_i) + I(x_{i+1})}{2}(x_{i+1} - x_i) \tag{A2}$$

Separation resolution is defined as the quotient of the separation peak distances over the average width of the two peaks and is employed to evaluate the performance of the separation:

$$Rs = \frac{PD_2 - PD_1}{2(\sigma_1 + \sigma_2)} \tag{A3}$$

This equation applies when the peaks are Gaussian. Actually, our peaks have small tailing, but still could be treated as Gaussian as approximation.

A.4 Orientational Order Parameter

In order to measure the degree of order in each packed structure in this study, a parameter called orientational order parameter ψ is used, where ψ can be calculated as:

$$\psi = \frac{1}{N_p} \sum_{N_p} \frac{\exp(6i\beta)}{6} \tag{A4}$$

where β is the angle between the two lines joining the central particle to its nearest neighbours, as shown in Figure A.3 and N_p is the total number of particles in the

image. In order to calculate ψ for each structure, first the coordinates of the particle centres in an SEM image of the structure were defined using an image analysis software, ImageJ (NIH, http://rsb.info.nih.gov/ij/). Once the particle coordinates were known, for each particle in the image, the angle β between the lines connecting the centres of the central particle and its nearest neighbours can be calculated, as shown in Figure A3. Using the values of β, the expression $\sum \frac{\exp(6i\beta)}{6}$ was calculated for each particle in the image. The degree of order in the structure can be quantified by averaging the values of $\sum \frac{\exp(6i\beta)}{6}$ over the total number of the particles in the image N_p, as given by Eq. A4. For a perfect hexagonal structure, ψ assumes the value of one and for highly random structures ψ assumes values close to zero.

particle size (nm)	particle concentration (% w/v)	packing time (h)	pore size (nm)
100	20	12-16	15
320	10	6-8	48
700	6	0.5-1	105

Table A.1. Particle sizes and optimized particle concentrations used for packing in this study along with the packing time and resulting pore sizes.

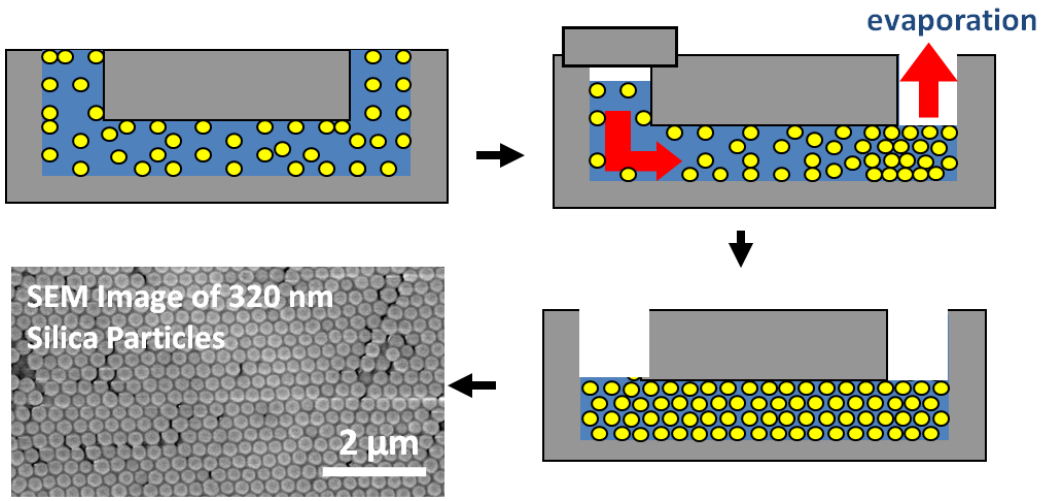

Figure A.1. Schematic description of the microfluidic packing scheme. Particle suspensions were ultrasonicated for 10-15 minutes prior to packing. Once the PDMS microchip was sealed to a clean glass slides, the device was filled with the particle suspension. All the reservoirs except than one were covered by PDMS pieces to prevent the solvent evaporation, so that the evaporation would take place only in open reservoir. Solvent evaporation induced the crystal nucleation in the channels connected to the open reservoir and the packed structure started to grow until the whole microchip was packed by silica nanoparticle. The SEM image shows a hexagonal packed structure using 320 nm silica particles.

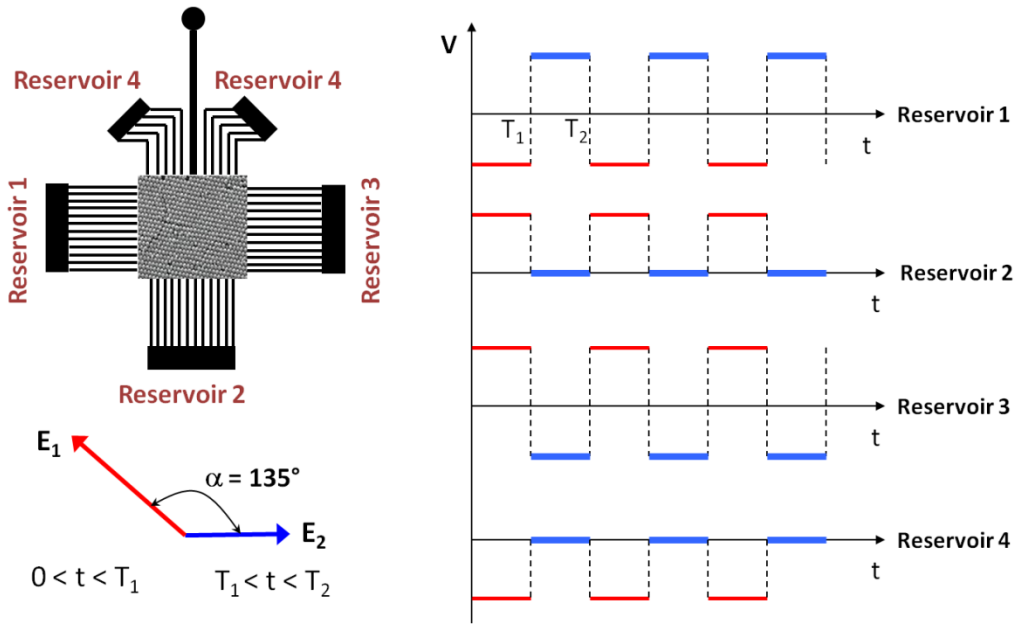

Figure A.2. Generation of obtuse angle pulsed electric field across the separation chamber. High-voltage square wave signals are applied to each buffer reservoirs in order to form electric fields in the directions of E_1 and E_2. Square wave signals generated using a four-channel function generator (TGA 1244, Thurlby Thandar Instruments Limited, Cambridgeshire, UK) and amplified using a two dual channel high voltage linear amplifiers (F20AD, FLC Electronics AB, Partille, Sweden). The resulting high voltage square wave signals are transferred to the reservoirs using platinum electrodes.

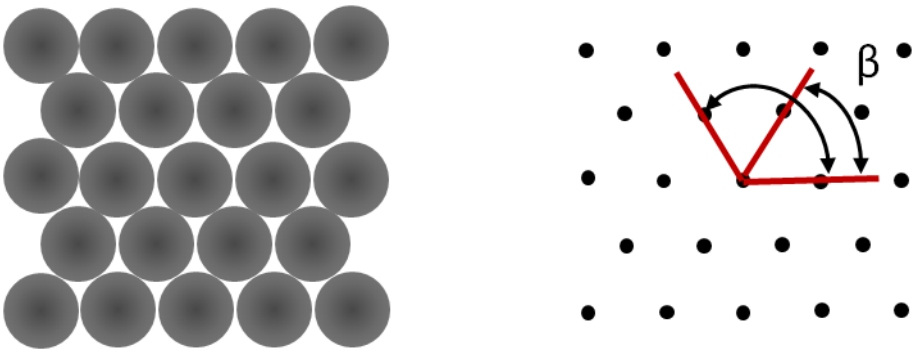

Figure A.3. Schematic of the scheme for calculation of orientational order parameter ψ. The particle centre coordinates in each SEM image of the structures were defined using ImageJ (NIH, http://rsb.info.nih.gov/ij/). Once the particle coordinates were known, for each particle in the image, the angle β between the lines connecting the centres of the central particle and its nearest neighbours was calculated. Using the values of β, the expression $\sum \frac{\exp(6i\beta)}{6}$ was calculated for each particle in the image and was averaged the total number of the particles in the image N_p.

APPENDIX B

Theoretical Analysis

B.1 Derivation of Geometric Model

The geometric was developed by assuming the DNA molecule as a flexible chain moving in the porous structure with either of its heads in the opposite direction of the applied electric fields (E_1 and E_2). Figure B.1 shows the displacement of a DNA chain at the end of one cycle. Three different locations of the chain in this figure correspond to 1) initial position of the chain at t = 0, 2) position of the chain at the end of half cycle right before the field changed to E_2, 3) position of the molecule at the end of one cycle right before the electric field changed back to E_1 for a new cycle. A comparison between the initial (1) and final (3) positions of the chain shows that there is a net angular displacement, θ, between the two positions. It can be seen from Figure B.1, that θ can be calculated as:

$$\tan\theta = \frac{d_{1x} - d_{2x}}{d_{1y} - d_{2y}} \tag{B1}$$

where d_{1x}, d_{2x}, d_{1y}, d_{2y} are the displacements in x and y directions under E_1 and E_2 electric fields, respectively and can be defined in terms of the chain mobilities μ_1, μ_2, chain length L, frequency f, and the angle between the two electric fields α:

$$
\begin{aligned}
d_{1x} &= \frac{\mu_1 E_1}{2f}\sin\alpha \\
d_{1y} &= \frac{\mu_1 E_1}{2f}\cos\alpha \\
d_{2x} &= L\sin\alpha + \frac{\mu_1 E_1}{2f} - L \\
d_{2y} &= L\cos\alpha
\end{aligned}
\tag{B2}
$$

Substituting Eq. B2 in Eq. B1, an expression can be derived to relate θ to the experimental parameters such as E_1, E_2, f and L:

$$
\begin{aligned}
\tan\theta &= \frac{(\frac{\mu_1 E_1}{2f} - L)\sin\alpha - \frac{\mu_2 E_2}{2f} + L}{(\frac{\mu_1 E_1}{2f} - L)\cos\alpha} \\
\tan\theta &= \tan\alpha - \frac{\frac{\mu_2 E_2}{2f} - L}{(\frac{\mu_1 E_1}{2f} - L)\cos\alpha}
\end{aligned}
\tag{B3}
$$

since $\alpha = 135°$, Eq. B3 can be further simplified to:

$$
\tan\theta = 1 - \sqrt{2}\,\frac{\frac{\mu_2 E_2}{2f} - L}{\frac{\mu_1 E_1}{2f} - L} \tag{B4}
$$

B.2 Description of FJC Model

Freely-jointed-chain (FJC) model of DNA was developed to study the frequency behaviour of a DNA chain under asymmetric electric field. The simulation is conducted using Working Model 2D software (Design Simulation

Technologies, Inc., Canton, MI, USA). DNA molecule is modeled as a chain of rigid rods jointed together with revolute joints. Figure B.2 shows the schematic of the FJC model. All segments have the same length equal to the Kuhn length of DNA chain. In order to simulate the electric fields, asymmetric external forces, F_1 and F_2 (F_1 = 1.4 F_2) with an obtuse angle of 135° (similar to the electric field configurations in our experiments) were exerted on each segment in a distributed fashion; one at the centre of the mass (CM), two at the two ends of each segment, and the other two applied half way between the CM and the two ends, as shown in Figure B.2.

The dynamic of this multi-body system of interconnected rigid rods under the pulsed external force is solved using a constraint force algorithm, which is a variation of Newton-Euler equations of motion. Working Model 2-d solves the equations of motion using Kutta-Merson (Rung-Kutta 5) integration method based on variable time step option. Table B.1 shows the parameters used in this simulation. The porous structure is modeled as a hexagonal array of posts. Since in packed structure of 700 nm particles, the pore sizes is around 105 nm and similar to the Kuhn length (100 nm), the distance between any two consecutive posts is set to be equal to the length of the segments of the freely-jointed-chain.

The simulation is conducted for different chains, N = 6 and N = 12 (N is the number of segments in each chain) at different pulse frequencies and the value of deflection angle θ, is measured at the end of the hexagonal array. For each frequency, the chain is released at five different initial positions inside the

injection channel and θ is calculated for each case, providing the average and standard deviation (error bars in Figure 4.12e).

properties	values
static friction coeff.	0.9
kinematic friction coeff.	0.8
elastic coeff.	0.0001

Table B.1. Parameters used in simulation of FJC model using Working Model 2D software (Design Simulation Technologies, Inc., Canton, MI, USA).

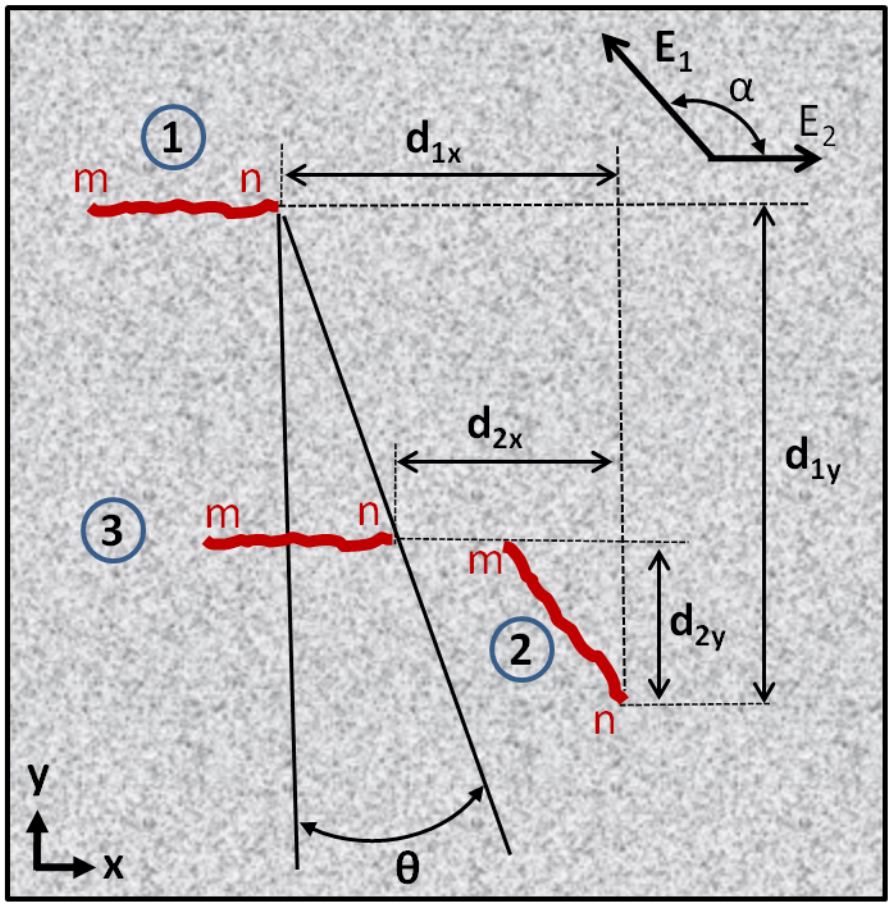

Figure B.1. Schematic of the migration of a DNA chain during one cycle under E_1 and E_2 as assumed for developing the geometric model. m and n are the two ends of the molecule. 1) initial position of the chain, 2) position of the chain and the end of half cycle, 3) position of the chain at the end of one cycle. θ is the net angular displacement of the chain during one cycle. d_{1x}, d_{1y}, d_{2x}, d_{2y} are the displacement of the chain in x and y directions under E_1 and E_2.

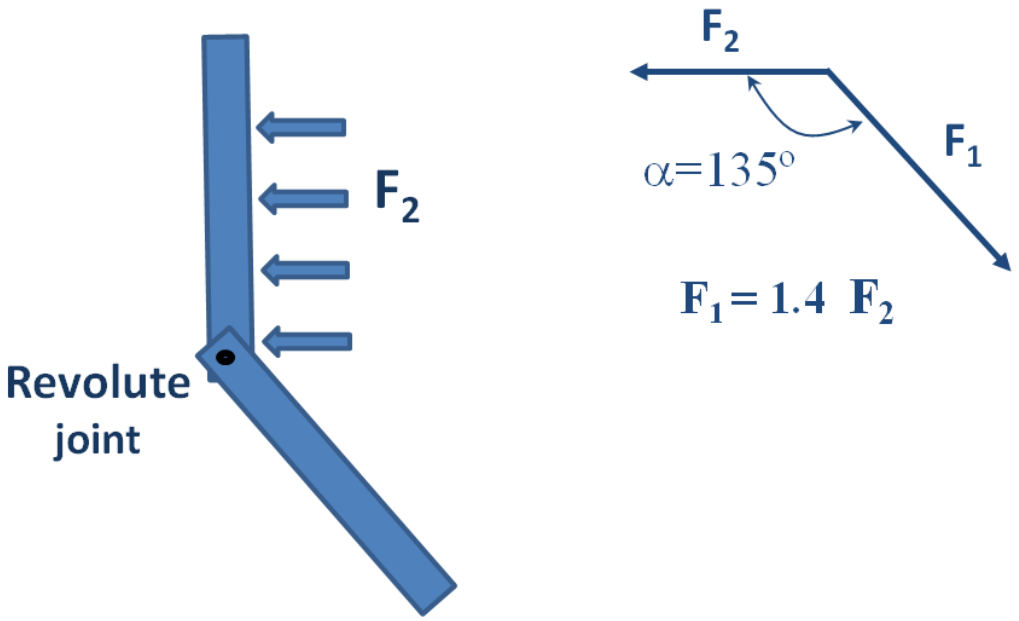

Figure B.2. Schematic of the freely-jointed-chain model of DNA. Rigid rods are connected with revolute joints. A constraint force algorithm is used to calculate the equation of motion of this chain under asymmetric pulsed external forces. The external force is pulsed between F_1 and F_2 with a configuration similar to the configuration of the pulsed electric fields in the DNA separation experiment. The force is applied on each segment in a distributed fashion; one at the centre of the mass (CM), two at the two ends of each segment, and the other two applied half way between the CM and the two ends.